UNIVERSITÉ DE MONTRÉAL

SYSTEMS OF DIFFERENTIAL-ALGEBRAIC EQUATIONS ENCOUNTERED IN THE
NUMERICAL MODELING OF HIGH-TEMPERATURE SUPERCONDUCTORS

SIMON BRAULT
DÉPARTEMENT DE GÉNIE ÉLECTRIQUE
ÉCOLE POLYTECHNIQUE DE MONTRÉAL

MÉMOIRE PRÉSENTÉ EN VUE DE L'OBTENTION
DU DIPLÔME DE MAÎTRISE ÈS SCIENCES APPLIQUÉES
(GÉNIE ÉLECTRIQUE)
JUILLET 2015

UNIVERSITÉ DE MONTRÉAL

ÉCOLE POLYTECHNIQUE DE MONTRÉAL

Ce mémoire intitulé :

SYSTEMS OF DIFFERENTIAL-ALGEBRAIC EQUATIONS ENCOUNTERED IN THE NUMERICAL MODELING OF HIGH-TEMPERATURE SUPERCONDUCTORS

présenté par : BRAULT Simon

en vue de l'obtention du diplôme de : Maîtrise ès Sciences Appliquées

a été dûment accepté par le jury d'examen constitué de :

M. LAFOREST Marc, Ph. D., président

M. SIROIS Frédéric, Ph. D., membre et directeur de recherche

M. DUFOUR Steven, Ph. D., membre et codirecteur de recherche

M. PRUDHOMME Serge, Ph. D., membre externe

DEDICACE

"Parler de ce qu'on ignore finit par vous l'apprendre."
-Albert Camus

REMERCIEMENTS

Tout d'abord, j'aimerais remercier le physicien et vulgarisateur Hubert Reeves qui a su me transférer sa passion pour la science à travers son livre *Poussière d'étoiles.* Je ne peux nier l'impact que cet auteur a eu sur ma vie et mon cheminement scientifique et je lui en suis encore aujourd'hui, très reconnaissant.

Ensuite, je tiens à remercier Martin Charest, professeur de physique au collège Ahunstic. C'est lors de son cours d'électromagnétisme que j'ai été initié à cette science et c'est aussi à ce moment qu'est né mon intérêt pour les supraconducteurs. Ma décision d'aller étudier en Génie Physique au Baccalauréat repose grandement sur le plaisir que j'ai eu à suivre ce cours.

Je n'écrirais probablement pas ces lignes si mon directeur, le Professeur Frédéric Sirois ne m'avait pas admis au Laboratoire en Énergie Électrique (LEE) en 2009 lorsque j'étais à la recherche d'un stage au Baccalauréat. J'aimerais le remercier pour avoir partagé sa passion pour l'analyse numérique et les supraconducteurs, mais aussi pour m'avoir donné de bonnes et uniques opportunités.

J'aimerais remercier le Professeur Steven Dufour, mon codirecteur, pour plusieurs raisons. Premièrement, pour m'avoir enseigné la méthode des éléments finis lorsque j'ai suivi son excellent cours sur le sujet en 2009. Deuxièmement, pour avoir accepté de codiriger ma maitrise, mais aussi pour m'avoir fourni un soutien académique continuel durant ces dernières années.

Je remercie le Professeur Marc Laforest du département de mathématiques de l'École Polytechnique Montréal pour m'avoir introduit à l'analyse numérique. J'aimerais aussi le remercier pour ses séminaires sur la modélisation des supraconducteurs à haute température critique, pour ses conseils et pour les excellentes discussions que nous avons eues. Je le remercie, ainsi que le Professeur Serge Prudhomme, d'avoir accepté de participer au jury d'examen de ce mémoire.

J'aimerais particulièrement remercier mes collègues Andy Wan et Charles-Henri Bonnard pour leur aide et leur implication dans mes travaux de maîtrise. J'aimerais aussi les remercier pour les bons moments que nous avons passés ensemble au LEE et ailleurs dans le monde. Je remercie aussi mes collègues Christian Lacroix et Mathieu Lambert pour les nombreuses discussions scientifiques que nous avons eu.

Je remercie le Professeur Thomas Gervais, qui m'a donné ma première chance en enseignement en m'engagent comme chargé de travaux dirigés pour le cours Mécanique pour ingénieur. Dans la même ligne d'idée, j'aimerais remercier le Docteur Donatien N'Dri, qui

m'a fait confiance en me donnant ma première charge de cours pour le cours Équations Différentielles.

Il n'aurait pas été possible que j'entame ma maitrise avec mes cheveux et sans tic nerveux sans le support et l'aide de mes collègues Nicolas Teyssedou et Darren Hall. Je ne peux compter le nombre de soirées et nuits que nous avons passées à l'université à travailler sur nos devoirs, laboratoires et projets tout en discutant de science en général. Merci d'avoir partagé votre passion avec moi.

Je remercie mes collègues David Lalonde et William Tsé pour leur support quotidien ainsi que leur flexibilité face à ma situation.

Je remercie mes parents, Serge et Suzanne pour leur encouragement et leur soutient financier et moral.

Finalement je remercie ma femme, Jennifer qui m'a soutenu à travers mes études depuis maintenant plus de 8 ans. Merci Jen.

RESUME

L'objectif principal de ce mémoire est d'étudier les systèmes d'Équations Différentielles et Algébriques (EDA) qui apparaissent lors de la modélisation numérique d'équipements électriques supraconducteurs à Haute Température Critique (HTC). Ces systèmes d'équations ainsi que le comportement non linéaire des matériaux supraconducteurs sont possiblement responsables des difficultés rencontrées lors de simulations numériques de ces appareillages. Dans la littérature, beaucoup d'attention a été portée aux problèmes liés à la nonlinéarité des matériaux, mais, au meilleur de notre connaissance, aucune étude des systèmes d'équations différentielles et algébriques n'a été répertoriée. Ainsi, il est essentiel d'approfondir nos connaissances à leur sujet dans le cadre de la simulation numérique d'équipements supraconducteurs à HTC.

Dans ce document, nous présentons une revue de la théorie des supraconducteurs de type I et de type II. Cette revue nous permet de bien comprendre le potentiel des supraconducteurs à HTC en électrotechnique. Ces derniers se démarquent notamment par leur capacité à opérer en fort champ et par leur température critique élevée. Nous discutons que la simulation numérique d'équipements supraconducteurs permet de les optimiser à faible coût en améliorant certaines caractéristiques d'opération tel que les pertes en courant alternatif.

Ensuite, nous présentons les principaux modèles physiques utilisés pour modéliser les équipements supraconducteurs. Plus précisément, nous décrivons un modèle 1-D utilisant une formulation en flux magnétique. Ce modèle est relativement simple mais son équation aux dérivées partielles possède une solution analytique connue. Ce modèle est donc utile pour s'introduire à la discipline et vérifier une méthode numérique implémentée dans un code. Puis, nous présentons des modèles 2-D et 3-D qui utilisent la formulation en champs magnétique. Ces modèles sont une meilleure approximation de la réalité que le modèle 1-D. Ils peuvent notamment considérer des matériaux de différentes natures et géométries. Cependant, ils sont plus complexes. Finalement, nous présentons un modèle qui utilise la formulation en potentiel vecteur magnétique sous sa forme intégrale. Ce modèle peut tenir compte d'effets 3-D en utilisant la bonne définition pour l'intégrale du potentiel vecteur.

Nous présentons deux méthodes numériques pour discrétiser les équations des modèles physiques dans l'espace, soit la Méthode des Éléments Finis (MEF) et la Méthode Semi-Analytique (MSA). Nous montrons que la MEF est utilisée pour discrétiser une forme faible des équations à l'aide d'une approximation discrète de la solution sur un maillage constitué d'éléments. Nous introduisons deux types d'éléments: les éléments finis nodaux et les éléments d'arrête (edge elements). Finalement, nous présentons brièvement la MSA qui est

utilisée pour discrétiser dans l'espace les équations de la formulation en potentiel vecteur magnétique sous sa forme intégrale. Cette méthode consiste à trouver une expression analytique reliant des champs et des potentiels aux termes sources sur une certaine discrétisation puis à résoudre le système d'équations résultant numériquement. Il s'agit d'une méthode à collocation par point.

Ensuite, nous introduisons les systèmes d'EDA. Ces systèmes d'équations sont obtenus après avoir discrétisé les équations des modèles physiques dans l'espace. Nous mentionnons que la structure mathématique d'un système d'EDA peut-être décrite par l'index. L'index est le nombre de dérivées nécessaires pour qu'un système d'EDA devienne un système d'Équations Différentielles Ordinaires (EDO). Il existe une structure de système d'EDA particulière qu'on retrouve souvent dans les problèmes variationnels. Il s'agit du système d'EDA d'index 2 de forme Hessenberg.

Nous décrivons quelques stratégies pour discrétiser les systèmes d'EDA. Nous montrons que nous pouvons les discrétiser principalement de trois façons, soit par discrétisation directe, par réduction d'index ou en reformulant un système d'index 0 en forme semi-explicite. La méthode de discrétisation directe consiste à appliquer directement une méthode numérique implicite au système d'équations, sans réduire son ordre. Dans la plupart des cas, une telle opération mène à un système d'équations nonlinéaires. La réduction d'index consiste à réduire l'index du système et à réévaluer sa structure. Nous pouvons aussi écrire les systèmes d'EDA d'index 0 sous forme semi-explicite pour ensuite appliquer une méthode explicite. Nous introduisons deux solveurs temporels, i.e. *Differential-Algebraic System SoLver* (DASSL) et *Implicit Differential-Algebraic Solver* (IDAS). Ces solveurs utilisent la stratégie de discrétisation directe.

Ensuite, nous étudions les systèmes d'EDA obtenus lors de la modélisation numérique de supraconducteurs à HTC avec la MEF pour un modèle physique en 1-D. Nous documentons comment discrétiser les équations pour obtenir les systèmes d'EDA. En fonction de la façon dont les conditions frontières sont appliquées, l'index du système peut être 0 ou 1. Nous recommandons de résoudre les systèmes d'EDA d'index 0 et 1 par discrétisation directe. Ensuite, nous vérifions un code que nous avons développé dans le cadre de ce projet en comparant les approximations obtenues avec une solution analytique. La stratégie de discrétisation directe est implémentée dans le code et aucun problème n'a été répertorié lors du calcul des approximations. Nous concluons que la stratégie de discrétisation directe fonctionne pour un problème typique de modélisation d'équipements supraconducteurs à HTC en 1-D.

Dans la même lignée, nous étudions les systèmes d'EDA obtenus lors de la modélisation numérique de supraconducteur à HTC en 2-D en utilisant une MEF basée sur des éléments

d'arrête. Nous écrivons comment appliquer la MEF pour obtenir les systèmes d'EDA. En fonction des conditions frontières, le système d'équations résultant peut être d'index 0 ou de forme Hessenberg d'index 2. Ensuite, nous proposons des stratégies pour résoudre les systèmes d'EDA. Pour le système d'index 2, nous ne pouvons conclure si il est mieux de le discrétiser directement ou de réduire son index. Nous remarquons que la réduction d'index de 2 à 1 nous permet d'obtenir directement un système d'EDO mais qu'il faut inverser une matrice. Enfin, nous vérifions un code développé pour ce projet en comparant les résultats obtenus avec des solutions analytiques linéaires. La stratégie de discrétisation directe est implémenté dans le code à travers le solveur IDAS et fonctionne pour les problèmes considérés. Le code donne de bonnes approximations aux solutions, excepté aux endroits où les solutions ne sont pas linéaires. On peut améliorer les approximations à ces endroits en raffinant le maillage.

Finalement, nous étudions les systèmes d'EDA obtenus lors de la modélisation numérique de supraconducteurs à HTC en utilisant la MSA. Si le problème à l'étude utilise une source de tension comme source d'énergie, le système d'EDA résultant est d'index 0. Si le problème utilise une source de courant, il est d'index 2 et de forme Hessenberg. Nous notons que ce système d'EDA est semblable à celui obtenu avec la MEF en utilisant des éléments d'arrête et ainsi, les mêmes stratégies de discrétisation peuvent être appliquées. Enfin, nous analysons deux stratégies pour discrétiser un système d'EDA d'index 2 de forme Hessenberg simple: la stratégie de discrétisation directe et la stratégie de réduction d'index. Pour les deux stratégies, nous obtenons les ordres de convergence prédits pour les méthodes numériques utilisées. Cependant, nous notons que la méthode de réduction d'index est moins directe que celle de discrétisation directe et qu'elle est plus risquée puisqu'il faut que les conditions initiales satisfassent l'équation algébrique et sa dérivée. Pour cette analyse, nous utilisons une solution manufacturée.

ABSTRACT

The main objective of this thesis is to study the systems of Differential-Algebraic Equations (DAE) encountered in the numerical modeling of electrical devices made of High-Temperature Superconductors (HTS). These systems of equations and the nonlinear behavior of HTS are possibly responsible for the difficulties faced when simulating HTS devices. In the literature, much attention is paid to the issues related to the nonlinearity of HTS but, to the best of our knowledge, there is no in-depth study of the problems related to the systems of DAE. Consequently, it is essential to improve our knowledge about those systems, in the context of HTS modeling.

In this document, we review the theory of type I and type II superconductors. This review is useful to understand the potential of HTS materials for power engineering applications. Their potential is mainly due to their ability to operate in strong fields and their high critical temperatures. We discuss that numerical simulation can be used to optimize HTS devices at low cost, by improving some quantities of interest, e.g. AC losses.

We introduce the main physical models used for the modeling of HTS devices. We describe a 1-D model based on a magnetic flux density formulation. This model is relatively simple but has a known analytical solution for a nonlinear HTS problem. It is convenient to use as an introduction to the methodology used in this thesis and to verify a code. Then, we introduce a 2-D and a 3-D model based on a magnetic field formulation. These models provide a better representation of the reality than the 1-D model. They can consider materials with different properties and complex geometries. However, they are more complicated than the 1-D model. Finally, we review a model based on a magnetic vector potential formulation in integral form $(\boldsymbol{A} - V)$. This model can take into account 3-D effects by using the proper definition for the magnetic vector potential integral.

We summarize two numerical methods to discretize the equations of the physical models in space, i.e. the Finite Element Method (FEM) and the Semi-Analytical Method (SAM). The FEM is used to discretize a weak form of the equations of the models using a discrete approximation of the solution over a mesh made of geometrical elements. We introduce two types of elements: nodal elements and edge elements. Then, we review the SAM, a numerical method used to discretize the equations of the magnetic vector potential formulation in integral form. It is a collocation method.

We introduce systems of DAE. These systems of equations are obtained after discretizing the equations of the physical models in space. We discuss that the mathematical structure of a system of DAE can be described by a notion called the index. The index is the number

of derivation required for a system of DAE to become a system of Ordinary Differential Equations (ODEs). We note that systems of DAE of index 2 in Hessenberg form are recurrent in variational problems.

Subsequently, we discuss three strategies to discretize systems of DAE in time, i.e. direct discretization, reduction of the index and reformulation into semi-explicit form. The direct discretization strategy consists in applying directly an implicit time integration scheme to a system of DAE without reducing its index. In most cases, this yields a system of nonlinear equations. The reduction of index consists in reducing the index of the system of DAE and then reassess its structure. Systems of DAE of index 0 can be reformulated into a semi-explicit form and then discretized using an explicit method. We introduce two time transient solvers that use the direct discretization strategy, i.e. *Differential-Algebraic System SoLver* (DASSL) and *Implicit Differential-Algebraic Solver* (IDAS).

We study the systems of DAE encountered in the numerical modeling of HTS devices using the FEM with a 1-D model. We document how to discretize the equations of the model in space to obtain a system of DAE. Depending on how the boundary conditions are enforced, the system of DAE can be of index 0 or 1. We suggest to discretize the systems of DAE of index 0 and 1 directly. We verify the code developed for this research work against an analytical solution to a nonlinear problem. The code uses the IDAS library and consequently, the direct discretization strategy. We show that this strategy works for both the system of DAE of index 0 and 1.

Similarly, we study the systems of DAE encountered in the numerical modeling of HTS devices using the FEM with edge elements for a 2-D model. We give the discretization of the equations in space and identify the resulting system of DAE. Depending on the boundary conditions, the resulting system of DAE can be of index 0 or 2 in Hessenberg form. For the system of DAE of index 2, we cannot conclude if it is better to discretize it directly or to reduce its index. We note that reducing the index from 2 to 1 yields a system of ODEs for the Degrees Of Freedom (DOFs) of interest but that a matrix needs to be inverted. We verify the code develop for this project against two analytical solutions for three different problems. The strategy of direct discretization is implemented in the code through the IDAS library. There are no difficulties reported when computing the approximations with the direct discretization strategy. Therefore, this strategy works for the problems considered. We show that the code gives good approximations for all the problems implemented, except where the solution is not linear. The approximations get better when the mesh is refined.

In conclusion, we study the systems of DAE encountered in the numerical modeling of HTS using the SAM. We summarize how to discretize the equation of the $\boldsymbol{A} - V$ formulation with this method. For a voltage driven problem, the SAM yields a system of DAE of index

0. For a current driven problem, the SAM gives a system of DAE of index 2 in Hessenberg form. We note that this system of DAE is similar to the one obtained using the FEM with edge elements in 2-D and as a result, the same strategies to discretize the system of DAE can be applied. Finally, we study two strategies to discretize a simple system of DAE of index 2 in Hessenberg form, i.e. the direct discretization and the reduction of the index. We report that the reduction of index is less straightforward than the direct discretization. It is also more risky because the initial conditions need to satisfy both the algebraic equation and its time derivative. We use a manufactured solution to study those strategies.

TABLE OF CONTENTS

LIST OF TABLES

LIST OF FIGURES

LIST OF APPENDICES

LIST OF ACRONYMS AND ABBREVIATIONS

HTS   High-Temperature Superconductors

LTS   Low-Temperature Superconductors

T_c Critical Temperature

H_c Critical Magnetic Field Strenght

B_c Critical Magnetic Flux Density

DC   Direct Current

AC   Alternating Current

YBCO   Ytrium Barium Copper Oxide

BSCCO Bismuth Strontium Calcium Copper Oxide

DAE   Differential-Algebraic Equations

ODE   Ordinary Differential Equation

PDE   Partial Differential Equation

DOF   Degree Of Freedom

FEM   Finite Element Method

SAM   Semi-Analytical Method

BDF   Backward Differentiation Formula

CHAPTER 1

INTRODUCTION

1.1 Problematics and Objectives

Superconducting materials with high critical temperatures represent a technological avenue of choice for solving important problems experienced in modern power systems. However, the superconducting equipments used in power engineering are still being developed, and the associated experiments are expensive. Therefore, it is important to first improve the geometry of the superconducting devices using numerical simulations. However, the challenges related to the highly nonlinear behavior of superconducting materials and the need to solve systems of differential-algebraic equations (DAE) in time are such that the use of free or expensive commercial software is often ill-suited for the task. When the simulations are possible, the long calculation times are not reasonable for device enhancement.

As a result, it is common in the modeling community to develop their own codes specifically designed to deal with the problems encountered in the numerical modeling of high-temperature superconductors (HTS). However, these codes are generally badly documented and focus on solving the problems associated with the nonlinear behavior of HTS, and not on the systems of DAE. Furthermore, to the best of our knowledge, systems of DAE have never been studied in the context of HTS modeling.

The main objective of this project is to *study the systems of DAE encountered in the numerical modeling of HTS devices.* The specific objectives of this thesis are as follows:

- *Show that numerical methods used for the discretization in space of HTS problems lead to systems of DAE;*

- *Identify the structures and indexes of the resulting systems of DAE;*

- *Give strategies to discretize the systems of DAE in time;*

- *Model problems based on the implementation of various numerical strategies for the discretization in space and time of DAE.*

1.2 Structure of The Thesis

In chapters 2 to 6, we introduce the concepts needed to achieve the objectives of this thesis. More precisely, in chapter 2, we introduce type I and type II superconductivity.

Then, in chapter 3, we give the main physical models used to study HTS devices. First, we give a 1-D model based on a magnetic flux density formulation. Then, we describe a 2-D and a 3-D model based on a magnetic field formulation. We finally review a model based on a magnetic vector potential formulation in integral form. In chapter 4, we introduce two numerical methods used to discretized the equations of the physical models in space, i.e. the Finite Element Method (FEM) and the Semi-Analytical Method (SAM). With both methods, the discretization of the equations leads to systems of DAE. In chapter 5, we introduce these systems, the notion of index and systems of DAE in Hessenberg form. In chapter 6, we propose some strategies to discretize systems of DAE in time.

Then, in chapters 7 to 9, we apply the concepts introduced in the previous chapters of the thesis to three different problems:

- Discretization of HTS problems using nodal finite elements in 1-D;

- Discretization of HTS problems using edge elements in 2-D;

- Discretization of HTS problems using the SAM.

We show typical HTS device problems and propose models to discretize them. We discretize the equations of the models in space using either the FEM or the SAM. In all cases, the spatial discretization leads to systems of DAE. These systems are identified and we propose strategies to discretize them in time. In chapters 7 and chapter 8, we verify the codes developed for this project against analytical solutions. In chapter 9, we investigate some of the proposed strategies with a simple problem with a manufactured solution. Note that in this research work, we use the power law to model the resistivity of HTS because it is widely used by the HTS modeling community.

CHAPTER 2

SUPERCONDUCTIVITY

This chapter introduces the physics of superconductor. It is divided in four sections. In section 2.1, we review concepts related to type I superconductivity. In section 2.2, we extend those concepts and introduce new ones to cover type II superconductivity. In section 2.3, we introduce high temperature superconductors (HTS) and a model that is widely used to represent their $E - J$ characteristics, the power law. Finally, in section 2.4, we discuss some quantities of interest that require optimization to enhance HTS devices. The concepts reported herein are general and come from multiple references: [1], [2], [7], [8], [9] and [10].

2.1 Type I Superconductivity

2.1.1 Electrical Resistance and the Thermodynamic Variables T_c, H_c and J_c

Let us consider a metal with a crystalline lattice containing a certain amount of impurities. At a temperature higher than $0\,\text{K}$, the atoms of this metal are vibrating with a given amplitude and frequency. Conductive electrons carrying a current in such a structure experience resistance due to the vibration of the lattice and the presence of impurities.

When the temperature is lowered, the vibrations of the lattice become less important and the electrons can flow more easily. At $0\,\text{K}$, the lattice doesn't vibrate and the only resistance to the flow of current is the presence of impurities in the crystal. Therefore, in a perfect crystal without impurities at $0\,\text{K}$, the resistivity is expected to be $0\,\Omega\text{m}$. These two scenarios are depicted in Figure 2.1.

In 1911, Karlingh Onnes observed that this is not the case for all metals [1]. When some metals are cooled to very low temperatures, their resistivity suddenly drops to $0\,\Omega\text{m}$, even for metals with impurities, as shown in Figure 2.2. This is the *critical temperature* T_c. Below this temperature, the metal is said to be a *superconductor* or in a *superconducting state.*

About half of the metals of the periodic table of elements are known to be superconductors below a certain temperature. There is also a good amount of alloys that share the same properties, even if some of these are composed of non-superconducting metals.

For metallic elements, alloys, and metallic compounds, T_c is low. It is below $10\,\text{K}$ for metallic elements and below $39\,\text{K}$ for metallic compounds and alloys[1]. This is why we refer to these superconductors as *Low-Temperature Superconductors* (LTS).

---

[1]The binary compound MgB_2 has a critical temperature of 39 K.
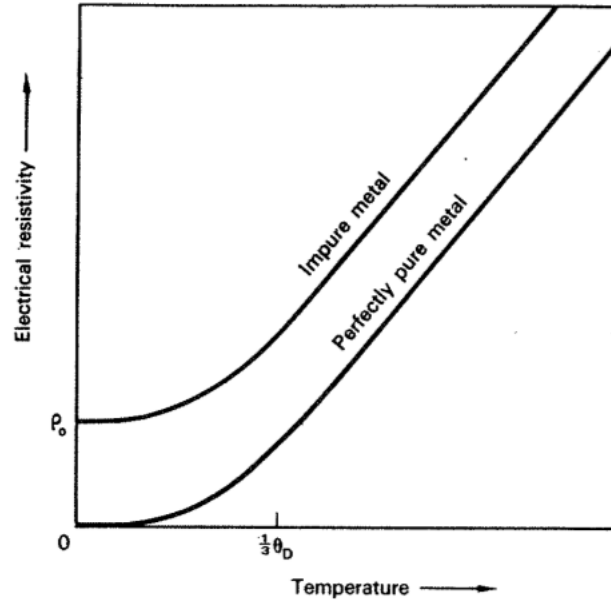
Figure 2.1 Expected resistivity as a function of the temperature for impure and pure metals. (Source of figure: [1])
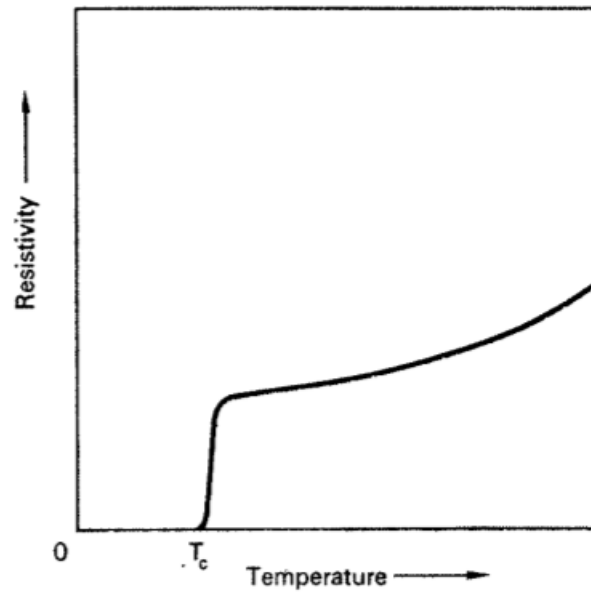
Figure 2.2 Resistivity as a function of the temperature for superconductors. We see that the resistivity drops to $0\,\Omega$m when the temperature reaches T_c. (Source of figure: [1])

When cooled below the critical temperature T_c, two other thermodynamic variables can cause a superconductor to return to its normal state, i.e. the critical field H_c and the critical current density J_c. If a superconductor is subjected to a magnetic field that is larger than H_c, it will transition back to its normal state. The same scenario will occur if it carries a current that is larger than its critical current. In the literature, the critical field is often written in terms of the critical magnetic flux density B_c, because of its physical significance.

The three thermodynamic variables, T_c, H_c and J_c all depend on each other and therefore, the transition between the normal and the superconducting state can be represented by a critical surface in the $J - H - T$ (or $J - B - T$) phase diagram, as shown in Figure 2.3.

2.1.2   The Meissner Effect

Another unique property of type I superconductors is called the *Meissner effect*, discovered by Walther Meissner and Robert Ochsenfeld in 1933 [1]. The Meissner effect is the ability of a type I superconductor to expel the magnetic flux density out of its volume, i.e. to exhibit *perfect diamagnetism*. Therefore, inside such a material, we always have

$$B = 0. \tag{2.1}$$

The perfect diamagnetism that results from the Meissner effect is a property that is
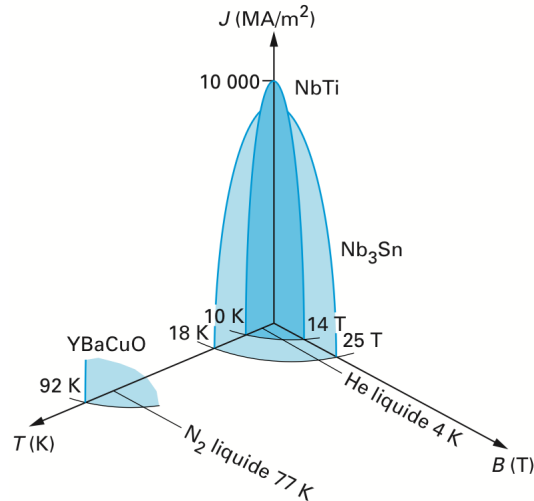
Figure 2.3 Critical surfaces (shaded) for various materials. These surfaces separate the normal and the superconducting states as a function of the thermodynamic variables $J - B - T$. Note that the YBaCuO exhibits type II superconductivity. Type II superconductors are discussed in section 2.2. (Source of figure: [2])

unique to superconductors since this is not the expected scenario for 'perfect conductors', i.e. a material without resistivity such as a pure metal that is not in a superconducting state at $0\,\mathrm{K}$.

Let us consider the resistanceless closed circuit shown in Figure 2.4 a). In this figure, we see that the total amount of flux passing through the resistanceless ring is given by $\Phi = AB_a$ where A is the area enclosed by the ring and B_a is the applied field. According to Faraday's law of induction, the equation that governs this circuit is given by

$$-A\frac{dB_a}{dt} = Ri + L\frac{di}{dt},$$

(2.2)

where R is the resistance of the circuit, i is the current and L is the inductance. Since the ring has no electrical resistance, we have $R = 0$, which yields

$$\frac{d}{dt}(AB_a + Li) = 0.$$

(2.3)

This means that the total flux passing through the ring *does not vary with time.* If we change the amplitude of the applied flux density B_a, the current i will compensate so that the total flux is always constant. This is depicted in Figure 2.4 b).

Let us now consider a bulk specimen such as the one shown in Figure 2.5. When cooled, this specimen becomes resistanceless, i.e. a perfect conductor. As discussed above, the magnetic flux passing through any closed path within this specimen is always constant. If the
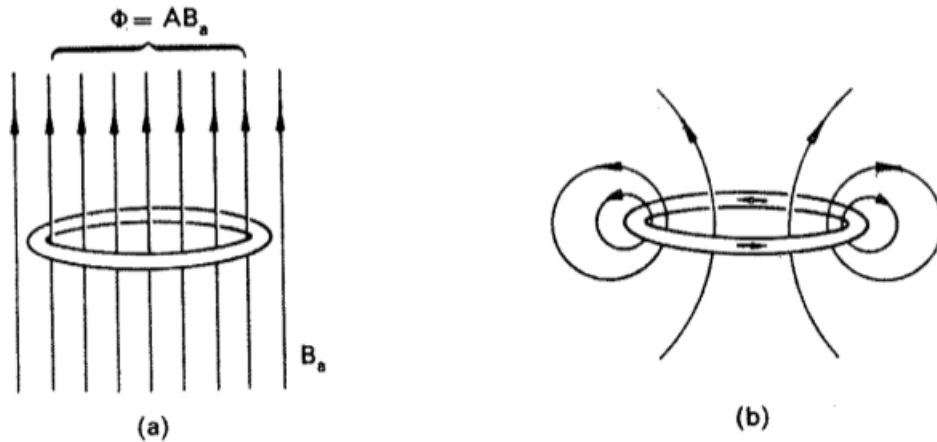
Figure 2.4 a) Resistanceless closed circuit subjected to an applied magnetic flux $\Phi = AB_a$ and no initial current. b) When the applied field is removed, a current flows in the ring to keep the flux constant. (Source of figure: [1])

specimen is cooled in the absence of a field, the net magnetic flux passing through it is always zero, even if a field is applied afterwards. This is shown in Figure 2.5 a), b), c) and d). If the specimen is cooled in the presence of a field B_a, the internal flux distribution will not be zero and it will remain constant even if we remove that field thereafter (see Figure 2.5 e), f) and g)). Therefore, the magnetic flux inside a resistanceless conductor depends on the sequence of application of the magnetic field.

For a superconductor, this is not the case. Independently of the sequence of application of the magnetic field, it is always zero inside, as shown in Figure 2.6.

2.1.3   Electrodynamics of Type I Superconductivity

In a superconductor, only a certain portion of the electrons carry the resistanceless current, i.e. the *superelectrons*. The others remain normal electrons and behave accordingly. The ratio of normal electrons is higher when the temperature of the superconductor is close to T_c and goes to zero when the temperature approaches $0\,\mathrm{K}$. This model that describes the currents observed in superconductors is known as the *two-fluid model*.
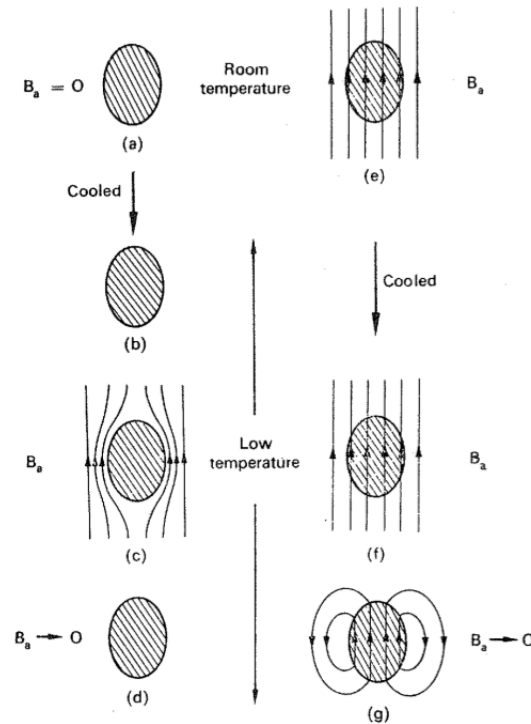
Figure 2.5 The magnetic field inside a resistanceless conductor is always constant. Therefore, the magnetic flux distribution inside the material *depends* on the sequence of application of the magnetic field. (Source of figure: [1])
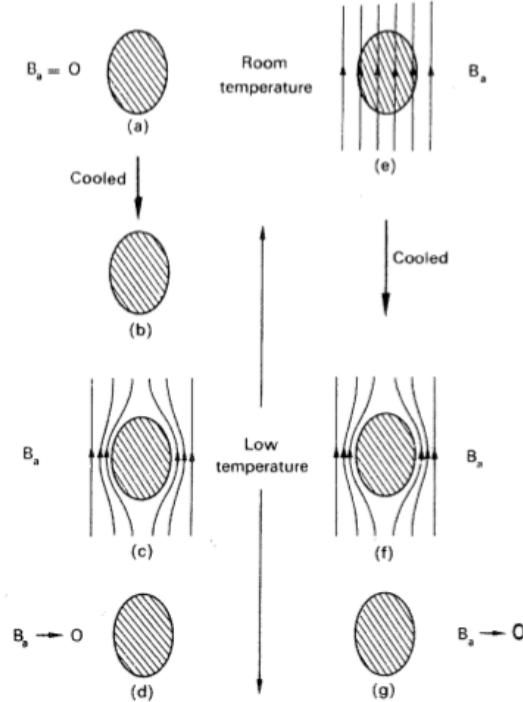
Figure 2.6 The magnetic field inside a superconductor is always zero. Therefore the magnetic flux distribution inside the material *does not depend* on the sequence of application of the magnetic field. (Source of figure: [1])

The superelectrons are normal electrons that gained the ability to carry current without resistance by pairing each other to form *Cooper pairs*. The concept of Cooper pairs is explained by the *Bardeen-Cooper-Schrieffer* (BCS) theory, which is out of the scope of this project. The interested reader is referred to [1] and [8] for a thorough introduction.

For the two-fluid model, the current density is defined by

$$\boldsymbol{J} = \boldsymbol{J}_s + \boldsymbol{J}_n, \tag{2.4}$$

where $\boldsymbol{J}_s$ and $\boldsymbol{J}_n$ are the current densities due to the superelectrons and to the normal electrons, respectively. All of these electrons obey Maxwell's equations, however, some restrictions need to be applied so that they predict the proper observed behaviors, i.e. the absence of resistance and the Meissner effect.

For the normal electrons, subjected to resistivity ρ_n, we use the linear $E - J$ characteristic:

$$\boldsymbol{E} = \rho_n \boldsymbol{J}_n. \tag{2.5}$$

For the superelectrons, this does not apply since there is an electric field $\boldsymbol{E}$ that is nonzero,

even if $\rho_s = 0\,\Omega\text{m}$. This is why we need to add an equation to Maxwell's equations to take into account the fact that superconductors are resistanceless. This equation is the first *London equation*

$$\frac{\partial \boldsymbol{J}_s}{\partial t} = -\frac{1}{\mu_0 \lambda_L^2} \boldsymbol{E}, \tag{2.6}$$

where λ_L, the *London penetration depth*, is explained below. This equation describes two important behaviors of superconductors:

1. A Direct Current (DC) can exist in a superconductor in the absence of an electric field. In this case, there is absolutely no loss in the superconductor.

2. If an Alternating Current (AC) is applied to a superconductor, there will be an electric field and as a result, losses. These losses are very small at low frequencies but can be large at high frequencies ($\gtrsim 10^{11}\,\text{Hz}$).

As mentioned earlier, superconductors act as perfect diamagnetic materials due to the Meissner effect. When a magnetic field is applied to type I superconductors, there are screening currents that circulate at their surfaces in a very thin layer. These currents create a field that is equal and in the opposite direction to the applied field. As a result, the magnetic flux density inside the superconductors is zero. The thickness of the layer where the surface currents circulate can be approximated by the London penetration depth λ_L, which can be computed using the second London equation

$$\nabla \times \boldsymbol{J}_s = -\frac{1}{\mu_0 \lambda^2} \boldsymbol{B}. \tag{2.7}$$

The London penetration depth λ_L is about $10^{-8}\,\text{m}$. This is a fair approximation since experimentally, it has been observed that the penetration depth is at least twice this length. Therefore, the London theory is good for a first approximation but has some limits. A more refined theory called the *Ginzburg-Landau Theory* predicts a penetration depth that is more accurate. However, this theory is out of the scope of this project.

2.2 Type II Superconductivity

In 1957, Alexei A. Abrikosov [1] suggested that a second category of superconductors with different inherent features could exist. Today, this second category is known as *type II superconductivity*.

2.2.1 The Differences Between Type I and Type II Superconductivity

For a type I superconductor, the energy released (free energy) when a superconducting and normal interface is created, is positive. Therefore, such interfaces are not energetically favorable for the material and they are minimized. As a result, the Meissner effect is observed for all applied fields that are less than H_c.

For a type II superconductor, it is the opposite: when the strength of the applied field is larger than a *lower critical field* H_{c1}, such that $H_{c1} < H_c$, the free energy released when normal and superconducting interfaces are created is negative. Therefore, it becomes advantageous for the superconductor to create those interfaces. As a result, small cylindrical normal regions parallel to the applied field begin to form inside the superconductor. These cylindrical normal regions are called *normal cores* and they form the most energetically favorable configuration. With these normal regions inside the superconductor, it is said to be in a *mixed state*.

As those normal cores progressively form, magnetic flux density lines, called *fluxons*, enter those areas. A fluxon is a quantum of magnetic flux and is given by $\Phi_0 = 2.07 \cdot 10^{-15}$ Wb.

Since the superconducting regions of the material are still perfectly diamagnetic, there are screening currents that circulate around the fluxons to expulse the magnetic flux out of those regions. The combination of a fluxon with the screening current around it is called a *vortex* and the final configuration of the material is called the *fluxon lattice*, as shown in Figure 2.7. The superconductor remains in the mixed state until the applied field strength reaches the *critical upper field* H_{c2}, with $H_{c2} \gg H_c$. At fields beyond H_{c2}, the superconductor returns to
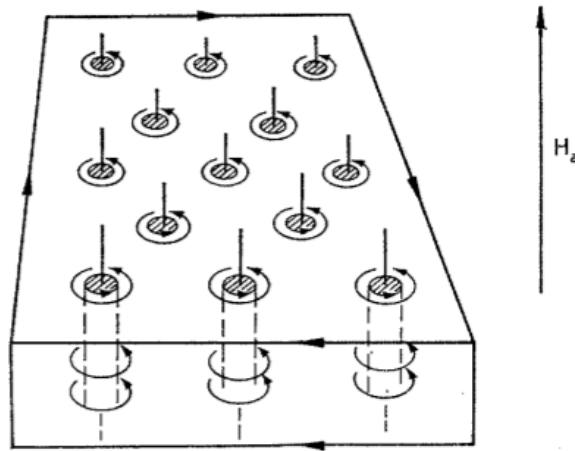
Figure 2.7 Fluxon lattice of a type II superconductor in the mixed state. The current circulating around the fluxons helps in maintaining the perfect diamagnetism of the superconducting regions. (Source of figure: [1])

its normal state.

As a result, for type II superconductors, the *Meissner effect is not observed* for magnetic field strengths that are between $H_{c1} < H < H_{c2}$. However, since their upper critical field is much higher than the critical field of type I superconductors, they are useful for high field applications such as power engineering devices and high field magnets.

2.2.2 Flux Pinning, the Critical State and Flux Flow

When a transport current $\boldsymbol{J}_T$ is applied to a type II superconductor, there is a resulting force called the *Lorenz force* that applies to the vortices in the lattice. This force is defined as

$$\boldsymbol{F}_L = \boldsymbol{J} \times \boldsymbol{\Phi}_0. \tag{2.8}$$

If nothing holds the vortices in place, they start to move under the influence of this force. However, in reality, there are impurities and irregularities in the crystal lattice of the superconductors. This results in a force that is equal and in the opposite direction to the Lorentz force and helps to keep the vortices in place. This force is called the *pinning force* $\boldsymbol{F}_p$. As long as the magnitude of the pinning force is larger than the magnitude of the Lorentz force ($F_{pmax} > F_L$), the vortices do not move and the current circulates according to the London equations discussed previously.

When the equilibrium between the magnitude of the two forces is reached, $F_L = F_{pmax}$, the superconductor is said to be in the *critical state*. The current needed to reach this state is called the *critical current* J_c. Beyond this current, the Lorentz force is larger than the pinning force and the vortices start to move in the superconductor; it is in the *flux flow* regime.

The vortices move with velocity $\boldsymbol{v}$ and generate an electric field according to

$$\boldsymbol{E} = \boldsymbol{B} \times \boldsymbol{v}, \tag{2.9}$$

which means that there is also a local power dissipation

$$p = \boldsymbol{J} \cdot \boldsymbol{E}. \tag{2.10}$$

Therefore, the superconductor is not a lossless conductor anymore.

Since there is an electric field in the superconductor, the London equations can be superseded by an appropriate $E - J$ characteristic. For LTS, we use the *flux flow model*:

$$\boldsymbol{E} = \rho_{ff}(\boldsymbol{J} - J_c), \tag{2.11}$$

where ρ_{ff} is a resistivity related to the viscous force that opposes to the motion of the vortices.

Generally, for power engineering applications, LTS are not economically viable because of the cooling costs. This is why HTS are generally used for this type of applications. They, however, exhibit a different $E - J$ characteristic, which we describe in the next section.

2.3 High-Temperature Superconductors (HTS)

HTS are type II superconductors that have a critical temperature that is higher than $77\,K$. Therefore, they can be cooled using *liquid nitrogen*, a low cost coolant compared to the ones needed for LTS, e.g. liquid helium.

Due to their high T_c and because they can operate in large magnetic fields ($H_{c2} >> H_c$), they are promising for power engineering applications. Typical HTS are made of Yttrium Barium Copper Oxide ($YBCO$) and Bismuth Strontium Calcium Copper Oxide ($BSCCO$) with specific stoichiometry.

Seeing that HTS operate at high temperatures, their $E - J$ characteristic is affected by thermal effects and unfortunately, the flux flow model cannot be used. Instead, it is common to use the *power law model* [7]:

$$\rho(\boldsymbol{J}) = \frac{E_c}{J_c} \left(\frac{||\boldsymbol{J}||_2}{J_c} \right)^{n-1} , \tag{2.12}$$

where n is an exponent related to the material, usually between 20 and 50, and typically $E_c = 10^{-4}\,\text{V/m}$, a criterion used to define J_c.

For HTS, the critical current density J_c depends on the magnetic flux B and the temperature T. These dependencies could be taken into account in the power law by using the appropriate model for J_c such as the Kim model [11] which is not described in this document.

2.4 Quantities of Interest for HTS Devices

As discussed in section 2.2.2, type II superconductors, and therefore HTS, can exhibit losses if the current density flowing in them is large enough for the vortices to move and create an electric field. These losses generate heat that needs to be extracted from the system to keep the superconductor below its critical temperature. As a result, one of the objectives of the numerical modeling of HTS is to compute these losses, often called the AC *losses*, in order to minimize them. The optimization parameters are generally the geometry of the device, the material, and the nominal conditions of operation. Other quantities of interest are:

- The magnetic/electric field distribution, its amplitude and its orientation;

- The current density distribution, its amplitude and its orientation;

- The normal zone propagation velocity;

- etc...

CHAPTER 3

MODELING OF HTS DEVICES

We now introduce physical models used to model HTS devices. This chapter is divided into two sections. First, in section 3.1, we describe models based on the H-field formulation in 1-D, 2-D and 3-D. In section 3.2, we report a 2-D general model based on the magnetic vector potential formulation ($\boldsymbol{A} - V$) in integral form. The $\boldsymbol{A} - V$ formulation in integral form is also known as the Integral Equations (IE) formulation.

For the HTS models introduced in this chapter, we propose to use the power law for the $E - J$ characteristic. Note that this is not a restriction and other $E - J$ models can be used as well. For the remainder of this document, $\hat{\boldsymbol{i}}$, $\hat{\boldsymbol{j}}$ and $\hat{\boldsymbol{k}}$ are the unit vectors along the x, y and z axes respectively of a 3-D Cartesian coordinate system.

3.1 Modeling of HTS Devices Using the H-field Formulation

In this section, the 1-D model is written in terms of the magnetic flux density $\boldsymbol{B}$ (the dependent variable) in accordance with the notation used in the literature. For the same reason, the 2-D and 3-D models are written in terms of the magnetic field strength, $\boldsymbol{H}$. Either way, when modeling HTS, we usually assume that $\boldsymbol{B} = \mu_0 \boldsymbol{H}$, which is accurate as long as the local field $B \gg B_{c1}$, typically a few mT at most.

3.1.1 1-D Model: Infinite Slab

This model is used to compute the diffusion of the magnetic flux density as a function of time and depth in a 1-D HTS slab, using Dirichlet boundary conditions as illustrated in Figure 3.1. The main reference used for the description of this model is [3]. For convenience, since $\boldsymbol{B}(x,t) = B_y(x,t)\hat{\boldsymbol{j}}$, we use $B_y(x,t) = B(x,t)$.

The Partial Differential Equation (PDE) to solve for the flux diffusion is

$$-\frac{\partial}{\partial x}\left[\frac{\rho(J)}{\mu_0}\frac{\partial B(x,t)}{\partial x}\right] + \frac{\partial B(x,t)}{\partial t} = 0, \tag{3.1}$$

with $x \in]-a, a[$, $t \in [0, \infty[$ and the initial conditions are

$$B(x,0) = B_0 \quad \text{and} \quad \dot{B}(x,0) = \dot{B}_0. \tag{3.2}$$
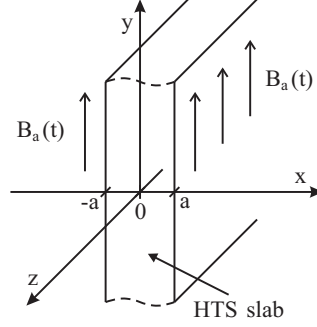
Figure 3.1 One-dimensional geometry used to compute the magnetic flux density across the width of a slab. (Source of figure: [3])

The Dirichlet boundary conditions are given by

$$B(-a, t) = B_a(t) \quad \text{and} \quad B(a, t) = B_a(t). \tag{3.3}$$

Finally, the constitutive equation for the $E - J$ characteristic can be modeled using the power law. For the 1-D case, we have

$$\rho(J) = \frac{E_c}{J_c} \left| \frac{J}{J_c} \right|^{n-1} \quad \text{where} \quad J = -\frac{1}{\mu_0} \frac{\partial B}{\partial x}. \tag{3.4}$$

The equations of this model can be solved analytically or discretized to be solved numerically. Both scenarios will be extensively reported in chapter 7 for a typical problem. The quantities of interest can then be analyzed either directly, e.g. for B and H, or by post-processing the results, e.g. for the AC losses and J.

3.1.2   2-D and 3-D Models

In this subsection, we generalize the 1-D model described above to 2-D and 3-D geometries. The references used for this subsection are [12] and [13].

Consider a 2-D domain Ω with k subdomains Ω_i, where $i = 1, ..., k$. A domain Ω with two subdomains Ω_1 and Ω_2 are shown in Figure 3.2. The domain Ω is in the $x - y$ plane in Cartesian coordinates. The 3-D domain and subdomains are not shown but they are similar to the 2-D case.

Over a domain Ω and for a time interval T, we want to solve:

$$\begin{cases} \mu \dfrac{\partial \boldsymbol{H}}{\partial t} + \nabla \times (\rho \nabla \times \boldsymbol{H}) = \boldsymbol{0}; \\ \nabla \cdot (\mu \boldsymbol{H}) = 0, \end{cases} \tag{3.5}$$
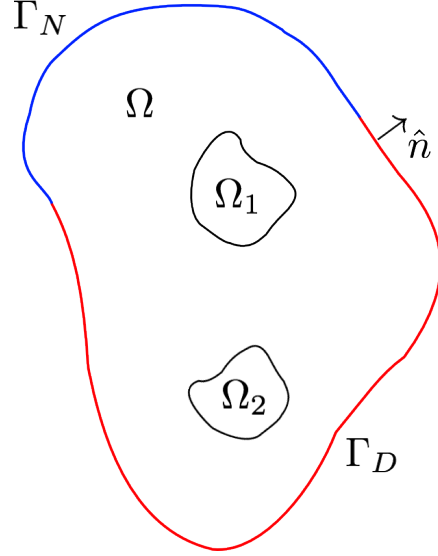
Figure 3.2 Two-dimensional domain Ω with subdomains Ω_1 and Ω_2. The domain is in the $x - y$ plane. Dirichlet boundary conditions are applied on the boundary Γ_D and Neumann boundary conditions are applied on the boundary Γ_N. The unit vector $\hat{\boldsymbol{n}}$ is the normal vector to the boundary of the domain Ω.

with the initial and boundary conditions:

$$
\begin{cases}
\boldsymbol{H}(\boldsymbol{x}, 0) = \boldsymbol{H}_0(\boldsymbol{x}); & \\
\hat{\boldsymbol{n}} \times \boldsymbol{H} = \boldsymbol{f} & \text{on} \quad \Gamma_D; \\
\hat{\boldsymbol{n}} \times (\rho \nabla \times \boldsymbol{H}) = \boldsymbol{g} & \text{on} \quad \Gamma_N.
\end{cases}
\tag{3.6}
$$

Different materials can be considered in the subdomains Ω_i, as in a HTS device, e.g. type II superconductors, insulating dielectrics and ferromagnetic materials. As a result, the definition of μ and ρ may or may not change for the different subdomains.

If the domain Ω or some of the subdomains Ω_i are HTS, we use $\mu = \mu_0$ for the permeability and the power law for the resistivity. For the 2-D and 3-D cases we have

$$
\rho(\boldsymbol{J}) = \frac{E_c}{J_c} \left(\frac{\|\boldsymbol{J}\|_2}{J_c} \right)^{n-1} \quad \text{where} \quad \boldsymbol{J} = \nabla \times \boldsymbol{H}.
\tag{3.7}
$$

For other materials, the proper permeability and resistivity need to be used.

For the 2-D model, we make the following assumptions:

1. The current density $\boldsymbol{J}$ is only flowing along the z-axis:

$$\boldsymbol{J} = J_z \hat{\boldsymbol{k}}. \tag{3.8}$$

2. The magnetic field component H_z is zero and therefore

$$\boldsymbol{H} = H_x \hat{\boldsymbol{i}} + H_y \hat{\boldsymbol{j}}. \tag{3.9}$$

Other assumptions can be made for the boundary conditions but they will depend on the specific geometry of the problem considered.

For the 3-D case, there are no assumptions to be made since the geometry of the model is closer to real-world problems. However, for a given problem, specific assumptions can be made on a case-by-case basis.

The boundary conditions can be used to apply an external magnetic field to the geometry of the model. A current can be imposed in the different subdomains Ω_i by adding current constraints to the set of equations (3.5):

$$I_{\Omega_i} = \int_{\Omega_i} \nabla \times \boldsymbol{H} \, d\Omega_i. \tag{3.10}$$

3.2 Modeling of HTS Devices Using the A-V Formulation in Integral Form

The *magnetic vector potential* formulation $(\boldsymbol{A} - V)$ in integral form, i.e. using the Biot-Savart law, has been widely used by the HTS modeling community. It was first introduced by Brandt (the Brandt Method) [14] for specific geometries and then generalized by Sirois with the Semi-Analytical Method (SAM) [6] for superconductors of arbitrary shapes.

Consider a 2-D domain Ω with k subdomains Ω_i, where $i = 1, ..., k$, such as the one shown in Figure 3.3 for $i = 1, 2$. Again, each Ω_i can represent different materials that are a part of a HTS device but with this model, ferromagnetic materials cannot be used; the permeability of all materials must be $\mu = \mu_0$.

We want to solve

$$\boldsymbol{E} = -\frac{\partial \boldsymbol{A}}{\partial t} - \nabla V \tag{3.11}$$

for the current density $\boldsymbol{J}$ on Ω using the constitutive relation

$$\boldsymbol{E} = \rho(\boldsymbol{J})\boldsymbol{J}, \tag{3.12}$$
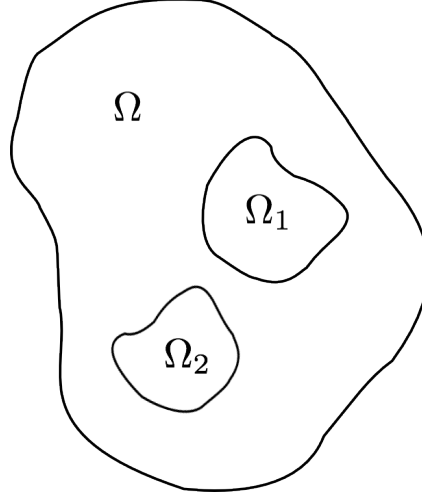
Figure 3.3 General 2-D domain Ω with subdomains Ω_1 and Ω_2. The domain is in the $x - y$ plane.

with the power law and where the magnetic vector potential is given by

$$\boldsymbol{A}(\boldsymbol{r}) = \frac{\mu_0}{4\pi} \int_\Omega \boldsymbol{J} \log |\boldsymbol{r} - \boldsymbol{r}'| \, d\Omega + \boldsymbol{A}_{ext}. \tag{3.13}$$

Here, $\boldsymbol{r} = x\hat{\boldsymbol{i}} + y\hat{\boldsymbol{j}}$ and $\boldsymbol{A}_{ext}$ is used to model an external magnetic field. In the case of an homogeneous and constant field $\boldsymbol{B}_{ext} = b_x\hat{\boldsymbol{x}} + b_v\hat{\boldsymbol{y}}$ in the $x - y$ plane, we have

$$\boldsymbol{A}_{ext}(x, y) = yb_x - xb_y. \tag{3.14}$$

The resulting equation in $\boldsymbol{J}$ is given by

$$\rho(\boldsymbol{J})\boldsymbol{J} = -\frac{\partial}{\partial t} \left[\frac{\mu_0}{4\pi} \int_\Omega \boldsymbol{J} \log |\boldsymbol{r} - \boldsymbol{r}'| \, d\Omega + \boldsymbol{A}_{ext} \right] - \nabla V. \tag{3.15}$$

The subdomains Ω_i can be conductors that are either driven by a current source or by a voltage source. For the subdomains that are driven by a current source, a current constraint expressed as a function of the current density $\boldsymbol{J}$ must be used in addition to equation (3.15), i.e.

$$I_{\Omega_i} = \int_{\Omega_i} \boldsymbol{J} d\Omega_i. \tag{3.16}$$

On those subdomains, the voltage V is constant in the $x - y$ plane and is an unknown of the problem. In the case where the conductors represented by the subdomains Ω_i are voltage driven, the voltage V on these subdomains are known and equation (3.15) only needs to be solved for $\boldsymbol{J}$.

Even if the model is 2-D, it can take into account 3-D effects by defining the proper kernel for the integral of $\boldsymbol{A}$. Interesting geometries have been modeled this way such as the twisted tapes of Siahrang [15] and the superconducting transformer windings of Carlier [16]. If the subdomains Ω_i are thin conductors, it is possible to approximate them using a 1-D geometry inside the 2-D domain Ω. Such models, called 1.5-D models, have been implemented by Brambilla in [17] and [18] and have shown to be an effective and accurate strategy.

3.3   Other Models

More models can be found in the literature for HTS devices and it would be out of the scope of this research work to introduce all of them in details. Table 3.1 lists other models that are widely used for HTS modeling. Moreover, a general review of the status of numerical modeling for HTS devices design can be found in [19].

Table 3.1 Physical models used for HTS devices.

Physical model description	Main reference
Minimum Magnetic Energy Variation (MMEV)	[20]
Current vector potential ($\boldsymbol{T} - \Omega$)	[21]
Magnetic vector potential, differential form ($\boldsymbol{A} - V$)	[22]

CHAPTER 4

NUMERICAL METHODS FOR SPATIAL DISCRETIZATION

The equations in the models introduced in the previous chapter can be solved numerically by discretizing them in *space* and in *time*. In this chapter, we describe two methods to discretize these equations in space, i.e. the Finite Element Method (FEM) and the Semi-Analytical Method (SAM). In both cases, the discretization in space leads to systems of DAE which are introduced in the next chapter. The main references used to describe the numerical methods are [4], [5], [6], [23], [24] and [25].

4.1 The Finite Element Method

4.1.1 The Variational Problem

The problem described below is one-dimensional for the sake of clarity, however, the extension to higher dimensions is straightforward. Let us consider the following function spaces:

$$U([a,b]) = \{u(x) : u(x) \in C^2([a,b]); \ u(a) = u_a, \ u(b) = u_b\}, \tag{4.1}$$

$$V([a,b]) = \{v(x) : v(x) \in C^2([a,b]); \ v(a) = 0, \ v(b) = 0\}, \tag{4.2}$$

where $C^2([a,b])$ is the space of twice continuously differentiable functions, and the functional

$$I(\omega) = \int_a^b F\left(x, \omega, \frac{d\omega}{dx}\right) dx, \tag{4.3}$$

where $\omega(x) \in U([a,b])$ and F is a real-valued function. Function spaces are studied in a branch of mathematics known as functional analysis. More information about functional analysis and function spaces can be found in [4].

We want to find a function $u(x) \in U([a,b])$, assuming it exists, such that

$$I(u) \le I(\omega), \ \forall \omega(x) \in U([a,b]). \tag{4.4}$$

If $\omega(x) = u(x) + \alpha v(x)$, it is equivalent to write inequality (4.4) as

$$I(u) \le I(u + \alpha v), \ \forall \alpha \in \mathbb{R}, \ \forall v(x) \in V([a,b]). \tag{4.5}$$

Using equation (4.3), this yields

$$I(u) \leq \int_a^b F\left(x, u + \alpha v, \frac{du}{dx} + \alpha \frac{dv}{dx}\right) dx = \tilde{I}(\alpha). \tag{4.6}$$

Since $u(x)$ minimizes the functional I, we see that I will be at its minimum when $\alpha = 0$, therefore

$$\left.\frac{d\tilde{I}}{d\alpha}\right|_{\alpha=0} = 0, \ \forall v(x) \in V([a,b]). \tag{4.7}$$

If we use $\tilde{I}$ from (4.6) in (4.7), we have that

$$\left.\frac{d\tilde{I}}{d\alpha}\right|_{\alpha=0} = \int_a^b \left[\frac{\partial F}{\partial \omega} v + \frac{\partial F}{\partial \omega'}\frac{dv}{dx}\right] dx = 0, \tag{4.8}$$

where $\omega' = \frac{d\omega}{dx}$. The second term on the right can be integrated by parts to yield

$$\int_a^b \left[\frac{\partial F}{\partial \omega'}\frac{dv}{dx}\right] dx = \left.\frac{\partial F}{\partial \omega'} v\right|_a^b - \int_a^b v\frac{d}{dx}\left(\frac{\partial F}{\partial \omega'}\right) dx. \tag{4.9}$$

According to the definition of $V([a,b])$, we have $v(a) = 0$ and $v(b) = 0$. Therefore, if we use equation (4.9) in (4.8), we get

$$\int_a^b \left[\frac{\partial F}{\partial \omega} - \frac{d}{dx}\left(\frac{\partial F}{\partial \omega'}\right)\right] v \, dx = 0, \ \forall v(x) \in V([a,b]). \tag{4.10}$$

Consequently, to minimize the functional I, we need to find the solution $w(x) \in U([a,b])$ of the *Euler-Lagrange* equations:

$$\begin{cases} \dfrac{\partial F}{\partial \omega} - \dfrac{d}{dx}\left(\dfrac{\partial F}{\partial \omega'}\right) = 0; \\ \omega(a) = u_a; \\ \omega(b) = u_b. \end{cases} \tag{4.11}$$

Note that the functions $u(x)$ and $v(x)$ can be in different function spaces than the ones used for this demonstration. The choice of a proper function space depends on the boundary conditions of the problem. Equation (4.10) is also known as the weak form of the differential equation in expression (4.11), used in the context of the finite element method.

4.1.2 The FEM with nodal elements

The FEM is a numerical method used for the discretization of PDEs in boundary value problems. Let us consider the following differential equation:

$$-\frac{d}{dx}\left(q\frac{du}{dx}\right) = f(x), \tag{4.12}$$

where $x \in]0, L[$ and q is a constant, and the boundary conditions:

$$\begin{cases} u(0) = 0; \\ u(L) = 0. \end{cases} \tag{4.13}$$

The first step of the FEM consists in multiplying the differential equation (4.12) by a test function $v(x) \in H_0^1([0, L])$ where $H_0^1([0, L])$ is a Sobolev space, to integrate over the domain $[0, L]$, and to integrate by parts in order to get the weak form

$$\int_0^L q\frac{du}{dx}\frac{dv}{dx}\,dx = \int_0^L fv\,dx \quad \forall\,v \in H_0^1. \tag{4.14}$$

Note that since $v(x) \in H_0^1([0, L])$, we have $v(0) = 0$ and $v(L) = 0$. More information about Sobolev spaces can be found in [4].

The next step consists in building the *mesh*. The mesh is a spatial discretization of the domain $[0, L]$ using nel geometrical elements K_i for $i = 1, .., nel$. An example of a mesh for $[0, L]$ is shown in Figure 4.1. The Degrees of Freedom (DOFs) of the problem, e.g. u_i for $i = 1, ..., ndof$ are assigned at different positions in the mesh and are stored in a vector written $\boldsymbol{u}$. For nodal elements, they are usually associated with the nodes of the elements. On an element K_i, there are $n_d^{K_i}$ DOFs.

On an arbitrary element $K = [x_1^K, x_2^K]$, the elementary weak form is given by

$$\int_{x_1^K}^{x_2^K} q\frac{du}{dx}\frac{dv}{dx}\,dx - \left[q\frac{du}{dx}v\right]_{x_1^k}^{x_2^k} = \int_{x_1^K}^{x_2^K} fv\,dx \tag{4.15}$$
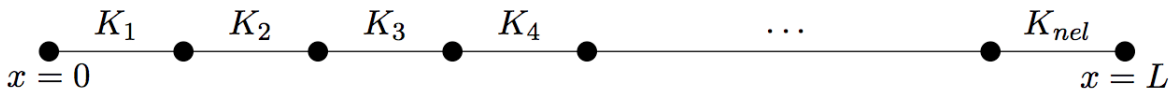
Figure 4.1 One-dimensional mesh built with *nel* elements. The elements are denoted K_i for $i = 1, ..., nel$. (Source of figure: [4])

and an approximation of the solution $u(x)$ is given by

$$u(x)\Big|_K \approx u^K(x) = \sum_{j=1}^{n_d^K} u_j^K \Psi_j^K(x), \qquad (4.16)$$

where u_j^K for $j = 1, ..., n_d^K$ are the DOFs on element K and $\Psi_j^K(x)$ for $j = 1, ..., n_d^K$ are the shape functions on K. If $v(x) = \Psi_i^K$ for $i = 1, ..., n_d^K$, we have the *elementary system of equations*

$$M^K \boldsymbol{u}^K = \boldsymbol{F}^K + \boldsymbol{S}^K. \qquad (4.17)$$

where

$$M_{ij}^K = \int_{x_1^K}^{x_2^K} q \frac{d\Psi_j^K(x)}{dx} \frac{d\Psi_i^K(x)}{dx} \, dx, \qquad (4.18)$$

$$F_i^K = \int_{x_1^K}^{x_2^K} f(x) \Psi_i^K(x) \, dx, \qquad (4.19)$$

$$S_i^K = S_{12}^K \Psi_i^K(x) + S_{11}^K \Psi_i^K(x), \qquad (4.20)$$

where $S_{11}^K = -q\frac{du(x_1^K)}{dx}$ and $S_{12}^K = q\frac{du(x_2^K)}{dx}$, and $\boldsymbol{u}^K$ is the vector containing the DOFs on element K.

To evaluate the elementary system of equations, we use a transformation on a reference element $\hat{K} = [-1, 1]$. An example of 1-D linear shape functions on $\hat{K}$, is shown in Figure 4.2. The reference element is introduced in details in chapter 7.

For each element K_i, $i = 1, ...nel$, there is an elementary system of equations (4.17).
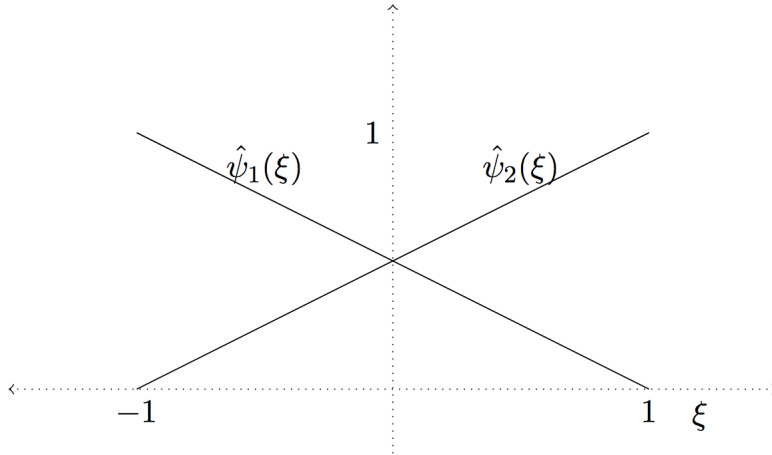
Figure 4.2 One-dimensional linear shape functions over the element $\hat{K} = [-1, 1]$. (Source of figure: [4])

These different systems of equations are coupled because one DOF can belong to more than one element. To account for this coupling, we assemble a *global system of equations* of the form

$$M\boldsymbol{u} = \boldsymbol{F} + \boldsymbol{S}. \tag{4.21}$$

This system of equations can then be solved for $\boldsymbol{u}$ using either LU decomposition or an iterative method.

Nodal elements have shown mitigated results for the modeling of HTS devices in 2-D and 3-D. For general electromagnetic problems, Jin [5] stated three main difficulties encountered with the use of this type of elements:

- Difficulty in enforcing the divergence free condition $\nabla \cdot \boldsymbol{B} = 0$ and, as a result, non-physical solutions are observed (spurious modes);

- Difficulty in imposing the continuity conditions of electric and magnetic fields at the different materials interfaces;

- Difficulty to deal with conducting and dielectric edges because of field singularities.

As a result, nodal elements are seldomly used for the numerical modeling of HTS devices in 2-D and 3-D.

4.1.3 Edge Elements

Nédélec's edge elements are vectorial elements for which the DOFs are associated with the edges of the elements rather than the nodes [25]. More precisely, they represent an approximation of the tangential component of the dependant variable along each edge. For an edge e and a DOF h_e:

$$\boldsymbol{H} \cdot \boldsymbol{t}_e = h_e, \tag{4.22}$$

where $\boldsymbol{t}_e$ is a unit vector tangent to the edge. As a result, an approximation of the dependant variable $\boldsymbol{H}$ on a triangular element K, with $n_d^K = 3$ DOFs, is given by

$$\boldsymbol{H}\bigg|_K \approx \boldsymbol{h}^K(\boldsymbol{x}) = \sum_{e=1}^{n_d^K} h_e^K \boldsymbol{N}_e^k(\boldsymbol{x}), \tag{4.23}$$

where h_e^K for $e = 1, ..., n_d^K$ are the DOFs and $\boldsymbol{N}_e^K$ for $e = 1, ..., n_d^K$ are the shape functions. A vectorial representation of these functions is shown in Figure 4.3.

For the numerical modeling of HTS, edge elements are popular because they don't suffer from the main limitations reported by Jin [5] for nodal elements. First, the basis functions
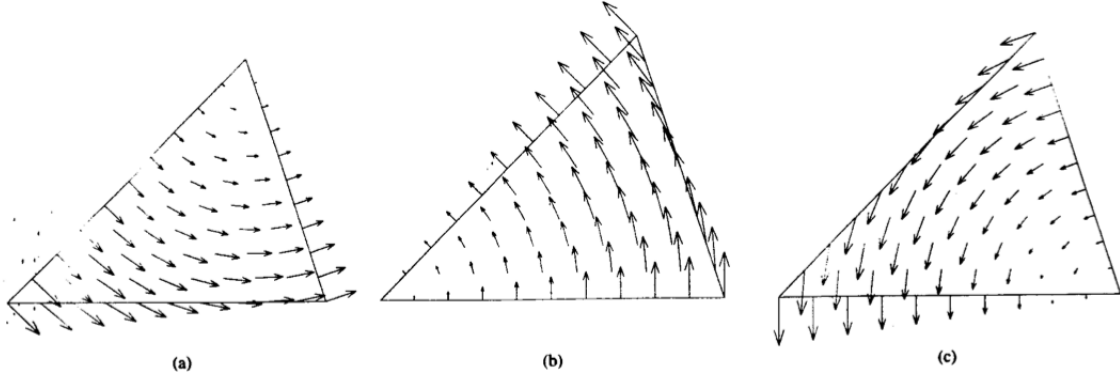
Figure 4.3 Vectorial interpretation of the 2-D shape functions for edge elements over a triangular element K. a) The function associated with edge #1: $\boldsymbol{N}_1^K$; b) Edge # 2: $\boldsymbol{N}_2^K$; c) Edge # 3: $\boldsymbol{N}_3^K$. (Source of figure: [5])

implicitly satisfy the divergence free condition on each element, i.e. $\nabla \cdot \boldsymbol{N}_e^K = 0$. If $\boldsymbol{h}^K$ is an approximation of the magnetic field on element K and if μ is constant in space, we have

$$\nabla \cdot \boldsymbol{h}^K(\boldsymbol{x}) = \sum_{e=1}^{n_d^K} h_e^K \nabla \cdot \boldsymbol{N}_e^K(\boldsymbol{x}) = 0. \tag{4.24}$$

The definition of the functions $\boldsymbol{N}_e^K$ for $e = 1, ..., n_d^K$ are discussed in chapter 8. Secondly, the materials interface conditions between the different domains are easier to implement because the tangential components of the fields are continuous across all edges. Finally, the normal component of the fields across an edge is not continuous which makes it easier to deal with singularities at conducting and dielectric interfaces.

4.2   The Semi-Analytical Method

The Semi-Analytical Method (SAM) is used to discretize in space the equations of the $\boldsymbol{A} - V$ formulation in integral form. A physical model based on this formulation has been introduced in section 3.2.

The SAM is a *point collocation* method and it consists in computing the current density $\boldsymbol{J}$ at n nodes of a mesh composed of n_e elements. The mesh is in the $x - y$ plane with $\boldsymbol{J}$ being perpendicular to that plane, but 3-D effects can still be taken into account using the integral definition of the magnetic vector potential. An example of a typical mesh is shown in Figure 4.4.
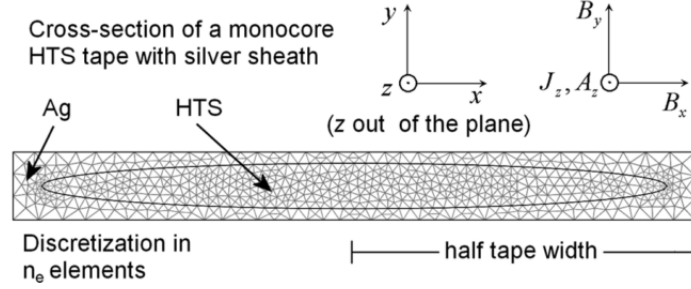
Figure 4.4 Typical two-dimensional mesh for the SAM. (Source of figure: [6])

We write

$$\boldsymbol{J}_v = \begin{bmatrix} J_1 \\ J_2 \\ \vdots \\ J_n \end{bmatrix}, \tag{4.25}$$

where J_i for $i = 1, .., n$ are the DOFs for the current density at each node of the mesh. Therefore, $\boldsymbol{J}_v$ is a discrete version of $\boldsymbol{J}$. By considering the current density $\boldsymbol{J}$ to be either linear or constant per element, we can get an expression for the magnetic potential vector at each node of the mesh:

$$A_i = [\text{coeff}]_{1 \times n} \boldsymbol{J}_v + A_{ext,i}. \tag{4.26}$$

The line vector $[\text{coeff}]_{1 \times n}$ is obtained by computing analytically the integral for the magnetic vector potential introduced in section 3.2, i.e.

$$\boldsymbol{A}(\boldsymbol{r}) = \frac{\mu_0}{4\pi} \int_\Omega \boldsymbol{J} \log |\boldsymbol{r} - \boldsymbol{r}'| \, d\Omega. \tag{4.27}$$

This integral depends only on the geometry of the conducting parts of the domain Ω. The term $A_{ext,i}$ is a discrete version of $\boldsymbol{A}_{ext}$ which was introduced in section 3.2. We recall that $\boldsymbol{A}_{ext}$ is used to model an external magnetic field. Since the contribution of $A_{ext,i}$ does not impact the structure of the equations, it will not be considered hereafter.

We recall the equation for the current density $\boldsymbol{J}$ that was introduced in section 3.2:

$$-\frac{\partial \boldsymbol{A}}{\partial t} - \rho \boldsymbol{J} - \nabla V = 0. \tag{4.28}$$

If we apply the collocation method described above to this equation, we obtain the system of ODEs:

$$M_A \dot{\boldsymbol{J}}_v - \Lambda_\rho \boldsymbol{J}_v - D\boldsymbol{V} = 0. \tag{4.29}$$

Here, M_A is a dense invertible $n \times n$ matrix whose entries are given by equation (4.26). The coefficients Λ_ρ is a diagonal $n \times n$ matrix with its diagonal elements given by the definition of ρ. The vector $\boldsymbol{V}$ contains the DOFs V_i for $i = 1, ..., nbcond$ where $nbcond$ is the number of conductors and D is a matrix of size $n \times nbcond$.

CHAPTER 5

INTRODUCTION TO SYSTEMS OF DAE

As discussed in the previous chapter, the numerical methods used to discretize the equations modeling HTS devices in space lead to systems of DAE. This chapter introduces systems of DAE. It is divided into 3 sections. In section 5.1, we report basic definitions for systems of DAE. In section 5.2 we describe a notion used to classify systems of DAE, i.e. the index. Finally, in section 5.3, we discuss an important type of system of DAE known as the Hessenberg form. The references used for this chapter are [26], [27], and [28].

5.1 Definition of a System of DAE

The first order *explicit* system of Ordinary Differential Equations (ODEs)

$$\dot{\boldsymbol{x}} = \boldsymbol{f}(t, \boldsymbol{x}), \tag{5.1}$$

contains m ODE. It can also be written in a more general *implicit* form

$$\boldsymbol{G}(t, \boldsymbol{x}, \dot{\boldsymbol{x}}) = \boldsymbol{0}, \tag{5.2}$$

where the Jacobian matrix of $\boldsymbol{G}$ with respect to $\dot{\boldsymbol{x}}$

$$\frac{\partial \boldsymbol{G}(t, \boldsymbol{x}, \dot{\boldsymbol{x}})}{\partial \dot{\boldsymbol{x}}} = \begin{bmatrix} \frac{\partial G_1}{\partial \dot{x}_1} & \cdots & \frac{\partial G_1}{\partial \dot{x}_m} \\ \vdots & \ddots & \vdots \\ \frac{\partial G_m}{\partial \dot{x}_1} & \cdots & \frac{\partial G_m}{\partial \dot{x}_m} \end{bmatrix} \tag{5.3}$$

is assumed to be nonsingular. If we add a system of algebraic equations $\boldsymbol{g}$ of size ℓ and ℓ *algebraic variables*, i.e. $\boldsymbol{z}$ to the system of equations (5.1), we have:

$$\begin{cases} \dot{\boldsymbol{x}} = \boldsymbol{f}(t, \boldsymbol{x}, \boldsymbol{z}); \\ \boldsymbol{0} = \boldsymbol{g}(t, \boldsymbol{x}, \boldsymbol{z}), \end{cases} \tag{5.4}$$

which is a *semi-explicit* system of DAE of size $n = m + \ell$. The solution of this system must satisfy both systems of differential and algebraic equations.

A more general form of DAE is the *semi-explicit nonlinear* system:

$$\begin{cases} \boldsymbol{h}(t, \boldsymbol{x}, \dot{\boldsymbol{x}}, \boldsymbol{z}) = \boldsymbol{0}; \\ \boldsymbol{g}(t, \boldsymbol{x}, \boldsymbol{z}) = \boldsymbol{0}, \end{cases} \tag{5.5}$$

where $\boldsymbol{h}$ only contains the differential equations and $\boldsymbol{g}$ contains the algebraic equations.

The systems of equations (5.4) and (5.5) can be written as

$$\boldsymbol{F}(t, \boldsymbol{y}, \dot{\boldsymbol{y}}) = \boldsymbol{0}, \tag{5.6}$$

with

$$\boldsymbol{y} = \begin{bmatrix} \boldsymbol{x} \\ \boldsymbol{z} \end{bmatrix} \tag{5.7}$$

which is called an *implicit* system of DAE. This time, the Jacobian matrix of $\boldsymbol{F}$ with respect to $\dot{\boldsymbol{y}}$, i.e. $\frac{\partial \boldsymbol{F}(t, \boldsymbol{y}, \dot{\boldsymbol{y}})}{\partial \dot{\boldsymbol{y}}}$ is singular. To explain this statement, let us write

$$\boldsymbol{y} = \begin{bmatrix} y_1 \\ y_2 \\ \vdots \\ y_n \end{bmatrix}, \quad \dot{\boldsymbol{y}} = \begin{bmatrix} \dot{y}_1 \\ \dot{y}_2 \\ \vdots \\ \dot{y}_n \end{bmatrix}, \tag{5.8}$$

and

$$\boldsymbol{x} = \begin{bmatrix} y_1 \\ y_2 \\ \vdots \\ y_m \end{bmatrix}, \quad \boldsymbol{z} = \begin{bmatrix} y_{m+1} \\ y_{m+2} \\ \vdots \\ y_n \end{bmatrix}, \tag{5.9}$$

where n is the length of vectors $\boldsymbol{y}$ and $\dot{\boldsymbol{y}}$, m is the length of vector $\boldsymbol{x}$ and $\ell = (n - m)$ is the length of vector $\boldsymbol{z}$. Since $\boldsymbol{z}$ contains algebraic variables, its time derivative

$$\dot{\boldsymbol{z}} = \begin{bmatrix} \dot{y}_{m+1} \\ \dot{y}_{m+2} \\ \vdots \\ \dot{y}_n \end{bmatrix} \tag{5.10}$$

does not appear in $\boldsymbol{F}$. As a result, columns $(m + 1)$ to n of $\frac{\partial \boldsymbol{F}(t, \boldsymbol{y}, \dot{\boldsymbol{y}})}{\partial \dot{\boldsymbol{y}}}$ are given by a vector of

zeros of length n, i.e.

$$\frac{\partial \boldsymbol{F}(t,\boldsymbol{y},\dot{\boldsymbol{y}})}{\partial \dot{\boldsymbol{y}}} = \begin{bmatrix} \frac{\partial F_1}{\partial \dot{y}_1} & \cdots & \frac{\partial F_1}{\partial \dot{y}_m} & 0 & \cdots & 0 \\ \vdots & \ddots & \vdots & \vdots & \ddots & \vdots \\ \frac{\partial F_n}{\partial \dot{y}_1} & \cdots & \frac{\partial F_n}{\partial \dot{y}_m} & 0 & \cdots & 0 \end{bmatrix}. \tag{5.11}$$

Consequently, $\frac{\partial \boldsymbol{F}(t,\boldsymbol{y},\dot{\boldsymbol{y}})}{\partial \ddot{\boldsymbol{y}}}$ is singular.

5.2   The Index of a System of DAE

Let us consider the following system of DAE, taken from Ascher [26]:

$$\begin{cases} \dot{y}_1 = y_2; \\ y_1 = q(t). \end{cases} \tag{5.12}$$

If we differentiate the second equation in this system, we have $\dot{y}_1 = \dot{q}(t)$ and $y_2 = \dot{q}(t)$. Then, if we differentiate the first equation, we have $\dot{y}_2 = \ddot{y}_1$ and therefore $\dot{y}_2 = \ddot{q}(t)$. This yields the following system of ODEs:

$$\begin{cases} \dot{y}_1 = \dot{q}(t); \\ \dot{y}_2 = \ddot{q}(t). \end{cases} \tag{5.13}$$

Since it took two differentiations to transform the original system of DAE into a system of ODEs, its *index* is 2. The minimum number of differentiation needed to obtain an *explicit system of ODEs* from a system of DAE is called the *index*. Therefore, systems of ODEs are systems of DAE of index 0. Systems of DAE with indexes that are higher than one are called *higher index systems of DAE*.

The initial or boundary conditions specified for the system of DAE (5.13) need to be *consistent*. This means that they need to satisfy the algebraic constraint $y_1 = q(t)$ but also $y_2(t) = \dot{q}(t)$. The latter equation is called a *hidden constraint* because it does not appear in the initial or final system of equations.

5.3   The Hessenberg Form of a DAE

Some systems of DAE have a particular mathematical structure called *Hessenberg form.* Generally and explicitly, a system of DAE of index r in Hessenberg form is written as [27]

$$
\begin{bmatrix}
I_1 & 0 & \cdots & \cdots & 0 \\
0 & I_2 & \ddots & & \vdots \\
\vdots & \ddots & \ddots & \ddots & \vdots \\
\vdots & & \ddots & I_{r-1} & 0 \\
0 & \cdots & \cdots & 0 & 0
\end{bmatrix}
\begin{bmatrix}
\dot{\boldsymbol{y}}_1 \\ \vdots \\ \vdots \\ \vdots \\ \dot{\boldsymbol{y}}_r
\end{bmatrix}
+
\begin{bmatrix}
B_{11} & \cdots & \cdots & B_{1,r-1} & B_{1r} \\
B_{21} & \cdots & \cdots & B_{2,r-1} & 0 \\
0 & \ddots & & \vdots & \vdots \\
\vdots & \ddots & \ddots & \vdots & \vdots \\
0 & \cdots & 0 & B_{r,r-1} & 0
\end{bmatrix}
\begin{bmatrix}
\boldsymbol{y}_1 \\ \vdots \\ \vdots \\ \vdots \\ \boldsymbol{y}_r
\end{bmatrix}
=
\begin{bmatrix}
\boldsymbol{f}_1 \\ \vdots \\ \vdots \\ \vdots \\ \boldsymbol{f}_r
\end{bmatrix}.
\tag{5.14}
$$

If the vectors $\boldsymbol{y}_i$ for $i = 1, ..., r$ have length n_{y_i}, then the I_i are identity matrices of size $n_{y_i} \times n_{y_i}$, the $B_{i,j}$ are matrices of size $n_{y_i} \times n_{y_j}$ for $i, j = 1, ..., r$ and the f_i are known vectors of length n_{y_i}. The most common indices for Hessenberg DAEs are 2 and 3. For a system of DAE of index 2 in Hessenberg form, we have:

$$
\begin{cases}
\dot{\boldsymbol{y}}_1 + B_{11}\boldsymbol{y}_1 + B_{12}\boldsymbol{y}_2 = \boldsymbol{f}_1; \\
B_{21}\boldsymbol{y}_1 = \boldsymbol{f}_2,
\end{cases}
\tag{5.15}
$$

and for an index 3:

$$
\begin{cases}
\dot{\boldsymbol{y}}_1 + B_{11}\boldsymbol{y}_1 + B_{12}\boldsymbol{y}_2 + B_{13}\boldsymbol{y}_3 = \boldsymbol{f}_1; \\
\dot{\boldsymbol{y}}_2 + B_{21}\boldsymbol{y}_1 + B_{22}\boldsymbol{y}_2 = \boldsymbol{f}_2; \\
B_{32}\boldsymbol{y}_2 = \boldsymbol{f}_3.
\end{cases}
\tag{5.16}
$$

A system of DAE of index 2 in Hessenberg form can be expressed in a semi-explicit form:

$$
\begin{cases}
\dot{\boldsymbol{y}}_1 = \boldsymbol{h}(t, \boldsymbol{y}_1, \boldsymbol{y}_2); \\
\boldsymbol{0} = \boldsymbol{g}(t, \boldsymbol{y}_1),
\end{cases}
\tag{5.17}
$$

or in a semi-explicit nonlinear form:

$$
\begin{cases}
\boldsymbol{h}(t, \boldsymbol{y}_1, \dot{\boldsymbol{y}}_1, \boldsymbol{y}_2) = \boldsymbol{0}; \\
\boldsymbol{g}(t, \boldsymbol{y}_1) = \boldsymbol{0}.
\end{cases}
\tag{5.18}
$$

In both cases, the algebraic variable $\boldsymbol{y}_2$ is not in the system of algebraic equations $\boldsymbol{g}$. Systems of DAE in Hessenberg form are of *full index* r; all algebraic variables can be eliminated with the same number of derivations.

Systems of DAE in Hessenberg form are common in constrained variational problems. The algebraic variables are often associated with the *Lagrange multipliers* of the problem. For example, nonlinear systems of DAE of index 2 in Hessenberg form are encountered in the

modeling of the flow of an incompressible fluid using the *Navier-Stokes* equations:

$$\begin{cases} M\dot{\boldsymbol{u}} + (K + N(\boldsymbol{u}))\boldsymbol{u} + \boldsymbol{C}p = \boldsymbol{f}; \\ \boldsymbol{C}^T\boldsymbol{u} = 0. \end{cases} \tag{5.19}$$

The details of this system of DAE are omitted here but we can note that the algebraic variable, i.e. the pressure p, is only in the first system of equations.

In conclusion, we can note three main features of systems of DAE of Hessenberg type. First, they are often encountered in constrained variational problems. Second, all algebraic variables require the same number of derivations for the system of DAE to be reduced to a system of ODEs. Third, for a system of DAE of index 2 in Hessenberg form, the algebraic variables are not in the algebraic equations.

CHAPTER 6

THE DISCRETIZATION OF SYSTEMS OF DAE IN TIME

In this chapter, we introduce some strategies, time-integration schemes and transient solvers that are used to discretize systems of DAE in time. In section 6.1 we describe a direct discretization method that consists in discretizing systems of DAE directly. Then, in section 6.2, we cover how to discretize systems of DAE by reducing their index. Afterwards, in section 6.3, we briefly discuss how we can discretize systems of DAE of index 0 in semi-explicit form. Finally, in section 6.4, we introduce one of the main transient solver used to discretize systems of DAE, i.e. the Differential-Algebraic System SoLver (DASSL) and related solvers. The main references used in this chapter are [26], [27], [29] and [30].

6.1 Direct Discretization

Systems of DAE can be solved numerically by *direct discretization*. This method consists in discretizing directly the system of DAE in its full implicit form:

$$\boldsymbol{F}(t, \boldsymbol{y}, \dot{\boldsymbol{y}}) = \boldsymbol{0}, \tag{6.1}$$

or in its semi-explicit nonlinear form:

$$\begin{cases} \boldsymbol{f}(t, \boldsymbol{y}, \dot{\boldsymbol{y}}) = \boldsymbol{0}; \\ \boldsymbol{g}(t, \boldsymbol{y}) = \boldsymbol{0}, \end{cases} \tag{6.2}$$

or its semi-explicit form:

$$\begin{cases} \dot{\boldsymbol{y}} = \boldsymbol{f}(t, \boldsymbol{y}); \\ \boldsymbol{0} = \boldsymbol{g}(t, \boldsymbol{y}), \end{cases} \tag{6.3}$$

using an implicit method such as a multistep *Backward Differentiation Formula* (BDF). Other methods can be used but in this thesis, we concentrate our efforts on the BDF schemes due to their use in the software DASSL, which is described in forthcoming sections.

An approximation of the time derivative at time $t = t_n$ using a BDF method of order k is written as [27]

$$\dot{y}_n \approx \frac{1}{\beta_0 \triangle t} \sum_{j=0}^{k} \alpha_j y_{n-j}, \tag{6.4}$$

where β_0 and α_j are the coefficients of the method and $\triangle t$ is the time-step size. Note that

the first order accurate BDF method is the backward Euler method.

For a system of DAE, initial conditions are said to be consistent when they satisfy the differential equations, the algebraic equations and the hidden constraints as explained in section 5.2. For consistent initial conditions, a convergence analysis reported by Brenan [27] shows that BDF methods of order k with $k < 7$ achieve the same convergence rate for systems of DAE of index 1 as they do for systems of ODEs. Furthermore, the same rate of convergence can be achieved with semi-explicit nonlinear systems of DAE of index 2, under certain conditions[1].

For most of the systems of DAE, the discretization of the time derivative with an implicit method yields a nonlinear system of equations that needs to be linearized using Newton's method. For the fully implicit system, the nonlinear system is

$$\boldsymbol{F}\left(t_n, \boldsymbol{y}_n, \frac{1}{\beta_0 \triangle t} \sum_{j=0}^{k} \alpha_j \boldsymbol{y}_{n-j}\right) = \boldsymbol{0}, \tag{6.5}$$

for the semi-explicit nonlinear form, it is:

$$\begin{cases} \boldsymbol{f}\left(t_n, \boldsymbol{y}_n, \frac{1}{\beta_0 \triangle t} \sum_{j=0}^{k} \alpha_j \boldsymbol{y}_{n-j}\right) = \boldsymbol{0}; \\ \boldsymbol{g}(t_n, \boldsymbol{y}_n) = \boldsymbol{0}, \end{cases} \tag{6.6}$$

and for the semi-explicit form, it is:

$$\begin{cases} \frac{1}{\beta_0 \triangle t} \sum_{j=0}^{k} \alpha_j \boldsymbol{y}_{n-j} = \boldsymbol{f}(t_n, \boldsymbol{y}_n); \\ \boldsymbol{0} = \boldsymbol{g}(t_n, \boldsymbol{y}_n). \end{cases} \tag{6.7}$$

6.2   Reduction of Index

In some situtations, it could be advantageous to reduce the index of the system of DAE before discretizing its time derivative. This process consists in the three following steps:

1. Reduce the index of the system of DAE;

2. Identitfy the resulting system of DAE;

3. As a function of item 2, discretize the system of DAE in time or reduce its index, again.

When reducing the index of a system of DAE, extra care must be taken to ensure that the initial conditions are consistent.

---

[1]see [27], theorem 3.2.2

6.3 Reformulation of Systems of DAE into Semi-Explicit Forms

The reformulation of systems of DAE into semi-explicit forms applies to systems of DAE of index 0. It consist in writing the DAE as a semi-explicit system of ODEs, i.e.

$$\dot{\boldsymbol{y}} = \boldsymbol{f}(t, \boldsymbol{y}), \tag{6.8}$$

and then discretize $\dot{\boldsymbol{y}}$ using an explicit method such as *forward Euler*. It is an efficient technique to avoid solving a nonlinear system of equations but it often requires to invert matrices. Note that this strategy has no use when the system of DAE to discretize is nonlinear.

The semi-explicit form, $\dot{\boldsymbol{y}} = \boldsymbol{f}(t, \boldsymbol{y})$, is the form solved by certain transient solvers such as `ode45` in MATLAB. Systems of DAE of index 0 can be reformulated into semi-explicit form to use these solvers.

6.4 DASSL and IDAS

DASSL was developed at Sandia National Laboratories by a team directed by Linda Petzold [29]. The way this solver works is similar to the direct discretization method applied to implicit systems of DAE introduced in section 6.1. DASSL is used to discretize initial value problems of the form

$$\boldsymbol{F}(t, \boldsymbol{y}, \dot{\boldsymbol{y}}) = \boldsymbol{0}, \quad \boldsymbol{y}(t_0) = \boldsymbol{y}_0, \quad \dot{\boldsymbol{y}}(t_0) = \dot{\boldsymbol{y}}_0. \tag{6.9}$$

The time derivatives are discretized using BDF methods. As a result, at each time step, a nonlinear system of the form

$$\boldsymbol{F}\left(t_n, \boldsymbol{y}_n, \frac{1}{\beta_0 \triangle t} \sum_{j=0}^{k} \alpha_j \boldsymbol{y}_{n-j}\right) = \boldsymbol{0} \tag{6.10}$$

needs to be solved using a variant of Newton's method. The linearization of this system of equations leads to a linear system of equations that is solved using dense or banded direct methods.

The BDF methods used in DASSL have a variable order of precision and the time-steps have variable size. The order of precision of the BDF methods vary from 1 to 5. DASSL discretizes systems of DAE of index 0 and of index 1, but it was shown to give good results in solving nonlinear semi-explicit systems of DAE of index 2.

IDAS (Implicit Differential-Algebraic Solver) is an extension of DASSL. The main difference is that iterative methods have been added to solve the linear system resulting from the linearization of the nonlinear system. Since it uses iterative methods, IDAS can be used to study large-scale problems.

CHAPTER 7

DISCRETIZATION OF HTS PROBLEMS USING NODAL FINITE ELEMENTS IN 1-D

In this chapter, we study the systems of DAE obtained from the discretization in space of HTS problems using nodal finite elements in 1-D. More precisely, in section 7.1, we describe a typical HTS problem that can be studied using a 1-D physical model. Afterwards, in section 7.2, we give the discretization in space of the equations of this model using the FEM with nodal elements. This discretization in space leads to systems of DAE. In section 7.3, we identify the structure and index of those systems of DAE and propose strategies to discretize them in time. Finally, in section 7.4, we describe and verify the code that was developed for this research work.

Despite their simplicity, we decided to study 1-D problems for two reasons. First, the 1-D case is used to introduce the general methodology of this research work. Second, Mayergoyz [31] and Wan [12] both derived analytical solutions for the 1-D model of the HTS slab which can be used to verify the developed code. The main references used to write this chapter are [4] and [23].

7.1 Typical Problem

Let us consider an HTS domain whose width and length are much larger than its thickness, often referred to the *slab* geometry [3]. We want to compute the current density distribution in the HTS slab as a function of the magnetic flux density applied parallel to the slab at $x = a$ and $-a$, i.e.:

$$\begin{cases} B(-a,t) = B_a t^p; \\ B(a,t) = -B_a t^p, \end{cases} \tag{7.1}$$

where B_a is the magnitude of the flux density and $p \geq 1$.

Since the slab is long and wide compared to its thickness, it can be approximated using a 1-D geometry of finite thickness. We can then use the 1-D model described in section 3.1.1. We recall the main characteristics of the model. The PDE for the flux density diffusion is given by

$$-\frac{\partial}{\partial x}\left[\frac{\rho(J)}{\mu_0}\frac{\partial B(x,t)}{\partial x}\right] + \frac{\partial B(x,t)}{\partial t} = 0, \tag{7.2}$$

with $x \in]-a, a[$ and $t \in [0, \infty[$. The initial conditions are given by:

$$\begin{cases} B(x,0) = 0; \\ B_t(x,0) = 0. \end{cases} \tag{7.3}$$

The parallel magnetic flux density is applied using Dirichlet boundary conditions:

$$\begin{cases} B(-a,t) = B_a t^p; \\ B(a,t) = -B_a t^p. \end{cases} \tag{7.4}$$

For the resistivity of the HTS slab, we use the power law model:

$$\rho(J) = \frac{E_c}{J_c} \left| \frac{J}{J_c} \right|^{n-1}, \tag{7.5}$$

and the current density is given by

$$J = -\frac{1}{\mu_0} \frac{\partial B}{\partial x}. \tag{7.6}$$

7.2 Discretization in Space Using the FEM with Nodal Elements

7.2.1 The Weak Form

We want to discretize the PDE (7.2) over the 1-D domain Ω shown in Figure 7.1. This domain represents the width of the slab. The first step consists in multiplying this PDE by a test function $v(x)$ taken in the Sobolev space $H_0^1(\Omega)$ and we integrate over the domain Ω:

$$-\int_{-a}^{a} \frac{\partial}{\partial x} \left[\frac{\rho(J)}{\mu_0} \frac{\partial B(x,t)}{\partial x} \right] v(x)\, dx + \int_{-a}^{a} \frac{\partial B(x,t)}{\partial t} v(x)\, dx = 0. \tag{7.7}$$
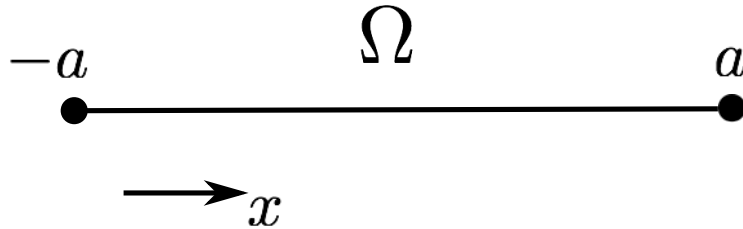
Figure 7.1 Domain Ω that represents the width of the HTS slab.

We then integrate the first term of equation (7.7) by parts to get

$$\int_{-a}^{a} \frac{\partial B(x,t)}{\partial t} v(x) \, dx + \int_{-a}^{a} \frac{\rho(J)}{\mu_0} \frac{\partial B(x,t)}{\partial x} \frac{dv(x)}{dx} \, dx - \left[\frac{\rho(J)}{\mu_0} \frac{\partial B(x,t)}{\partial x} v(x) \right]_{-a}^{a} = 0. \quad (7.8)$$

Since $v(x)$ is in $H_0^1(\Omega)$, we have $v(-a) = v(a) = 0$. Therefore, the last term in equation (7.8) is zero and we have

$$\int_{-a}^{a} \frac{\partial B(x,t)}{\partial t} v(x) \, dx + \int_{-a}^{a} \frac{\rho(J)}{\mu_0} \frac{\partial B(x,t)}{\partial x} \frac{dv(x)}{dx} \, dx = 0, \quad (7.9)$$

which is a weak form of equation (7.2).

7.2.2 The Mesh

The next step consists in building a spatial discretization of the domain of definition of the problem Ω using *nel* elements K_i for $i = 1, ..., nel$. Elements do not need to be of the same size h. Each element K_i is defined using $n_g^{K_i} = 2$ *geometric nodes*, as shown in Figure 7.2.

An arbitrary element $K = [x_1^K, x_2^K]$ contains n_c^K *computation nodes*. For the problem studied in this chapter, the computation nodes are at the geometric nodes and therefore $n_c^K = n_g^K = 2$. The total number of nodes is *nnodes*.

The x coordinate of each node is stored in a table called COOR. An example of a table COOR is shown in Table 7.1. The relationship between an element and the nodes within this element is stored in a table called CONNEC. An example of a table CONNEC is shown in Table 7.2. For the problem studied in this chapter, the DOFs are an approximation of the magnetic flux density at the computation nodes and there is only one DOF associated with each node. As a result, there are $n_d^K = 2$ DOFs in an element K and *ndof* DOFs on Ω. The DOFs are time-dependent and written as $b_i(t)$ with $i = 1, ..., ndof$.

The DOFs are unknowns except for the DOFs related to Dirichlet boundary conditions.
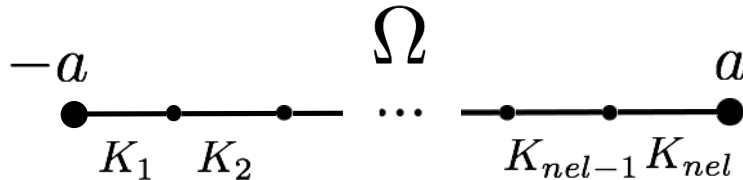
Figure 7.2 Domain Ω discretized using *nel* elements K_i. Each element have $n_g^K = 2$ geometrical nodes.

Table 7.1 The x coordinate of each node is stored in a table called COOR.

COOR	
Node	x coordinate
1	-0.5
2	-0.4
$\vdots$	$\vdots$
$nnodes$	0.5

Table 7.2 The relationship between an element K_i for $i = 1, ...nel$ and the nodes within this element is stored in a table called CONNEC.

CONNEC		
Element	Node #1	Node #2
K_1	1	2
K_2	2	3
$\vdots$	$\vdots$	$\vdots$
K_{nel}	$nnodes - 1$	$nnodes$

We write

$$\boldsymbol{B} = \begin{bmatrix} b_1 \\ b_2 \\ \vdots \\ b_{ndof} \end{bmatrix} = \begin{bmatrix} \boldsymbol{B}_U \\ \boldsymbol{B}_D \end{bmatrix}, \tag{7.10}$$

where $\boldsymbol{B}$ is the *global vector* containing the DOFs of B, $\boldsymbol{B}_U$ is a vector containing the unknown DOFs and $\boldsymbol{B}_D$ is a vector containing the known DOFs on the boundary where the Dirichlet boundary conditions are imposed. Similarly, for the time derivative of the DOFs, we can write

$$\dot{\boldsymbol{B}} = \begin{bmatrix} \dot{b}_1 \\ \dot{b}_2 \\ \vdots \\ \dot{b}_{ndof} \end{bmatrix} = \begin{bmatrix} \dot{\boldsymbol{B}}_U \\ \dot{\boldsymbol{B}}_D \end{bmatrix}. \tag{7.11}$$

The DOFs are numbered using a table called NUMBER. It has dimensions $ndof \times 1$. It gives the number of the DOF associated with each node. To get the structure of the global

vector as in equation (7.10), the DOFs that are unknown are numbered first, then a number is given to the DOFs that are known. An example of this table is shown in Table 7.3.

7.2.3 The Elementary System of Equations

Let us consider an element $K = [x_1^K, x_2^K]$. By defining

$$S_{11}^K = -\frac{\rho(J)}{\mu_0} \frac{\partial B(x,t)}{\partial x}\bigg|_{x=x_1^K}, \tag{7.12}$$

and

$$S_{12}^K = \frac{\rho(J)}{\mu_0} \frac{\partial B(x,t)}{\partial x}\bigg|_{x=x_2^K}, \tag{7.13}$$

the elementary weak form of equation (7.2) can be written as

$$\int_{x_1^K}^{x_2^K} \frac{\partial B(x,t)}{\partial t} v(x)\, dx + \int_{x_1^K}^{x_2^K} \frac{\rho(J)}{\mu_0} \frac{\partial B(x,t)}{\partial x} \frac{dv(x)}{dx}\, dx = S_{12}^K v(x_2^K) + S_{11}^K v(x_1^K). \tag{7.14}$$

Let us suppose we can approximate $B(x,t)$ on K using

$$B(x,t)|_K \approx b^K(x,t) = \sum_{j=1}^{n_d^K} b_j^K(t)\Psi_j^K(x), \tag{7.15}$$

where the $b_j^K(t)$ are the DOFs on element K and the $\Psi_j^K(x)$ are shape functions defined on K. We recall that $n_d^K = 2$ for the problem studied in this chapter. Replacing equation (7.15)

Table 7.3 The NUMBER table gives the number of the DOF associated with each node.

NUMBER	
Node	Number of the DOF
1	$ndof - 1$
2	1
$\vdots$	$\vdots$
$nnodes$	$ndof$

in the elementary weak form (7.14), we have

$$\sum_{j=1}^{n_d^K} \left[\dot{b}_j^K(t) \int_{x_1^K}^{x_2^K} \Psi_j^K(x) v(x)\, dx + b_j^K(t) \int_{x_1^K}^{x_2^K} \frac{\rho(J)}{\mu_0} \frac{d\Psi_j^K(x)}{dx} \frac{dv(x)}{dx}\, dx \right]$$
$$= S_{12}^K v(x_2^K) + S_{11}^K v(x_1^K). \tag{7.16}$$

Taking $v(x) = \Psi_i^K(x)$ for $i = 1, ..., n_d^K$, we get the nonlinear *elementary system of equations*

$$M^K \dot{\boldsymbol{B}}^K + A^K(J)\boldsymbol{B}^K = \boldsymbol{S}^K, \tag{7.17}$$

where $\boldsymbol{B}_i^K = b_i^K$ is the *elementary vector* of the DOFs, $\dot{\boldsymbol{B}}^K$ is its time derivative,

$$M_{ij}^K = \int_{x_1^K}^{x_2^K} \Psi_j^K(x)\Psi_i^K(x)\, dx, \tag{7.18}$$

$$A_{ij}^K = \int_{x_1^K}^{x_2^K} \frac{\rho(J)}{\mu_0} \frac{d\Psi_j^K(x)}{dx} \frac{d\Psi_i^K(x)}{dx}\, dx, \tag{7.19}$$

and

$$S_i^K = S_{12}^K \Psi_i^K(x_2^K) + S_{11}^K \Psi_i^K(x_1^K), \tag{7.20}$$

for $i, j = 1, ..., n_d^K$.

7.2.4 The Reference Element

Let us consider the following change of variable:

$$T^K: \quad \hat{K} \rightarrow K;$$
$$[-1, 1] \rightarrow [x_1^K, x_2^K];$$
$$\xi \rightarrow x = \frac{(x_1^K + x_2^K) + h^K \xi}{2}; \tag{7.21}$$
$$dx = \frac{h^K}{2} d\xi,$$

and the inverse change of variable:

$$(T^K)^{-1}: \quad K \to \hat{K};$$

$$[x_1^K, x_2^K] \to [-1, 1];$$

$$x \to \xi = \frac{2x - (x_1^K + x_2^K)}{h^K};$$

$$d\xi = \frac{2}{h^K} dx,$$

(7.22)

where h^K is the size of element K, $\hat{K} = [-1, 1]$ is the reference element and ξ is the independent variable on $\hat{K}$. On this element, we have

$$\Psi_i^K(x) = \Psi_i^K(T^K(\xi)) = \Psi_i^K \left(\frac{(x_1^K + x_2^K) + h^K \xi}{2} \right) = \hat{\Psi}_i(\xi),$$

(7.23)

and

$$\frac{d\Psi_i^K(x)}{dx} = \frac{d\hat{\Psi}_i(\xi)}{d\xi} \frac{d\xi}{dx} = \frac{2}{h^k} \frac{d\hat{\Psi}_i(\xi)}{d\xi},$$

(7.24)

for $i = 1, ..., n_d^K$.

We choose $\hat{\Psi}_i(\xi)$ to be the linear Lagrange shape functions:

$$\begin{cases} \hat{\Psi}_1(\xi) = \dfrac{1 - \xi}{2}; \\ \hat{\Psi}_2(\xi) = \dfrac{1 + \xi}{2}, \end{cases}$$

(7.25)

which yield an approximation of J that is piecewise constant by element. The choice of the shape functions for HTS problems has been studied by Sirois and more information on this subject can be found in [3].

As a result, for the elementary system of equations on $\hat{K}$, we have

$$M_{ij}^K = \frac{h^K}{2} \int_{-1}^1 \hat{\Psi}_j(\xi) \hat{\Psi}_i(\xi) \, d\xi,$$

(7.26)

$$A_{ij}^K = \frac{4\rho^K(t)}{(h^K)^2 \mu_0} \int_{-1}^1 \frac{d\hat{\Psi}_j(\xi)}{d\xi} \frac{d\hat{\Psi}_i(\xi)}{d\xi} \, d\xi,$$

(7.27)

and

$$S_i^K = S_{12}^K \hat{\Psi}_i(1) + S_{12}^K \hat{\Psi}_i(-1),$$

(7.28)

for $i, j = 1, .., n_d^K$. Note that the HTS resistivity ρ^K is not in the integral of A_{ij}^K. This is

because it is independent of ξ, i.e.

$$\rho^K(t) = \frac{E_c}{J_c} \left| \frac{b_1^K(t) - b_2^K(t)}{\mu_0 J_c h^K} \right|^{n-1}.$$ (7.29)

This is shown in Appendix A.

7.2.5 Assembly of the Global System of Equations

We have the elementary system of equations (7.17) for each element K_i, $i = 1, ..., nel$. We cannot solve these systems independently because the DOFs are shared between elements. As a result, we need to assemble a *global system of equations*

$$M\dot{\boldsymbol{B}} + A(\boldsymbol{J})\boldsymbol{B} = \boldsymbol{S},$$ (7.30)

where $\boldsymbol{B}$ is the global vector described in equation (7.10), $\dot{\boldsymbol{B}}$ is its time derivative, A and M are matrices of dimensions $ndof \times ndof$ and $\boldsymbol{S}$ is a vector of length $ndof$. The entries of A and M come from the elementary contributions of A^{K_i} and M^{K_i} for $i = 1, ..., nel$. The coefficients of $\boldsymbol{S}$ come from the elementary contributions of the vectors $\boldsymbol{S}^{K_i}$, for $i = 1, ..., nel$.

For the problem studied in this chapter, we do not impose any jump in the approximation of the solution between the elements. Therefore, the coefficients S_i^K of $\boldsymbol{S}$ at the DOFs locations inside the domain Ω will either be zero or they will cancel. As a result, for the remainder of this chapter, we will have

$$\boldsymbol{S} = \begin{bmatrix} \boldsymbol{0} \\ \boldsymbol{S}_U \end{bmatrix},$$ (7.31)

where $\boldsymbol{S}_U$ is an unknown vector of length 2, i.e. one coefficient for each DOF on the boundary where Dirichlet boundary conditions are applied.

To assemble the global system of equations, we use a table called ADDRESS. This table gives the number of the DOFs on each element. An example of this table is shown in Table 7.4 and a thorough explanation of the assembly process can be found in [4].

7.3 Systems of DAE

Depending on how the Dirichlet boundary conditions are enforced, the discretization of equation (7.2) in space can lead to a system of DAE of index 0 or index 1. In this section, we give the structure of those systems and propose strategies for solving them.

Table 7.4 The ADDRESS table gives the number of the DOFs on each element K_i for $i = 1, ..., nel$.

ADDRESS		
Element	DOF #1	DOF #2
K_1	$ndof - 1$	1
K_2	1	2
$\vdots$	$\vdots$	$\vdots$
K_{nel}	$ndof - 2$	$ndof$

7.3.1   System of DAE of Index 0

As mentioned in subsection 7.2.2, the coefficients of vector $\boldsymbol{B}_D$ are known. Therefore, using

$$M\dot{\boldsymbol{B}} = \begin{bmatrix} M_{11} & M_{12} \\ M_{21} & M_{22} \end{bmatrix} \begin{bmatrix} \dot{\boldsymbol{B}}_U \\ \dot{\boldsymbol{B}}_D \end{bmatrix}, \tag{7.32}$$

and

$$A(J)\boldsymbol{B} = \begin{bmatrix} A_{11}(J) & A_{12}(J) \\ A_{21}(J) & A_{22}(J) \end{bmatrix} \begin{bmatrix} \boldsymbol{B}_U \\ \boldsymbol{B}_D \end{bmatrix}, \tag{7.33}$$

we can rearrange the global system of equations (7.30) to obtain two systems of equations:

$$\begin{cases} M_{11}\dot{\boldsymbol{B}}_U + A_{11}(J)\boldsymbol{B}_U + M_{12}\dot{\boldsymbol{B}}_D + A_{12}(J)\boldsymbol{B}_D = \boldsymbol{0}; \\ M_{21}\dot{\boldsymbol{B}}_U + A_{21}(J)\boldsymbol{B}_U + M_{22}\dot{\boldsymbol{B}}_D + A_{22}(J)\boldsymbol{B}_D = \boldsymbol{S}_U. \end{cases} \tag{7.34}$$

Only the first system of equation needs to be solved to find $\boldsymbol{B}_U$. Since we have no interest in computing $\boldsymbol{S}_U$ for the problem described in section 7.1, the only system of equations to solve is

$$M_{11}\dot{\boldsymbol{B}}_U + A_{11}(J)\boldsymbol{B}_U + M_{12}\dot{\boldsymbol{B}}_D + A_{12}(J)\boldsymbol{B}_D = \boldsymbol{0}. \tag{7.35}$$

This is a system of ODEs and therefore, it is a system of DAE of index 0.

We propose two strategies for solving the system of DAE of index 0:

- Direct discretization;

- Reformulation into a semi-explicit form.

Let us write $\boldsymbol{B}_U = \boldsymbol{B}$ in order to simplify the notation. The direct discretization consists in

discretizing directly

$$\boldsymbol{F}(t, \boldsymbol{B}, \dot{\boldsymbol{B}}) = M_{11}\dot{\boldsymbol{B}} + A_{11}(J)\boldsymbol{B} + M_{12}\dot{\boldsymbol{B}}_D + A_{12}(J)\boldsymbol{B}_D = \boldsymbol{0} \tag{7.36}$$

in time using a time integration scheme. The discretization of this system of DAE results in a nonlinear algebraic system of equations to be linearized using Newton's method.

For example, using a BDF time integration scheme of order k, at time $t = t_n$, we have the nonlinear system of equations

$$\boldsymbol{F}\left(t_n, \boldsymbol{B}_n, \frac{1}{\beta_0 \triangle t} \sum_{j=0}^{k} \alpha_j \boldsymbol{B}_{n-j}\right) = \boldsymbol{0}, \tag{7.37}$$

where β_0 and α_j are the coefficients of the BDF scheme, n is the time-step number, t_n is the time at time step n and $\triangle t$ is the time-step size. The vector $\boldsymbol{B}_n$ contains the DOFs at time step n, i.e.

$$\boldsymbol{B}_n = \begin{bmatrix} b_{1,n} \\ b_{2,n} \\ \vdots \\ b_{ndof,n} \end{bmatrix}, \tag{7.38}$$

where $b_{i,n} \approx b_i(t_n)$ for $i = 1, ..., ndof$.

We can reformulate the system of DAE of index 0 (7.35) as

$$\dot{\boldsymbol{B}}_U = M_{11}^{-1}\left(-A_{11}(J)\boldsymbol{B}_U - M_{12}\dot{\boldsymbol{B}}_D - A_{12}(J)\boldsymbol{B}_D\right). \tag{7.39}$$

Since M_{11} is not time dependent, $\dot{\boldsymbol{B}}_U$ only needs to be isolated once. We then discretize $\dot{\boldsymbol{B}}_U$ using a time integration scheme.

Since the system of DAE of index 0 studied in this chapter is nonlinear, the strategy of reformulation has no use. If we use an explicit method to discretize $\dot{\boldsymbol{B}}_U$ in equation (7.39), we get a nonlinear system of equations, similar to the one obtained with the direct discretization strategy. As a result, it is better to use the direct discretization strategy and avoid inverting the matrix M_{11}.

7.3.2   System of DAE of Index 1

Using the submatrices of equations (7.32) and (7.33), we define

$$\tilde{M} = \begin{bmatrix} M_{11} & M_{12} \end{bmatrix}, \tag{7.40}$$

and

$$\tilde{A}(J) = \begin{bmatrix} A_{11}(J) & A_{12}(J) \end{bmatrix}. \tag{7.41}$$

Note that $\tilde{M}$ and $\tilde{A}(J)$ are matrices of dimensions $(ndof - 2) \times ndof$. If we apply the boundary conditions as algebraic equations, we have

$$\begin{cases} \tilde{M}\dot{\boldsymbol{B}} + \tilde{A}(J)\boldsymbol{B} = \boldsymbol{0}; \\ \boldsymbol{B}_D = \boldsymbol{B}_a. \end{cases} \tag{7.42}$$

This is a nonlinear semi-explicit system of DAE of index 1 because one differentiation of the system of algebraic equations $\boldsymbol{B}_D = \boldsymbol{B}_a$ leads to a system of ODEs. The system of DAE (7.42) can also be written as

$$\begin{cases} \boldsymbol{f}(t, \boldsymbol{B}, \dot{\boldsymbol{B}}) = \boldsymbol{0}; \\ \boldsymbol{g}(t, \boldsymbol{B}_D) = \boldsymbol{0}, \end{cases} \tag{7.43}$$

where $\boldsymbol{f} = \tilde{M}\dot{\boldsymbol{B}} + \tilde{A}(J)\boldsymbol{B}$ and $\boldsymbol{g} = \boldsymbol{B}_D - \boldsymbol{B}_a$.

Since $\tilde{M}$ and $\tilde{A}$ are matrices of dimensions $(ndof - 2) \times ndof$, we propose two ways to discretize the system of DAE of index 1 in time:

- Reduction of the index;

- Direct discretization.

Reducing the index of the DAE results in a system of ODEs similar to the one obtained in the index 0 case. The same strategies can then be applied, e.g. the direct discretization. Note that when reducing the index, we need to verify that the initial conditions are consistent with the hidden constraints.

As discussed in chapter 6, BDF schemes of order k with $k < 7$ used with consistent initial conditions converge with the same order of accuracy for systems of ODEs and systems of DAE of index 1. Therefore, the system of DAE of index 1 can also be discretized directly using a BDF scheme. This yields a nonlinear system of equations:

$$\begin{cases} \boldsymbol{f}\left(t_n, \boldsymbol{B}_n, \frac{1}{\beta_0 \triangle t} \sum_{j=0}^{k} \alpha_j \boldsymbol{B}_{n-j}\right) = \boldsymbol{0}; \\ \boldsymbol{g}(t_n, \boldsymbol{B}_{D,n}) = \boldsymbol{0}, \end{cases} \tag{7.44}$$

which can be linearized using Newton's method.

When using the direct discretization strategy, we do not need to reduce the index and we do not need to verify that the initial conditions are consistent with the hidden constraints. As a result, it is more straightforward and less risky than the reduction of the index.

7.4 Code Development

We implemented a code to solve the problem described in section 7.1. We programmed the discretization in space in C and used the IDAS library for the transient solver. As discussed in chapter 6, IDAS uses the direct discretization strategy to discretize systems of DAE. As a result, the developed code does a direct discretization of the systems of DAE of index 0 and 1 described in the previous section. The implementation goes as follows:

- Discretization in space using the FEM;

- Programmation of a routine for computing the residual to be used by IDAS;

- Approximation of the Jacobian matrix using difference quotients (easier but slower);

- Selection of the parameters for the IDAS solver (absolute and relative tolerances).

7.4.1 Verification of the Code

In this section, we verify that the code developed for this project gives an accurate approximation of the solution for the equations described in section 7.1. We compare the computed approximation with an analytical solution derived by Wan [12] and described in Appendix B. Note that a similar solution was first derived by Mayergoyz [31] for the current density as the dependent variable.

A comparison between the analytic solution and the FEM approximation at time $t = 0.0025\,\text{s}$ for 40 elements is illustrated in Figure 7.3. Only the results for the index 1 case are shown but the results for the index 0 formulation are indistinguishable. We see that both solutions overlap. It therefore seems that the code gives the right approximation for a given system of equations. We note that we did not faced any issues when computing the FEM approximation for the system of DAE of index 0 and for the system of DAE of index 1. For this example, we consider the developed code as verified and we conclude that the direct discretization strategy works.
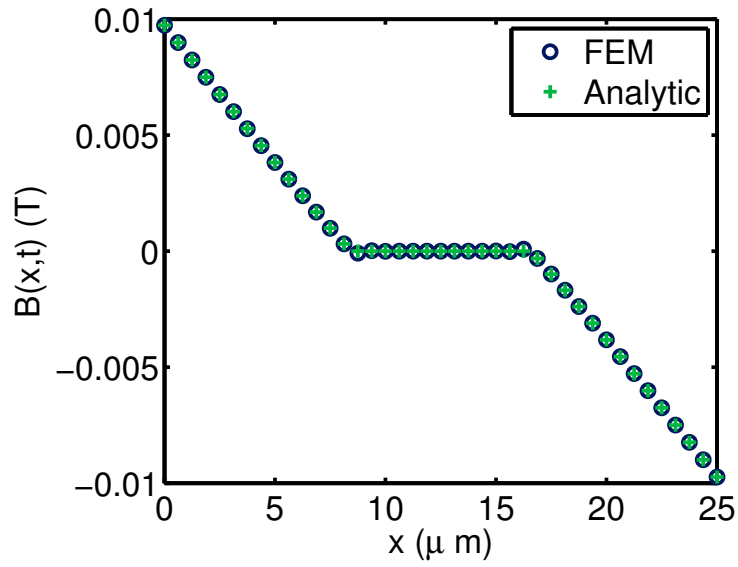
Figure 7.3 Comparisons between the analytical solution and the FEM approximation for the problem of equation (7.2) with $B(-a, t) = B_a t^p$ and $B(a, t) = -B(-a, t)$ at time $t = 0.0025s$ for 40 elements for the index 1 formulation.

CHAPTER 8

DISCRETIZATION OF HTS PROBLEMS USING EDGE ELEMENTS IN 2-D

In this chapter, we study the systems of DAE obtained from the discretization of HTS problems in space using edge elements in 2-D. For this, in section 8.1, we define a basic model for modeling HTS devices in a two-dimensional environment. In section 8.2, we give the discretization in space of the equations of the model using the FEM with edge elements. The discretization in space leads to systems of DAE. In section 8.3, we identify those systems and propose strategies to discretize them in time. Finally, in section 8.4, we describe and verify the code developed for this project. The main references used for this chapter are [4], [5], [12], [23] and [25].

8.1   Basic 2-D Model for the Study of HTS Devices

Let us consider long conductors that are surrounded by dielectrics. The conductors can be made of HTS or metal. We restrict our study to the case $\mu = \mu_0$. The conductors are so long that their electromagnetic behavior can be assumed to be constant along their length. We want to compute different electromagnetic quantities in these conductors, e.g. the current density distribution and the magnetic field strength as a function of an applied current or magnetic field.

Since the conductors are long and their electromagnetic behavior is assumed to be constant along their length, the electromagnetic quantities of interest can be computed on a cross-section and then be extrapolated to the full length of the geometry. As a result, we can model this problem using the 2-D model introduced in section 3.1.2. We recall the main characteristics of the model.

In a domain Ω and for a time interval T, we want to solve:

$$\begin{cases} \mu_0 \dfrac{\partial \boldsymbol{H}}{\partial t} + \nabla \times (\rho(\boldsymbol{J})\nabla \times \boldsymbol{H}) = \boldsymbol{0}; \\ \nabla \cdot \boldsymbol{H} = 0, \end{cases} \tag{8.1}$$

with the initial and boundary conditions:

$$\begin{cases} \boldsymbol{H}(\boldsymbol{x}, 0) = \boldsymbol{H}_0(\boldsymbol{x}); \\ \hat{\boldsymbol{n}} \times \boldsymbol{H} = \boldsymbol{f} & \text{on} \quad \Gamma_D; \\ \hat{\boldsymbol{n}} \times (\rho(\boldsymbol{J})\nabla \times \boldsymbol{H}) = \boldsymbol{g} & \text{on} \quad \Gamma_N. \end{cases} \tag{8.2}$$

The domain Ω and subdomains Ω_1 and Ω_2 are illustrated in Figure 3.2. There can be more than two subdomains. Note that we write $\rho(\boldsymbol{J})$ to show the nonlinearity but for materials that are not HTS, e.g. the air domain, ρ can be constant.

For the subdomains of Ω that represent HTS materials, we use the power law model for the resistivity:

$$\rho(\boldsymbol{J}) = \frac{E_c}{J_c} \left(\frac{||\boldsymbol{J}||_2}{J_c} \right)^{n-1} \quad \text{where} \quad \boldsymbol{J} = \nabla \times \boldsymbol{H}. \tag{8.3}$$

For other materials, we use the proper resistivity.

We make the following assumptions:

- The current density $\boldsymbol{J}$ is only flowing along the z-axis:

$$\boldsymbol{J} = J_z \hat{\boldsymbol{k}}. \tag{8.4}$$

- The magnetic field component H_z is zero and therefore

$$\boldsymbol{H} = H_x \hat{\boldsymbol{i}} + H_y \hat{\boldsymbol{j}}. \tag{8.5}$$

The boundary conditions can be used to apply a magnetic field on the device being modeled. A transport current can also be imposed in the different subdomains by adding current constraints to the set of equations. These constraints are defined as

$$I_i = \int_{\Omega_i} \nabla \times \boldsymbol{H} \, d\Omega_i, \tag{8.6}$$

for $i = 1, ..., n_c$ where n_c is the total number of constraints and Ω_i is a subset of Ω where this constraint is applied.

8.2 Discretization in Space using the FEM with Edge Elements

8.2.1 The Weak Form

Let us consider a subset V_0 of the Sobolev space $W^p(Curl : \Omega)$:

$$V_0 = \{\boldsymbol{u} \in W^p(Curl : \Omega) : \nabla \cdot \boldsymbol{u} = 0 \quad \text{on} \quad \Omega, \quad \hat{\boldsymbol{n}} \times \boldsymbol{u} = \boldsymbol{0} \quad \text{on} \quad \Gamma_D\}. \tag{8.7}$$

A thorough description of the Sobolev space $W^p(Curl : \Omega)$ can be found in [12]. The first step to obtain a weak form of the PDE in equation (8.1) is to mutiply it by a test function

$\boldsymbol{v}$ in V_0 and integrate over Ω. We have

$$\int_\Omega \mu_0 \frac{\partial \boldsymbol{H}}{\partial t} \cdot \boldsymbol{v} + \nabla \times (\rho(\boldsymbol{J})\nabla \times \boldsymbol{H}) \cdot \boldsymbol{v} \, d\Omega = 0. \tag{8.8}$$

Now, let us use the divergence theorem:

$$\int_\Omega \nabla \cdot (\boldsymbol{a} \times \boldsymbol{b}) \, d\Omega = \int_{\partial\Omega} (\boldsymbol{a} \times \boldsymbol{b}) \cdot \hat{\boldsymbol{n}} \, dS. \tag{8.9}$$

If we use the identity

$$\nabla \cdot (\boldsymbol{a} \times \boldsymbol{b}) = \boldsymbol{b} \cdot (\nabla \times \boldsymbol{a}) - \boldsymbol{a} \cdot (\nabla \times \boldsymbol{b}) \tag{8.10}$$

in equation (8.9), it yields

$$\int_\Omega \boldsymbol{b} \cdot (\nabla \times \boldsymbol{a}) \, d\Omega = \int_\Omega \boldsymbol{a} \cdot (\nabla \times \boldsymbol{b}) \, d\Omega + \int_{\partial\Omega} (\boldsymbol{a} \times \boldsymbol{b}) \cdot \hat{\boldsymbol{n}} \, dS. \tag{8.11}$$

Now, if $\boldsymbol{a} = \rho\nabla \times \boldsymbol{H}$ and $\boldsymbol{b} = \boldsymbol{v}$, we have

$$\int_\Omega \boldsymbol{v} \cdot [\nabla \times (\rho(\boldsymbol{J})\nabla \times \boldsymbol{H})] \, d\Omega = \int_\Omega \rho(\boldsymbol{J})\nabla \times \boldsymbol{H} \cdot \nabla \times \boldsymbol{v} \, d\Omega + \int_{\partial\Omega} (\rho(\boldsymbol{J})\nabla \times \boldsymbol{H} \times \boldsymbol{v}) \cdot \hat{\boldsymbol{n}} \, dS, \tag{8.12}$$

and if we replace equation (8.12) in (8.8), we get

$$\int_\Omega \mu_0 \frac{\partial \boldsymbol{H}}{\partial t} \cdot \boldsymbol{v} \, d\Omega + \int_\Omega \rho(\boldsymbol{J})\nabla \times \boldsymbol{H} \cdot \nabla \times \boldsymbol{v} \, d\Omega + \int_{\partial\Omega} (\rho(\boldsymbol{J})\nabla \times \boldsymbol{H} \times \boldsymbol{v}) \cdot \hat{\boldsymbol{n}} \, dS = 0. \tag{8.13}$$

Then, with the identity

$$(\boldsymbol{A} \times \boldsymbol{B}) \times (\boldsymbol{C} \times \boldsymbol{D}) = (\boldsymbol{A} \cdot (\boldsymbol{B} \times \boldsymbol{D}))\boldsymbol{C} - (\boldsymbol{A} \cdot (\boldsymbol{B} \times \boldsymbol{C}))\boldsymbol{D}, \tag{8.14}$$

and replacing $\boldsymbol{A}$ and $\boldsymbol{C}$ with the unit normal vector $\hat{\boldsymbol{n}}$, we have that

$$(\hat{\boldsymbol{n}} \times \boldsymbol{B}) \times (\hat{\boldsymbol{n}} \times \boldsymbol{D}) = (\hat{\boldsymbol{n}} \cdot (\boldsymbol{B} \times \boldsymbol{D}))\hat{\boldsymbol{n}}. \tag{8.15}$$

If we apply equation (8.15) in the third term of equation (8.13) with $\boldsymbol{B} = \rho\nabla \times \boldsymbol{H}$ and $\boldsymbol{D} = \boldsymbol{v}$, this yields

$$\int_\Omega \mu_0 \frac{\partial \boldsymbol{H}}{\partial t} \cdot \boldsymbol{v} \, d\Omega + \int_\Omega \rho(\boldsymbol{J})\nabla \times \boldsymbol{H} \cdot \nabla \times \boldsymbol{v} \, d\Omega + \int_{\partial\Omega} \hat{\boldsymbol{n}} \cdot [\hat{\boldsymbol{n}} \times (\rho(\boldsymbol{J})\nabla \times \boldsymbol{H}) \times (\hat{\boldsymbol{n}} \times \boldsymbol{v})] \, dS = 0. \tag{8.16}$$

Using $\boldsymbol{g} = \hat{\boldsymbol{n}} \times (\rho\nabla \times \boldsymbol{H})$, and since $\hat{\boldsymbol{n}} \times \boldsymbol{v} = 0$ on Γ_D, we have

$$\int_\Omega \mu_0 \frac{\partial \boldsymbol{H}}{\partial t} \cdot \boldsymbol{v} \, d\Omega + \int_\Omega \rho(\boldsymbol{J})\nabla \times \boldsymbol{H} \cdot \nabla \times \boldsymbol{v} \, d\Omega + \int_{\partial\Gamma_N} \hat{\boldsymbol{n}} \cdot [\boldsymbol{g} \times (\hat{\boldsymbol{n}} \times \boldsymbol{v})] \, dS = 0. \qquad (8.17)$$

For this research work, when applying Neumann boundary conditions, we want the tangential component of the electric field $\boldsymbol{E} = \rho\nabla \times \boldsymbol{H}$ to be zero at the boundary Γ_N, i.e.

$$\hat{\boldsymbol{n}} \times (\rho(\boldsymbol{J})\nabla \times \boldsymbol{H}) = \boldsymbol{g} = \boldsymbol{0} \quad \text{on} \quad \Gamma_N. \qquad (8.18)$$

As a result, the final weak form of the PDE in equation (8.1) is given by

$$\int_\Omega \mu_0 \frac{\partial \boldsymbol{H}}{\partial t} \cdot \boldsymbol{v} \, d\Omega + \int_\Omega \rho(\boldsymbol{J})\nabla \times \boldsymbol{H} \cdot \nabla \times \boldsymbol{v} \, d\Omega = 0, \quad \forall \boldsymbol{v} \in V_0. \qquad (8.19)$$

8.2.2 The Mesh

We discretize the domain Ω using *nel* triangular elements K_i for $i = 1, ..., nel$. Each element is defined using $n_g^{K_i} = 3$ geometrical nodes $X_1^{K_i}$, $X_2^{K_i}$ and $X_3^{K_i}$, and three edges, $e_1^{K_i}$, $e_2^{K_i}$ and $e_3^{K_i}$. These edges are where the elementary DOFs of the problem are computed. The length of the edges are $\ell_1^{K_i}$, $\ell_2^{K_i}$ and $\ell_3^{K_i}$, and the area of an element K_i is given by $\triangle^{K_i}$. The total number of nodes is *nnodes* and the total number of edges is *nedges*. An example of a discretized domain Ω using 16 elements is shown in Figure 8.1.
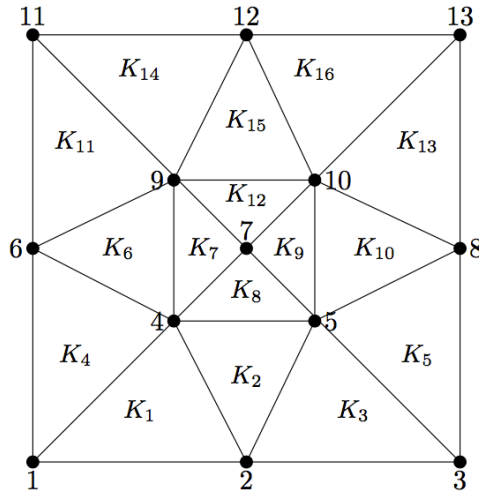
Figure 8.1 Domain Ω discretized using 16 elements. The nodes are numbered and the elements are denoted K_i for $i = 1, ..., 16$. The edges are not identified to simplify the illustration. (Source of Figure: [4])

Each edge e_i for $i = 1, ..., nedges$ is defined using the nodes $X_1^{e_i}$ and $X_2^{e_i}$. Each edge belongs to either a single element $K_1^{e_i}$ or two adjacent elements $K_1^{e_i}$ and $K_2^{e_i}$, depending if it is located at the boundary of the domain Ω or not.

The $x - y$ coordinates of each geometrical node are stored in a table called COOR. The relationship between the elements and their nodes is stored in a table called CONNEC. Examples of those tables for the mesh illustrated in Figure 8.1 are shown in Tables 8.1 and 8.2.

The information about the edges is stored in a table called EDGES. This table gives the indices of the nodes and elements associated with an edge. If the edge is on a boundary, the second element is numbered -1. An example of the table EDGES for the mesh illustrated in Figure 8.1 is shown in Table 8.3.

For the problems studied in this chapter, there is one DOF associated with each edge and, as a result, there are $n_d^K = 3$ DOFs in each element and $ndof = nedges$ DOFs in total. The DOFs h_i for $i = 1, ..., ndof$ are time-dependent approximations of the tangential component

Table 8.1 The $x - y$ coordinates of each geometrical node are stored in a table called COOR.

COOR		
Node	x coordinate	y coordinate
1	0.0	0.0
2	0.5	0.0
$\vdots$	$\vdots$	$\vdots$
13	1.0	1.0

Table 8.2 The relationship between the elements and their nodes is stored in a table called CONNEC.

CONNEC			
Element	Node #1	Node #2	Node #3
K_1	1	2	4
K_2	2	5	4
$\vdots$	$\vdots$	$\vdots$	$\vdots$
K_{16}	13	12	10

Table 8.3 The EDGES table gives the indices of the nodes and elements associated with an edge. If the edge is on a boundary, the second element is numbered -1.

EDGES				
Edge	Node #1	Node #2	Element #1	Element #2
e_1	1	2	K_1	-1
e_2	1	6	K_4	-1
$\vdots$	$\vdots$	$\vdots$	$\vdots$	$\vdots$
e_{28}	10	13	K_{13}	K_{16}

of the magnetic field along the length of an edge. We have

$$h_i(t) \approx \boldsymbol{H}(\boldsymbol{x}, t) \cdot \boldsymbol{t}_i, \tag{8.20}$$

for $i = 1, ..., ndof$, where $\boldsymbol{t}_i$ is a unit vector tangent to the edge and $\boldsymbol{H}$ is the magnetic field.

Since the DOFs associated with Dirichlet boundary conditions are known and the others are considered as unknown, we therefore have

$$\boldsymbol{H}_v = \begin{bmatrix} h_1 \\ h_2 \\ \vdots \\ h_{ndof} \end{bmatrix} = \begin{bmatrix} \boldsymbol{H}_U \\ \boldsymbol{H}_D \end{bmatrix}, \tag{8.21}$$

where $\boldsymbol{H}_v$ is the vector containing the DOFs, $\boldsymbol{H}_U$ is the vector containing the unknown DOFs and $\boldsymbol{H}_D$ is the vector containing the known DOFs. Likewise, the vectors

$$\dot{\boldsymbol{H}}_v = \begin{bmatrix} \dot{h}_1 \\ \dot{h}_2 \\ \vdots \\ \dot{h}_{ndof} \end{bmatrix} = \begin{bmatrix} \dot{\boldsymbol{H}}_U \\ \dot{\boldsymbol{H}}_D \end{bmatrix} \tag{8.22}$$

contain the time-derivatives of the DOFs.

The DOFs are numbered in a table called NUMBER. It gives the number of the DOF associated with the edge of the same index in the EDGES table. The DOFs that are unknown are numbered first, followed by the ones that are known. An example of a table NUMBER is shown in Table 8.4. Note that the last column of the table EDGES can be used to identify

which DOF is on an exterior boundary where a Dirichlet boundary condition is applied.

8.2.3 The Elementary System of Equations

Let us consider an element K. If we define

$$s^K = \hat{\boldsymbol{n}} \cdot [\hat{\boldsymbol{n}} \times (\rho \nabla \times \boldsymbol{H}) \times \hat{\boldsymbol{n}}], \tag{8.23}$$

according to equation (8.16), the weak form of the PDE in equation (8.1) on element K is

$$\int_K \mu_0 \frac{\partial \boldsymbol{H}}{\partial t} \cdot \boldsymbol{v} \, d\boldsymbol{x} + \int_K \rho(\boldsymbol{J}) \nabla \times \boldsymbol{H} \cdot \nabla \times \boldsymbol{v} \, d\boldsymbol{x} + \int_{\partial K} s^K \times \boldsymbol{v} \, dS = 0. \tag{8.24}$$

On element K, we suppose that we can approximate the magnetic field using

$$\boldsymbol{H} \approx \boldsymbol{h}^K = \sum_{j=1}^{n_d^K} h_j^K(t) \boldsymbol{N}_j^K(\boldsymbol{x}), \tag{8.25}$$

where the h_j^K are the DOFs on element K and the $\boldsymbol{N}_j^K$ are the shape functions defined on K. We therefore have

$$\sum_{j=1}^{n_d^K} \left[\dot{h}_j^K \int_K \mu_0 \boldsymbol{N}_j^K \cdot \boldsymbol{v} \, d\boldsymbol{x} + h_j^K \int_K \rho(\boldsymbol{J}) \nabla \times \boldsymbol{N}_j^K \cdot \nabla \times \boldsymbol{v} \, d\boldsymbol{x} \right] + \int_{\partial K} s^K \times \boldsymbol{v} \, dS = 0. \tag{8.26}$$

Table 8.4 The NUMBER table is used to number the DOFs. It gives the number of the DOF associated with the edge of the same index in the EDGES table.

NUMBER	
Edge	Number of the DOF
e_1	21
e_2	22
e_3	1
$\vdots$	$\vdots$
e_{28}	19

Note that $n_d^K = 3$ for the problem studied in this chapter. Taking $\boldsymbol{v} = \boldsymbol{N}_i^K$ for $i = 1, ..., n_d^K$, we get the elementary system of equations

$$M^K \dot{\boldsymbol{H}}^K + A^K(\boldsymbol{J})\boldsymbol{H}^K = \boldsymbol{S}^K, \tag{8.27}$$

where $\boldsymbol{H}_i^K = h_i^K$ is the elementary vector of the DOFs, $\dot{\boldsymbol{H}}^K$ is its derivative,

$$M_{ij}^K = \int_K \mu_0 \boldsymbol{N}_j^K \cdot \boldsymbol{N}_i^K \, d\boldsymbol{x}, \tag{8.28}$$

$$A_{ij}^K(\boldsymbol{J}) = \int_K \rho(\boldsymbol{J})\nabla \times \boldsymbol{N}_j^K \cdot \nabla \times \boldsymbol{N}_i^K \, d\boldsymbol{x}, \tag{8.29}$$

and

$$S_i^K = \int_{\partial K} \boldsymbol{s}^K \times \boldsymbol{N}_i^K \, dS, \tag{8.30}$$

for $i, j = 1, ..., n_d^K$.

8.2.4 The Reference Element

To simplify the calculations, equations (8.28) and (8.29) are discretized on a reference element $\hat{K}$. A transformation is used to transform element K into $\hat{K}$. For this project, we do not give the details of this transformation; we directly use the results on K provided by Jin in [5], as described below.

The functions $\boldsymbol{N}_j^K$ for $j = 1, 2, 3$ are the first-order edge element basis functions defined as:

$$\boldsymbol{N}_1^K(\boldsymbol{x}) = (L_1^K(\boldsymbol{x})\nabla L_2^K(\boldsymbol{x}) - L_2^K(\boldsymbol{x})\nabla L_1^K(\boldsymbol{x}))\ell_1^K; \tag{8.31}$$

$$\boldsymbol{N}_2^K(\boldsymbol{x}) = (L_2^K(\boldsymbol{x})\nabla L_3^K(\boldsymbol{x}) - L_3^K(\boldsymbol{x})\nabla L_2^K(\boldsymbol{x}))\ell_2^K; \tag{8.32}$$

and

$$\boldsymbol{N}_3^K(\boldsymbol{x}) = (L_3^K(\boldsymbol{x})\nabla L_1^K(\boldsymbol{x}) - L_1^K(\boldsymbol{x})\nabla L_3^K(\boldsymbol{x}))\ell_3^K, \tag{8.33}$$

where L_i, for $i = 1, 2, 3$, are the classical Lagrange shape functions, i.e.

$$\begin{bmatrix} L_1 \\ L_2 \\ L_3 \end{bmatrix} = \frac{1}{2\triangle^K} \begin{bmatrix} a_1^K & b_1^K & c_1^K \\ a_2^K & b_2^K & c_2^K \\ a_3^K & b_3^K & c_3^K \end{bmatrix} \begin{bmatrix} 1 \\ x \\ y \end{bmatrix}, \tag{8.34}$$

and where:

$$\begin{aligned}
a_1^K &= x_2^K y_3^K - y_2^K x_3^K, & b_1^K &= y_2^K - y_3^K, & c_1^K &= x_3^K - x_2^K; \\
a_2^K &= x_3^K y_1^K - y_3^K x_1^K, & b_2^K &= y_3^K - y_1^K, & c_2^K &= x_1^K - x_3^K; \\
a_3^K &= x_1^K y_2^K - y_1^K x_2^K, & b_3^K &= y_1^K - y_2^K, & c_3^K &= x_2^K - x_1^K,
\end{aligned} \tag{8.35}$$

the coefficient $\triangle^K$ is the area of element K, ℓ_j^K for $j = 1, 2, 3$ is the length of edge j and (x_i^K, y_i^K) are the coordinates of the nodes X_i^K for $i = 1, ..., nnodes$. According to Jin [5], we have

$$\nabla \times \boldsymbol{N}_i^K = \frac{\ell_i^K}{\triangle^K} \hat{\boldsymbol{k}}, \tag{8.36}$$

for $i = 1, 2, 3$. If we replace this result in equation (8.29), it yields

$$A_{ij}^K(\boldsymbol{J}) = \frac{\ell_j^K \ell_i^K}{(\triangle^K)^2} \int_\Omega \rho(\boldsymbol{J}) \, d\Omega \tag{8.37}$$

for $i, j = 1, 2, 3$. If the resistivity ρ is constant in space, we have that

$$A_{ij}^K = \rho \frac{\ell_j^K \ell_i^K}{\triangle^K}, \tag{8.38}$$

for $i, j = 1, 2, 3$, and if it is given by the power law, we have

$$A_{ij}^K(t) = \frac{\ell_j^K \ell_i^K}{(\triangle^K)^n} \frac{E_c}{J_c} \left| \frac{\sum_{j=1}^3 h_j^K(t) \ell_j^K}{J_c} \right|^{n-1}. \tag{8.39}$$

We show how to get this expression in Appendix C.

The calculations of the entries $M_{i,j}^K$ are more complex. According to Jin [5], we have:

$$\begin{aligned}
M_{11}^K &= \frac{\mu_0 (\ell_1^K)^2}{24 \triangle^K} (f_{22} - f_{12} + f_{11}); \\
M_{12}^K &= \frac{\mu_0 \ell_1^K \ell_2^K}{48 \triangle^K} (f_{23} - f_{22} - 2f_{13} + f_{12}); \\
M_{13}^K &= \frac{\mu_0 \ell_1^K \ell_3^K}{48 \triangle^K} (f_{21} - 2f_{23} - f_{11} + f_{13}); \\
M_{22}^K &= \frac{\mu_0 (\ell_2^K)^2}{24 \triangle^K} (f_{33} - f_{23} + f_{22}); \\
M_{23}^K &= \frac{\mu_0 \ell_2^K \ell_3^K}{48 \triangle^K} (f_{31} - f_{33} - 2f_{21} + f_{23}); \\
M_{33}^K &= \frac{\mu_0 (\ell_3^K)^2}{24 \triangle^K} (f_{11} - f_{13} + f_{33}),
\end{aligned} \tag{8.40}$$

where $f_{ij} = b_i^K b_j^K + c_i^K c_j^K$. Since M^K is symmetric, $M_{21}^K = M_{12}^K$, $M_{31}^K = M_{13}^K$ and $M_{32}^K = M_{23}^K$.

For an element K, the functions $\boldsymbol{N}_j^K$ for $j = 1, 2, 3$ are vectorial functions and therefore,

they have an orientation when evaluated on an edge e. Their orientation is counterclockwise with respect to the $x - y$ plane. Let us now consider two adjacent elements K_1 and K_2. For an edge e shared by the two elements, the two functions $\boldsymbol{N}_j^{K_1}$ and $\boldsymbol{N}_j^{K_2}$ associated with this edge have opposite signs and as a result, the approximation of the tangential component of the solution across the two elements is not continuous. To avoid this, we assign an orientation to the edges in the table EDGES, i.e. from the smaller node number to the largest, and we verify if it agrees with the orientation of the functions $\boldsymbol{N}_j^{K_1}$ and $\boldsymbol{N}_j^{K_2}$. If this is the case, there is no need to take action; if not, we multiply the functions by -1.

8.2.5   Assembly of the Global System of Equations

There is an elementary system of equations (8.27) for each element K_i for $i = 1, ..., nel$. These systems cannot be solved independently because the DOFs are shared between elements. To consider the coupling between the elements, we assemble a global system of equations

$$M\dot{\boldsymbol{H}}_v + A(\boldsymbol{J})\boldsymbol{H}_v = \boldsymbol{S}, \tag{8.41}$$

where M and A are matrices of dimensions $ndof \times ndof$, $\boldsymbol{S}$ is a vector of length $ndof$, $\boldsymbol{H}_v$ is a vector of length $ndof$ containing the DOFs and described by equation (8.21), and $\dot{\boldsymbol{H}}_v$ is the times derivative of $\boldsymbol{H}_v$.

The assembly of the global system of equations is done using a table called ADDRESS. For a given element, this table gives the number of the DOFs within the element. The numbers of the DOFs are the indices of the entries in the global system where the contributions of the elementary systems must be added. An example of this table is shown in Table 8.5 and a detailed explanation of the assembly process is given in [4]. Therefore, the entries of the matrices M and A are the added contributions of the local matrices A^{K_i} and M^{K_i} for $i = 1, ..., nel$. The components of the vector $\boldsymbol{S}$ are the added contributions of the local vectors $\boldsymbol{S}^{K_i}$ for $i = 1, ..., nel$. Note that for the problem studied in this chapter, we do not

Table 8.5 The ADDRESS table gives the number of the DOFs within an element.

ADDRESS			
Element	DOF #1	DOF #2	DOF #3
K_1	21	1	2
K_2	2	6	7
$\vdots$	$\vdots$	$\vdots$	$\vdots$
K_{16}	18	19	28

impose any jump in the approximation of the solution between the elements and the only Neumman boundary condition that we use is

$$\hat{\boldsymbol{n}} \times (\rho \nabla \times \boldsymbol{H}) = \boldsymbol{g} = \boldsymbol{0} \quad \text{on} \quad \Gamma_N. \tag{8.42}$$

As a result, the contributions to $\boldsymbol{S}$ that come from shared edges between two elements or from DOFs on Γ_N will either be zero or they will cancel out. Therefore, the vector $\boldsymbol{S}$ can be simplified as

$$\boldsymbol{S} = \begin{bmatrix} \boldsymbol{0} \\ \boldsymbol{S}_{\Gamma_D} \end{bmatrix}, \tag{8.43}$$

where $\boldsymbol{S}_{\Gamma_D}$ is a vector containing the contributions to $\boldsymbol{S}$ that come from the DOFs that are on the boundary Γ_D of Ω. The length of $\boldsymbol{S}_{\Gamma_D}$ is the same as the length of $\boldsymbol{H}_D$.

8.3 Systems of DAE

8.3.1 Dirichlet Boundary Conditions: System of DAE of Index 0

Ampere's law is used to apply an external magnetic field or a current constraint in a domain Ω if the symmetry of this domain allows it. The law is enforced using Dirichlet boundary conditions on all external boundaries of the domain. In such a case, the vector of known DOFs $\boldsymbol{H}_D$ contains as many DOFs as there are edges of elements on the boundary Γ_D. Let us write

$$M\dot{\boldsymbol{H}}_v = \begin{bmatrix} M_{11} & M_{12} \\ M_{21} & M_{22} \end{bmatrix} \begin{bmatrix} \dot{\boldsymbol{H}}_U \\ \dot{\boldsymbol{H}}_D \end{bmatrix}, \tag{8.44}$$

and

$$A(\boldsymbol{J})\boldsymbol{H}_v = \begin{bmatrix} A_{11}(\boldsymbol{J}) & A_{12}(\boldsymbol{J}) \\ A_{21}(\boldsymbol{J}) & A_{22}(\boldsymbol{J}) \end{bmatrix} \begin{bmatrix} \boldsymbol{H}_U \\ \boldsymbol{H}_D \end{bmatrix}. \tag{8.45}$$

If we replace equations (8.44) and (8.45) in the global system of equations (8.41), we have:

$$\begin{cases} M_{11}\dot{\boldsymbol{H}}_U + A_{11}(\boldsymbol{J})\boldsymbol{H}_U + M_{12}\dot{\boldsymbol{H}}_D + A_{12}(\boldsymbol{J})\boldsymbol{H}_D = \boldsymbol{0}; \\ M_{21}\dot{\boldsymbol{H}}_U + A_{21}(\boldsymbol{J})\boldsymbol{H}_U + M_{22}\dot{\boldsymbol{H}}_D + A_{22}(\boldsymbol{J})\boldsymbol{H}_D = \boldsymbol{S}_{\Gamma_D}. \end{cases} \tag{8.46}$$

The first expression in (8.46) yields $\boldsymbol{H}_U$ and therefore $\boldsymbol{H}_v$. This can be used in the second expression of (8.46) to find $\boldsymbol{S}_{\Gamma_D}$. However, for the problem considered in this chapter, we have no interest in solving for $\boldsymbol{S}_{\Gamma_D}$. As a result, the only system of equations to solve to find $\boldsymbol{H}_v$ is

$$M_{11}\dot{\boldsymbol{H}}_U + A_{11}(\boldsymbol{J})\boldsymbol{H}_U + M_{12}\dot{\boldsymbol{H}}_D + A_{12}(\boldsymbol{J})\boldsymbol{H}_D = \boldsymbol{0}. \tag{8.47}$$

This system of equations only contains differential equations; there is no algebraic equation. As a result, it is a system of ODEs, i.e. a system of DAE of index 0. This system is similar to the system of DAE of index 0 (7.34) studied in chapter 7. As a result, the same strategies for discretizing the system of DAE can be applied here.

8.3.2 Neumann Boundary Conditions: System of DAE of Index 2

Neumann boundary conditions with constraints are used to apply currents in conductors when the domain Ω is not symmetrical. In such a case, Ampere's law with Dirichet boundary conditions cannot be used to impose currents. A current constraint is defined as

$$I_i(t) = \int_{\Omega_i} \nabla \times \boldsymbol{H} d\Omega_i, \tag{8.48}$$

where i is the index of the constraint and Ω_i is the subset of Ω where the constraint is applied. There can be a total of n_c constraints. Let us define the Lagrangian

$$L = \sum_{i=1}^{n_c} \lambda_i(t) \left[\int_{\Omega_i} \nabla \times \boldsymbol{H} \, d\Omega_i - I_i(t) \right], \tag{8.49}$$

where $\lambda_i(t)$ is the Lagrange multiplier associated with the constraint i. If $\boldsymbol{H} = \boldsymbol{h} + \alpha \boldsymbol{v}$ where α is a constant, we have

$$L = \sum_{i=1}^{n_c} \lambda_i(t) \left[\int_{\Omega_i} \nabla \times (\boldsymbol{h} + \alpha \boldsymbol{v}) \, d\Omega_i - I_i(t) \right]. \tag{8.50}$$

If we add this Lagrangian to a functionnal I similar to equation (4.3) and then minimize the sum, we have

$$\frac{d}{d\alpha} \left[I + L \right] \bigg|_{\alpha=0} = 0, \tag{8.51}$$

where

$$
\begin{aligned}
\frac{dL}{d\alpha} &= \sum_{i=1}^{n_c} \lambda_i(t) \frac{d}{d\alpha} \left[\int_{\Omega_i} \nabla \times (\boldsymbol{h} + \alpha \boldsymbol{v}) \, d\Omega_i - I_i(t) \right]; \\
&= \sum_{i=1}^{n_c} \lambda_i(t) \frac{d}{d\alpha} \left[\int_{\Omega_i} \nabla \times \boldsymbol{h} \, d\Omega_i + \int_{\Omega_i} \nabla \times \alpha \boldsymbol{v} \, d\Omega_i - I_i(t) \right]; \\
&= \sum_{i=1}^{n_c} \lambda_i(t) \int_{\Omega_i} \nabla \times \boldsymbol{v} \, d\Omega_l.
\end{aligned}
\tag{8.52}
$$

This yields n_c additional terms to the weak form (8.16), i.e.

$$\int_\Omega \mu_0 \frac{\partial \boldsymbol{H}}{\partial t} \cdot \boldsymbol{v} \, d\Omega + \int_\Omega \rho \nabla \times \boldsymbol{H} \cdot \nabla \times \boldsymbol{v} \, d\Omega + \int_{\partial\Omega} \hat{\boldsymbol{n}} \cdot [\hat{\boldsymbol{n}} \times (\rho \nabla \times \boldsymbol{H}) \times (\hat{\boldsymbol{n}} \times \boldsymbol{v})] \, dS$$
$$+ \sum_{i=1}^{n_c} \lambda_i \int_{\Omega_i} \nabla \times \boldsymbol{v} \, d\Omega_i = 0. \tag{8.53}$$

As a result, for an element K in Ω_i, we have the weak form

$$\int_K \mu_0 \frac{\partial \boldsymbol{H}}{\partial t} \cdot \boldsymbol{v} \, d\boldsymbol{x} + \int_K \rho \nabla \times \boldsymbol{H} \cdot \nabla \times \boldsymbol{v} \, d\boldsymbol{x} + \int_{\partial K} \boldsymbol{s}^K \times \boldsymbol{v} \, dS + \lambda_i \int_K \nabla \times \boldsymbol{v} \, d\boldsymbol{x} = 0, \tag{8.54}$$

and the elementary system of equations is given by

$$M^K \dot{\boldsymbol{H}}^K + A^K \boldsymbol{H}^K + \boldsymbol{G}^K \lambda_i = \boldsymbol{S}^K, \tag{8.55}$$

where

$$G_i^K = \int_K \nabla \times \boldsymbol{N}_i^K \, d\boldsymbol{x}, \tag{8.56}$$

for $i = 1, ..., n_d^K$. Note that $n_d^K = 3$ for the problem studied in this chapter. According to Jin [5], $\nabla \times \boldsymbol{N}_{\boldsymbol{i}}^{\boldsymbol{K}} = \frac{\ell_i^K}{\triangle^K} \hat{\boldsymbol{k}}$ for $i = 1, 2, 3$. As a result

$$G_i^K = \frac{\ell_i^K}{\triangle^K} \int_K d\boldsymbol{x} = \ell_i^K, \tag{8.57}$$

for $i = 1, 2, 3$. The assembly process gives the global system of equations

$$M\dot{\boldsymbol{H}}_v + A(\boldsymbol{J})\boldsymbol{H}_v + \sum_{i=1}^{n_c} \boldsymbol{G}_i \lambda_i(t) = \boldsymbol{S}, \tag{8.58}$$

where M, A, $\dot{\boldsymbol{H}}_v$, $\boldsymbol{H}_v$ are the matrices and vectors of equation (8.41), $\boldsymbol{G}_i$ for $i = 1, ..., n_c$ are vectors of length $ndof$ containing the elementary contributions of $\boldsymbol{G}^{K_j}$ for $j = 1, ..., nel$. Since there are no Dirichlet boundary conditions, $\boldsymbol{S}_{\Gamma_D} = \boldsymbol{0}$ and $\boldsymbol{S} = \boldsymbol{0}$ and as a result,

$$M\dot{\boldsymbol{H}}_v + A(\boldsymbol{J})\boldsymbol{H}_v + \sum_{i=1}^{n_c} \boldsymbol{G}_i \lambda_i(t) = \boldsymbol{0}. \tag{8.59}$$

For the current constraints $I_i(t)$ for $i = 1, ..., n_c$, we have:

$$I_i(t) = \int_{\Omega_i} \nabla \times \boldsymbol{H} \, d\Omega_i = \sum_{n=1}^{nelc} \int_{K_n} \nabla \times \boldsymbol{H} \, d\boldsymbol{x}, \tag{8.60}$$

where *nelc* is the number of elements in Ω_i. Considering the approximation of $\boldsymbol{H}$ on each element K_n for $n = 1, ..., nelc$, we have

$$I_i(t) = \sum_{n=1}^{nelc} \left(\sum_{j=1}^{n_d^{K_n}} h_j^{K_n}(t) \int_{K_n} \nabla \times \boldsymbol{N}_j^{K_n} \, d\boldsymbol{x} \right), \tag{8.61}$$

which yields

$$I_i(t) = \sum_{n=1}^{nelc} \left(\sum_{j=1}^{n_d^{K_n}} h_j^{K_n}(t) \ell_j^{K_n} \right). \tag{8.62}$$

We can sum up the contribution of $I_i(t)$ using a vector $\boldsymbol{C}_i$:

$$\boldsymbol{C}_i^T \boldsymbol{H}_v = I_i(t). \tag{8.63}$$

If we add the algebraic current constraints to the global system of equations (8.59), we have

$$\begin{cases} M\dot{\boldsymbol{H}}_v + A(\boldsymbol{J})\boldsymbol{H}_v + \sum_{i=1}^{n_c} \boldsymbol{G}_i \lambda_i(t) = \boldsymbol{0}; \\ C\boldsymbol{H}_v(t) = \boldsymbol{I}(t), \end{cases} \tag{8.64}$$

where

$$C = \begin{bmatrix} \boldsymbol{C}_1^T \\ \boldsymbol{C}_2^T \\ \vdots \\ \boldsymbol{C}_{n_c}^T \end{bmatrix}, \tag{8.65}$$

$$\boldsymbol{I}(t) = \begin{bmatrix} I_1(t) \\ I_2(t) \\ \vdots \\ I_{n_c}(t) \end{bmatrix}, \tag{8.66}$$

and n_c is the number of applied constraints.

We see that the algebraic variables λ_i for $i = 1, .., n_c$ only appear in the differential equations and not in the algebraic equations. Moreover, there is only one vector $\boldsymbol{H}_v$ that is differentiated. Therefore, this system of equations is a DAE of index 2 in Hessenberg form. We recall the general nonlinear semi-explicit form of this sytem:

$$\begin{cases} \boldsymbol{p}(t, \boldsymbol{\lambda}, \boldsymbol{H}_v, \dot{\boldsymbol{H}}_v) = \boldsymbol{0}; \\ \boldsymbol{q}(t, \boldsymbol{H}_v) = \boldsymbol{0}, \end{cases} \tag{8.67}$$

where

$$\boldsymbol{\lambda} = \begin{bmatrix} \lambda_1 \\ \lambda_2 \\ \vdots \\ \lambda_{n_c} \end{bmatrix}. \tag{8.68}$$

Note that the system of DAE of index 2 (8.64) can also be written in its matrix form:

$$\begin{bmatrix} M & 0 \\ 0 & 0 \end{bmatrix} \begin{bmatrix} \dot{\boldsymbol{H}}_v \\ \dot{\boldsymbol{\lambda}} \end{bmatrix} + \begin{bmatrix} A & G \\ C & 0 \end{bmatrix} \begin{bmatrix} \boldsymbol{H}_v \\ \boldsymbol{\lambda} \end{bmatrix} = \begin{bmatrix} \boldsymbol{0} \\ \boldsymbol{I}(t) \end{bmatrix}, \tag{8.69}$$

where G is a matrix whose lines are $\boldsymbol{G}_i$ for $i = 1, ..., n_c$.

We propose two strategies to discretize the system of DAE of index 2 in time:

- Direct discretization;

- Reduction of the index.

Direct Discretization

It is possible to discretize the system of DAE of index 2 directly. As mentioned in section 6.1, the same level of accuracy can be achieved using BDF schemes for ODEs and nonlinear semi-explicit systems of DAE of index 2, under certain conditions. Such a direct discretization yields the nonlinear system of equations:

$$\begin{cases} \boldsymbol{p}\left(t_n, \boldsymbol{\lambda}, \boldsymbol{H}_{v,n}, \frac{1}{\beta_0 \triangle t} \sum_{j=0}^{k} \alpha_j \boldsymbol{H}_{v,n-j}\right) = \boldsymbol{0}; \\ \boldsymbol{q}(t_n, \boldsymbol{H}_{v,n}) = \boldsymbol{0}, \end{cases} \tag{8.70}$$

where β_0 and α_j are the coefficients of the BDF scheme, n is the time-step number, t_n is the time at time step n and $\triangle t$ is the time-step size. The vector $\boldsymbol{H}_{v,n}$ contains the DOFs at time step n, i.e.

$$\boldsymbol{H}_{v,n} = \begin{bmatrix} h_{1,n} \\ h_{2,n} \\ \vdots \\ h_{ndof,n} \end{bmatrix}, \tag{8.71}$$

where $h_{i,n} \approx h_i(t_n)$ for $i = 1, ..., ndof$. This system can be linearized using Newton's method.

Reduction of the Index

We can reduce the index of the system of DAE by differenciating its algebraic equations which yields:

$$\begin{cases} M\dot{\boldsymbol{H}}_v + A(\boldsymbol{J})\boldsymbol{H}_v + \sum_{i=1}^{n_c} \boldsymbol{G}_i \lambda_l(t) = \boldsymbol{0}; \\ C\dot{\boldsymbol{H}}_v(t) = \dot{\boldsymbol{I}}(t). \end{cases} \tag{8.72}$$

In matrix form, we can write

$$\begin{bmatrix} M & G \\ C & 0 \end{bmatrix} \begin{bmatrix} \dot{\boldsymbol{H}}_v \\ \boldsymbol{\lambda} \end{bmatrix} = \begin{bmatrix} -A\boldsymbol{H}_v \\ \dot{\boldsymbol{I}} \end{bmatrix}. \tag{8.73}$$

Nonlinearities are not written for the sake of clarity but are still present. From now on, the matrix on the left-hand side is denoted P. The matrix P is constant in time.

If we suppose that P is invertible, we write

$$P^{-1} = T = \begin{bmatrix} T_1 & T_2 \\ T_3 & T_4 \end{bmatrix}. \tag{8.74}$$

If we multiply equation (8.73) by T, we have

$$\begin{bmatrix} \dot{\boldsymbol{H}}_v \\ \boldsymbol{\lambda} \end{bmatrix} = \begin{bmatrix} T_1 & T_2 \\ T_3 & T_4 \end{bmatrix} \begin{bmatrix} -A\boldsymbol{H}_v \\ \dot{\boldsymbol{I}} \end{bmatrix}, \tag{8.75}$$

this yields the explicit system of DAE of index 1:

$$\begin{cases} \dot{\boldsymbol{H}}_v = -(T_1 A)\boldsymbol{H}_v + T_2 \dot{\boldsymbol{I}}; \\ \boldsymbol{\lambda} = -(T_3 A)\boldsymbol{H}_v + T_4 \dot{\boldsymbol{I}}. \end{cases} \tag{8.76}$$

The structure of this DAE is interesting for two reasons. First, we can solve the first equation for $\boldsymbol{H}_v$ using a time-integration scheme and then calculate $\boldsymbol{\lambda}$ with the second equation. However, in typical engineering HTS applications, we have no interest in calculating $\boldsymbol{\lambda}$ and therefore, we do not need to use the second equation. Second, we only need to invert the matrix P once at the beginning of the solving process. As a result, the problem is reduced to the system of ODEs

$$\dot{\boldsymbol{H}}_v = -(T_1 A)\boldsymbol{H}_v + T_2 \dot{\boldsymbol{I}}. \tag{8.77}$$

We can reduce the index of the system of DAE to zero by differentiating the second equation in (8.76). Performing this operation does not affect the first expression in (8.76). As a result, equation (8.77) can still be used to find $\boldsymbol{H}_v$ and reducing the index to zero has no added value.

With the information that we have, we cannot conclude if the strategy of direct discretization is better than the strategy of reduction of the index. However, when reducing the index, we need to do additional mathematical manipulations such as inverting the matrix P. This is a downside of this strategy.

8.4 Code Development

We implemented a code for the basic 2-D model described in section 8.1. The code was written by Dubois [32] and the candidate for this M.Sc. project. It can be summarized as follows:

- Discretization in space using the FEM;

- Programming of a routine for computing the residuals for IDAS;

- Approximation of the Jacobian matrix using difference quotients (easier but slower);

- Selection of the parameters of the solver (absolute and relative tolerances).

The transient solver IDAS uses the direct discretization strategy.

In the following subsections, we verify that the code gives the right solution for these three types of problems:

- System of DAE of index 0 with one domain;

- System of DAE of index 0 with multiple subdomains;

- System of DAE of index 2 in Hessenberg form with multiple subdomains.

8.4.1 System of DAE of Index 0 with One Domain: Verification of the Code Using Bessel's Equation

We consider the circular two-dimensional cross-section of a conductor shown in Figure 8.2. On this domain, we want to solve equations (8.1) for $\rho = 1\,\Omega\text{m}$ and $\mu_0 = 1\ \text{N/A}^2$ for convenience. Initial and boundary conditions are given by:

$$\begin{cases} \boldsymbol{H}(\boldsymbol{x}, 0) = \mathrm{J}_1(a \cdot ||\boldsymbol{x}||); \\ \hat{\boldsymbol{n}} \times \boldsymbol{H} = e^{-a^2 t} \hat{\boldsymbol{k}}, \qquad \text{on } \Gamma_D, \end{cases} \tag{8.78}$$

where J_1 is the Bessel function of the first kind and a is its first roots.
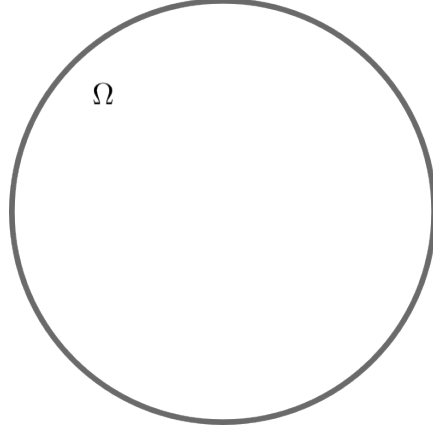
Figure 8.2 Circular 2-D cross section of a conductor.

There is a known analytical solution to this problem. Using the identity

$$\nabla \times \nabla \times \boldsymbol{H} = \nabla(\nabla \cdot \boldsymbol{H}) - \nabla^2 \boldsymbol{H}, \tag{8.79}$$

and the second equation of expression (8.1), we have

$$\frac{\partial \boldsymbol{H}}{\partial t} - \nabla^2 \boldsymbol{H} = 0. \tag{8.80}$$

Because of the symmetry of the problem in cylindrical coordinates, we can make the following assumptions:

$$H_z = H_r = \frac{\partial \boldsymbol{H}}{\partial \phi} = \frac{\partial \boldsymbol{H}}{\partial z} = 0, \tag{8.81}$$

which yields

$$\frac{\partial H_\phi}{\partial t} - \frac{\partial}{\partial r}\left[\frac{1}{r}\frac{\partial}{\partial r}(rH_\phi)\right] = 0, \tag{8.82}$$

and a few additional steps give us

$$r^2\frac{\partial^2 H_\phi}{\partial r^2} + r\frac{\partial H_\phi}{\partial r} = H_\phi + r^2\frac{\partial H_\phi}{\partial t}. \tag{8.83}$$

We propose a solution of the form:

$$H_\phi(r, t) = R(r)\exp(-a^2 t). \tag{8.84}$$

By replacing equation (8.84) in equation (8.83), we obtain Bessel's differential equation:

$$r^2\frac{d^2 R(r)}{dr^2} + r\frac{dR(r)}{dr} + ((ra)^2 - 1)R(r) = 0. \tag{8.85}$$

According to Arfken and Weber [33], the general solution to this equation is

$$R(r) = C_1 \mathrm{J}_\nu(a \cdot r) + C_2 N_\nu(a \cdot r), \tag{8.86}$$

where C_1 and C_1 are constants, N_ν is the Bessel function of the second kind and ν is the integral order of the Bessel functions. The function N_ν is unbounded at the origin. Since we want the solution to be finite at the origin, we exclude N_ν from the general solution and we have

$$R(r) = C_1 \mathrm{J}_\nu(a \cdot r). \tag{8.87}$$

Finally, using the initial and boundary conditions, we find the particular solution:

$$H_\phi(r, t) = \mathrm{J}_1(a \cdot r) \exp(-a^2 t). \tag{8.88}$$

The numerical approximation of H_ϕ computed at $t = 0.1$ s is shown at the top of Figure 8.3. The analytical solution is illustrated at the bottom of Figure 8.3. The problem has been discretized using a mesh of 542 elements and 837 edges, illustrated in Figure 8.4.

From Figure 8.3, the linear edge elements give a good approximation of the analytical solution of Bessel's problem. A cross section ($\phi = 0$) of the solution and its approximation, illustrated in Figure 8.5, shows that the approximation is better when it is nearly linear; the numerical approximation is not as good close to the boundaries.

There are two factors that can explain the discrepancies observed between the discrete approximation and the continuous solution. If we look at the mesh in Figure 8.4, there are approximately two elements between $r = 0.35$ m and $r = 0.481$ m, where the discrepancies are observed. We mentioned previously in this chapter that the shape functions that we use are linear. Therefore, it is expected that the approximation of the solution cannot flawlessly approximate the solution when this latter is not linear, specifically, with two elements. Moreover, we mentioned in section 4.1.3 of chapter 4 that the normal component of the field approximated using edge elements is not continuous between two elements. Therefore, nothing guarantees the continuity of H_ϕ between two elements, unless it is exactly tangential to an edge between two elements.
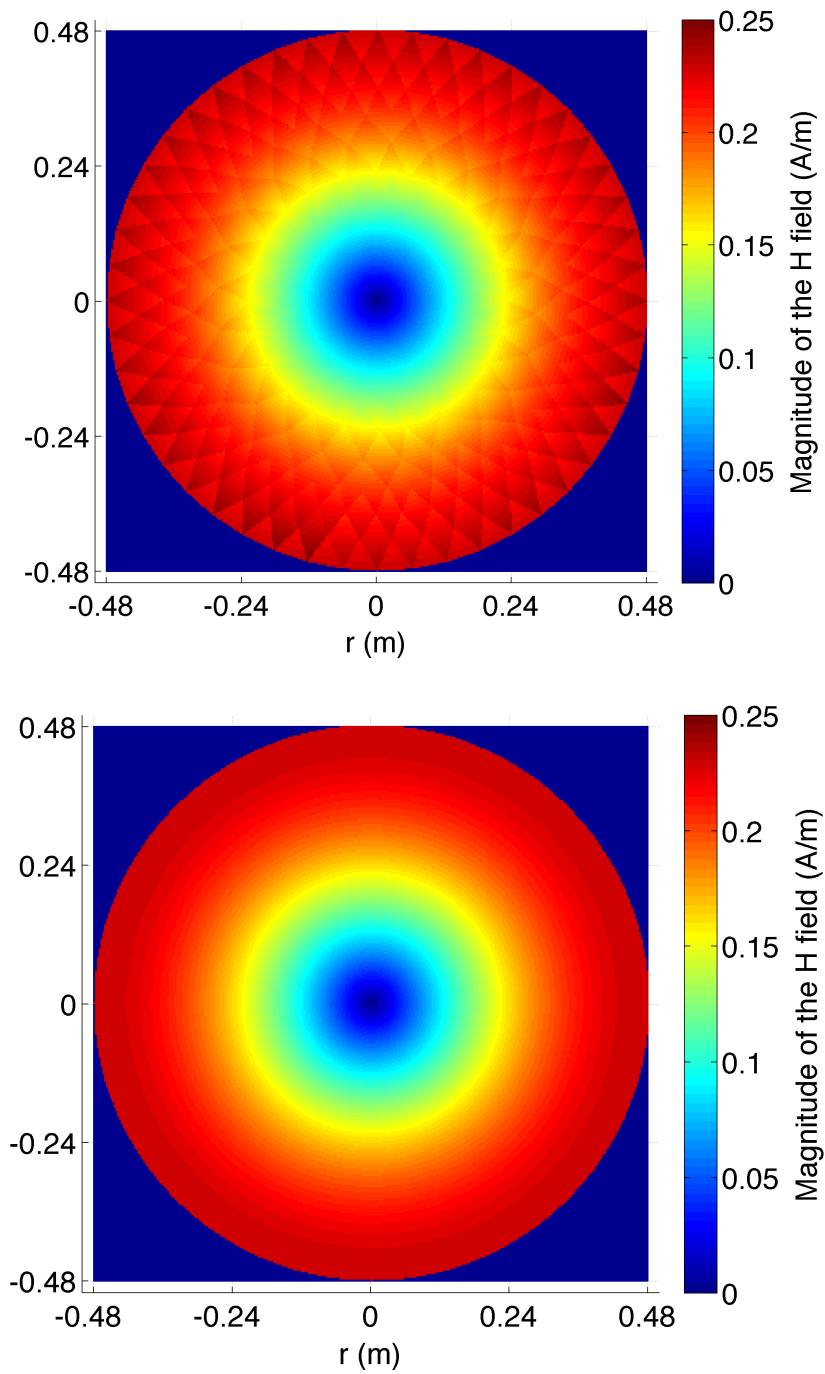
Figure 8.3 Numerical (top) and analytical solutions (bottom) to Bessel's problem at $t = 0.1$ s obtained with a mesh of 542 elements and 837 edges. The Figure shows the magnitude of the H field.

Figure 8.4 Mesh composed of 542 elements and 837 edges used to compute the numerical solution to Bessel's problem.
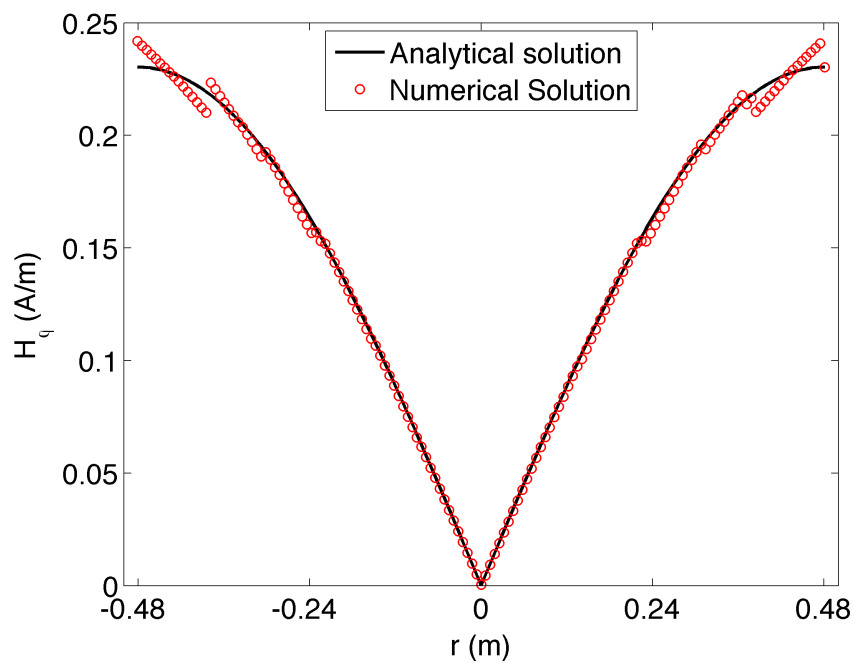
Figure 8.5 Analytical and numerical solutions for Bessel's problem at $t = 0.1$ s and $\phi = 0$. The numerical solution was computed using 542 elements and 837 edges.

We can get a better approximation by refining the mesh where the solution is not linear. Using a mesh made of 2178 elements and 3367 edges, illustrated in Figure 8.6, we get the approximation shown at the top of Figure 8.7. The bottom of Figure 8.7 shows the solution and the approximation at $\phi = 0$. We see that the approximation is better when there are more elements to approximate the solution.

Let us consider uniform meshes. If we compute the error in the L^2-norm, i.e.

$$||\boldsymbol{E}||_{L^2} = ||\boldsymbol{h} - \boldsymbol{H}||_{L^2} = \left(\int_{\Omega} (\boldsymbol{h} - \boldsymbol{H}) \cdot (\boldsymbol{h} - \boldsymbol{H}) d\Omega \right)^{\frac{1}{2}}, \tag{8.89}$$

as a function of the minimum element size, we observe that the numerical approximation converges to the solution of the continuous problem, as shown in Figure 8.8. Note that we cannot conclude on the rate of convergence using the L^2-norm.
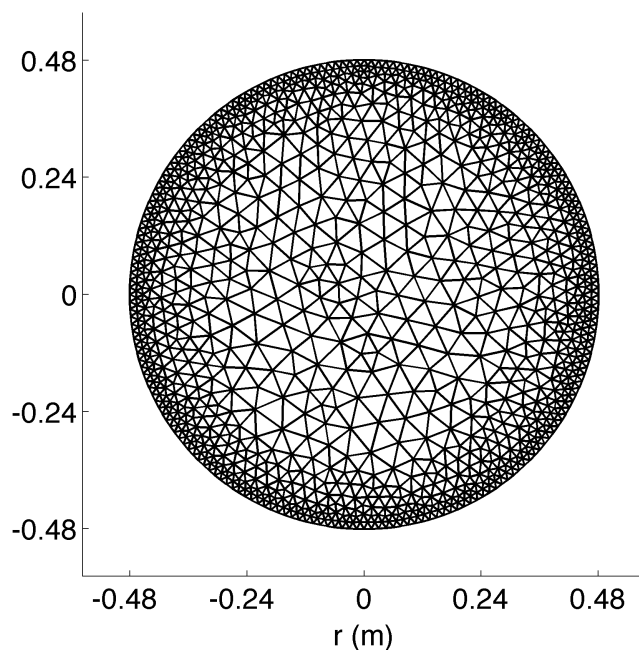
Figure 8.6 Refined mesh composed of 2178 elements and 3367 edges used to compute the numerical solution to Bessel's problem.

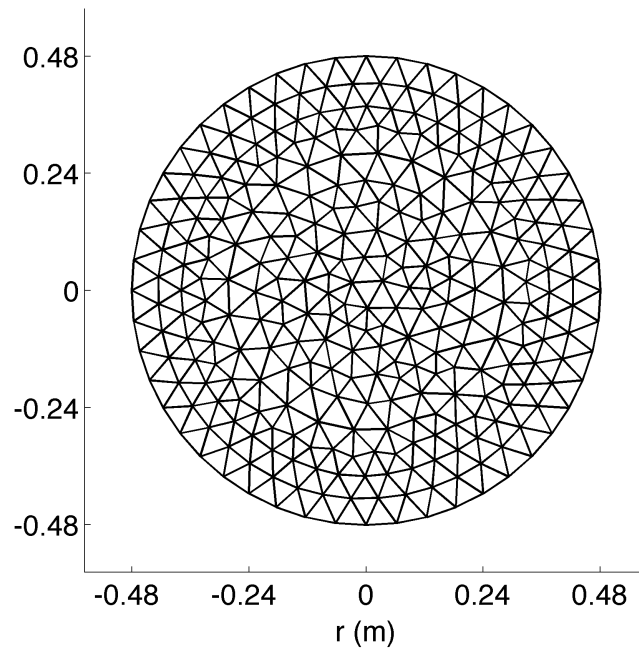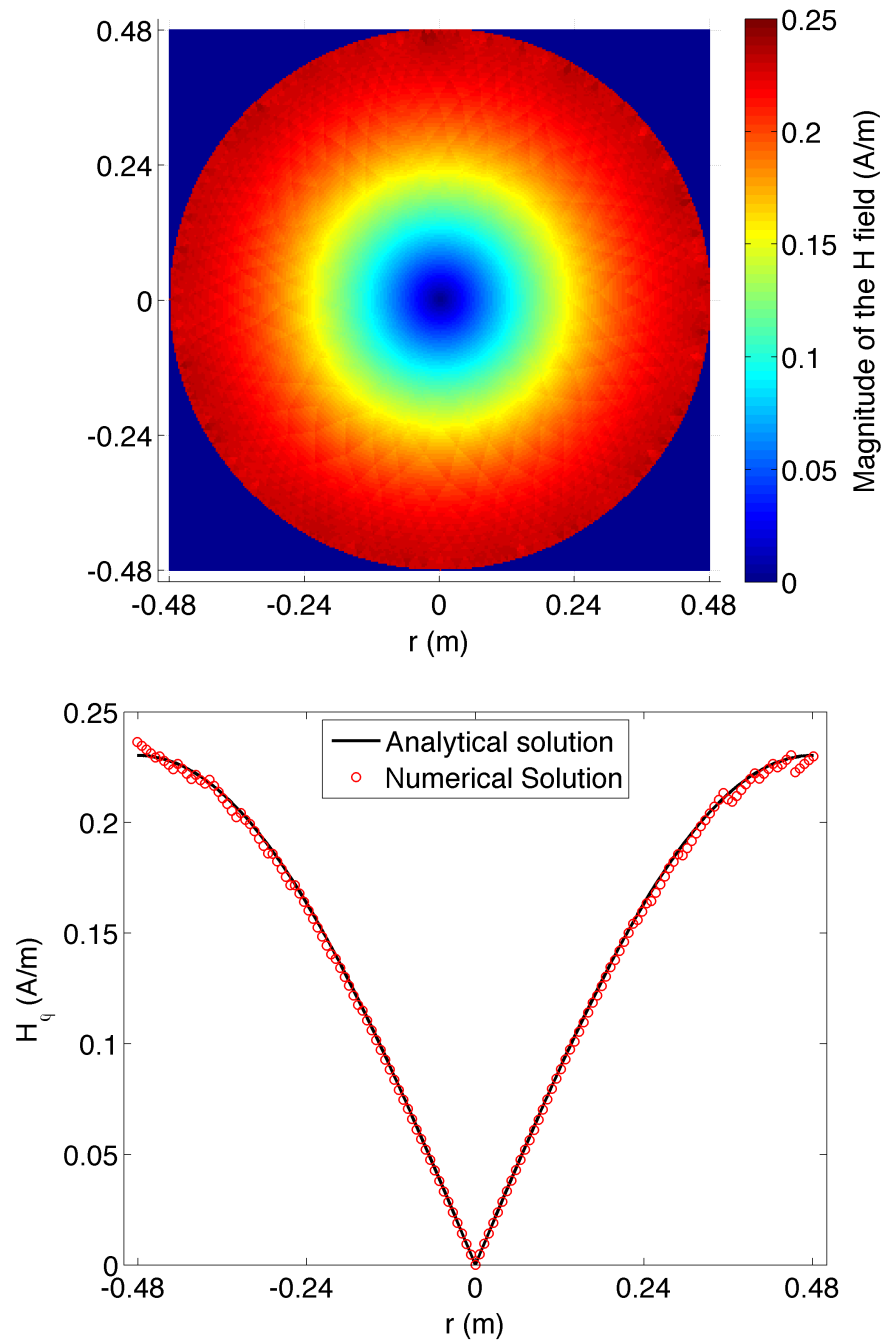Figure 8.7 At the top, the numerical approximation to Bessel's problem at $t = 0.1$ s obtained with a mesh of 2178 elements and 3367 edges. At the bottom, the analytical and numerical solutions for Bessel's problem at $\phi = 0$.
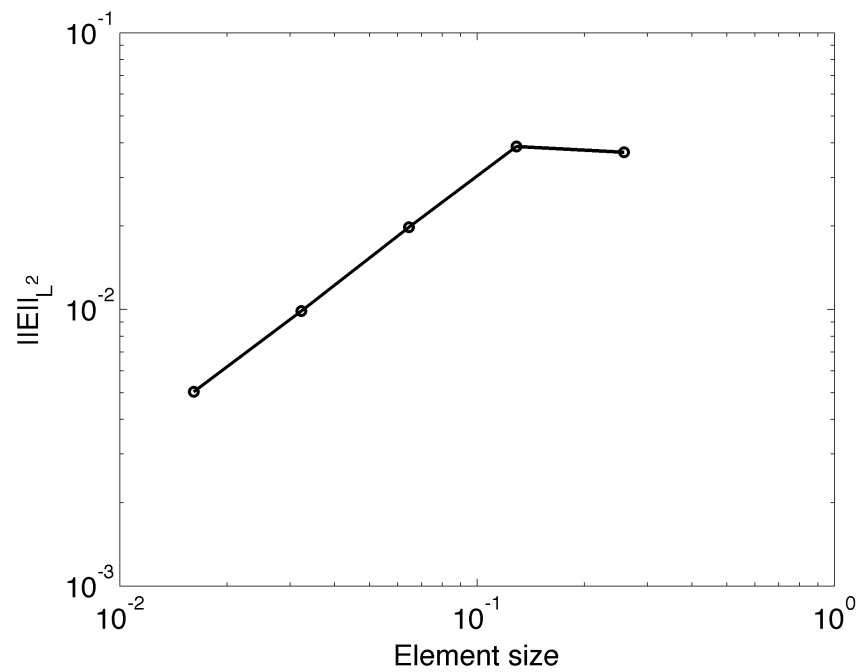
Figure 8.8 Error computed in the L^2-norm as a function of the size of the elements.

8.4.2 System of DAE of Index 0 with Multiple Subdomains: Verification of the Code Using Ampere's Law

In this subsection, we verify the code for a system of DAE of index 0 with multiple subdomains using Ampere's law and physical parameters. We consider a circular conductor inside a circular air domain, as shown in Figure 8.9 (not to scale). The conductor is made of copper with resistivity $1.68 \cdot 10^{-8}$ Ωm inside an air domain with resistivity 1.0 Ωm. The radius of the copper conductor is 0.1 m and the radius of the air domain is 1 m. The parameters for this problem are summarized in Table 8.6.

We want to impose a current in the copper conductor. The imposed current is given by the piecewise function

$$I(t) = \begin{cases} 0, & t = 0 \text{ s}; \\ 10t^2, & 0 < t \leq 1 \text{ s}; \\ 10, & t > 1 \text{ s}. \end{cases} \tag{8.90}$$

According to Ampere's law, the total current flowing in a 2-D domain is equivalent to the
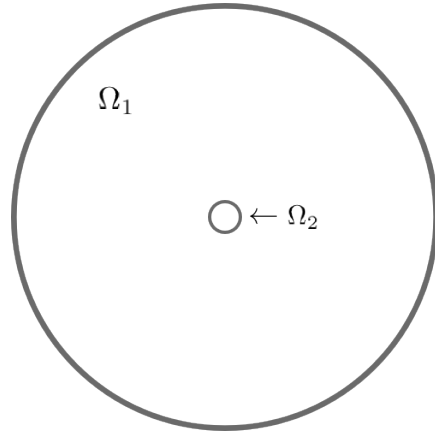
Figure 8.9 Circular conductor (Ω_2) inside of a circular domain (Ω_1) filled with air.

Table 8.6 Parameters for the Ampere's law problem.

ρ_{Ω_1}	$1.68 \cdot 10^{-8}$ Ωm
ρ_{Ω_2}	1 Ωm
μ_0	$4\pi \cdot 10^{-7}$ N/A^2
Radius of the domain Ω_1	1 m
Radius of the domain Ω_2	0.1 m

closed path integral of the magnetic field tangential to the contour of that region:

$$\oint \boldsymbol{H} \cdot d\boldsymbol{s} = I. \tag{8.91}$$

This equality and the definition of $I(t)$ give the boundary and initial conditions of the problem:

$$\boldsymbol{H}(\boldsymbol{x}, 0) = \boldsymbol{0}, \tag{8.92}$$

and

$$\hat{\boldsymbol{n}} \times \boldsymbol{H} = \begin{cases} \dfrac{10t^2}{C} & \text{on} \quad \Gamma_D \times]0, 1]; \\ \dfrac{10}{C} & \text{on} \quad \Gamma_D \times [1, T]. \end{cases} \tag{8.93}$$

For $t \gg 1\,\text{s}$, we expect the current to be distributed uniformly inside the copper conductor. A steady-state analytical solution can be obtained for H_ϕ using Ampere's law:

$$H_\phi(r) = \begin{cases} \dfrac{rI}{2\pi r_{conduc}^2}, & r \leq 0.1; \\ \dfrac{I}{2\pi r}, & r > 0.1. \end{cases} \tag{8.94}$$

Figure 8.10 shows the numerical approximation of H_ϕ as a function of the radius of the domain plotted on top of the analytical solution at $t = 10$ s. The mesh used consists of 1156 elements and 1758 edges. As discussed in section 8.4.1, the numerical solution gives a good approximation of the analytical solution but it is less accurate where the magnetic field is not linear. Again, this can be explained by the fact that the shape functions are linear and because the normal component of the magnetic field is not necessarily continuous between two elements.

8.4.3 System of DAE of Index 2 with Multiple Subdomains: Verification of the Code Using Ampere's Law

The objective of this section is to verify that the implemented code can properly discretize systems of DAE of index 2 in Hessenberg form with multiple domains. The problem under study is similar to the problem described in the previous subsection. The main difference is that instead of applying the current in the conductor using Ampere's law, we apply it directly as a current constraint using Neumann boundary conditions and Lagrange multipliers.

Using a mesh of 1156 elements and 1758 edges, we get the solution shown in Figure 8.11. We see that this solution is similar to the one computed with the Dirichlet boundary condi-

Figure 8.10 Numerical approximation of H_ϕ as a function of the radius of the domain plotted on top of the analytical solution for the copper conductor inside the air domain at $t = 10$ s. This approximation was obtained after the discretization in time of the system of DAE of index 0.

tions in section 8.4.2, i.e. the system of DAE of index 0. It gives a good approximation of the solution but there are some discrepancies where the magnetic field is not linear. The causes of those discrepancies are the same as the ones discussed for the Bessel problem.
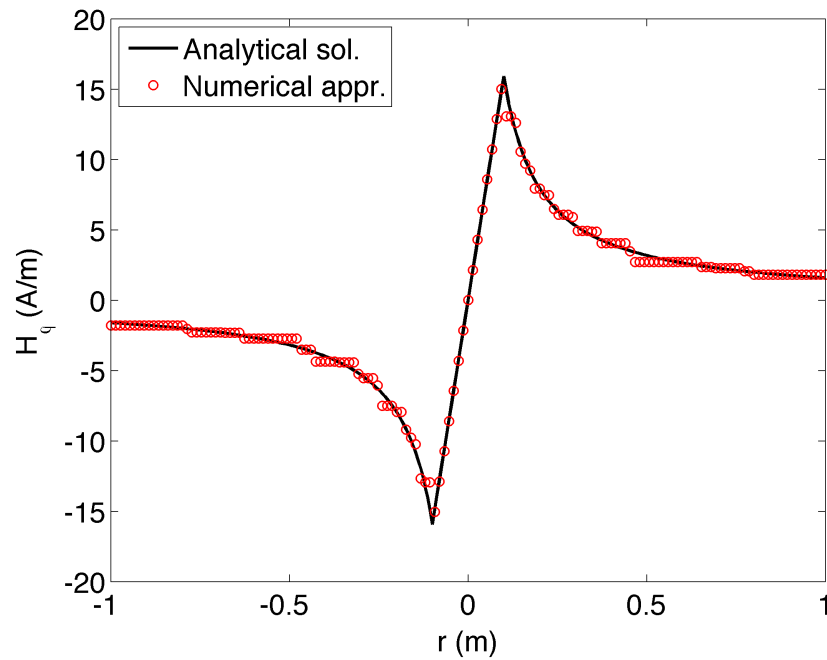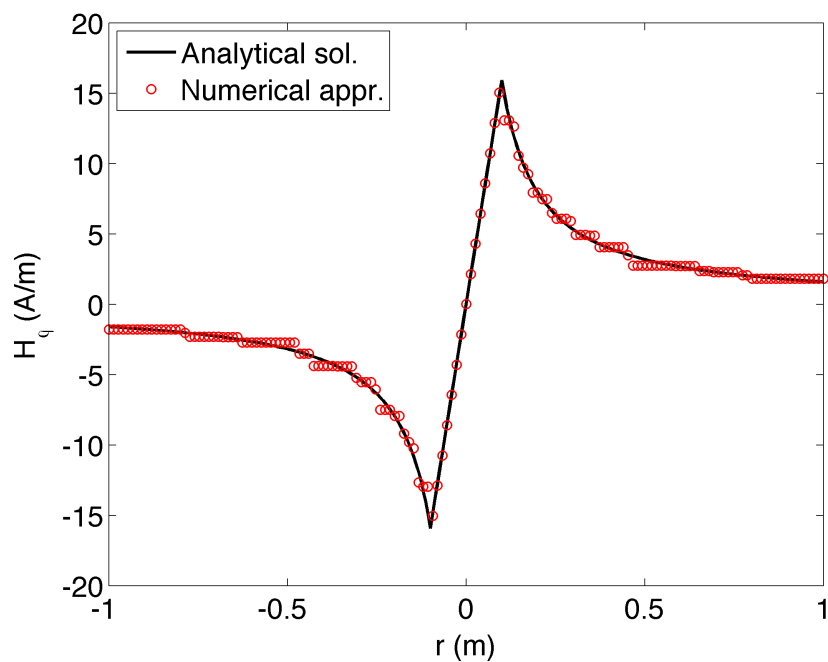
Figure 8.11 Numerical solution for H_ϕ as a function of the radius of the domain plotted on top of the analytical solution for the copper conductor inside the air domain at $t = 10$ s. This approximation was obtained after the discretization in time of the system of DAE of index 2.

CHAPTER 9

DISCRETIZATION OF HTS PROBLEMS USING THE SAM

In this chapter, we study systems of DAE obtained from the discretization in space of HTS problems using the Semi-Analytical Method (SAM). In section 9.1, we describe a typical problem for HTS devices that we discretize with the $\boldsymbol{A} - V$ formulation in integral form. We then give, in section 9.2, the discretization in space of the equations and we identify the resulting systems of DAE. We also propose various strategies to discretize these systems in time. Finally, in section 9.3, we investigate the use of the proposed strategies with a simple problem with a manufactured solution. The main references used for this chapter are [6], [26] and [27].

Note that the simple problem studied in this chapter is purely investigative. It serves as an introduction to the discretization of systems of DAE in time.

9.1 Typical Problem

We want to compute electromagnetic quantities of interest for a HTS device. The HTS device is either voltage or current driven and it is not made of ferromagnetic materials. The electromagnetic properties of the device can be assumed to be constant along its length. There exists an analytical expression to compute the integral (3.13) for the magnetic vector potential on a cross-section of its geometry.

We can solve this problem using an $\boldsymbol{A} - V$ formulation in integral form, introduced in section 3.2. We recall the main aspects of this model. Let us consider a 2-D domain Ω with subdomains Ω_i for $i = 1, ..., k$, where k is the total number of subdomains. We want to solve the following equation for $\boldsymbol{J}$:

$$\rho \boldsymbol{J} = -\frac{\partial}{\partial t} \left[\frac{\mu_0}{4\pi} \int_\Omega \boldsymbol{J} \log |\boldsymbol{r} - \boldsymbol{r}'| \, d\Omega \right] - \nabla V, \tag{9.1}$$

where ρ is the resistivity which is modeled using a power law for HTS, $r = x\hat{\boldsymbol{i}} + y\hat{\boldsymbol{j}}$ is the position vector and ∇V is the electric potential gradient.

The subdomains Ω_i can be conductors that are either driven by a current source or by a voltage source. For each subdomain that is driven by a current source, a current constraint that is a function of the current density $\boldsymbol{J}$ must be added to equation (9.1). This constraint

is given by

$$I_i = \int_{\Omega_i} \boldsymbol{J} \, d\Omega_i. \tag{9.2}$$

for $i = 1, ..., n_c$ where i is the index of the constraint, n_c is the total number of current constraints and Ω_i is the subset of Ω in which the constraint is applied. Note that the voltages of each current driven conductors, i.e. V_i for $i = 1, ..., n_c$, are unknown and constant in the $x - y$ plane. For the case of voltage driven conductors, the expression ∇V in equation (9.1) is known and as a result, equation (9.1) only needs to be solved for $\boldsymbol{J}$.

9.2 Systems of DAE

The discretization in space of the $\boldsymbol{A} - V$ formulation using the SAM is documented in [6], [15] and [16]. Therefore, it will not be explained in detail. Note that this method is briefly described in section 4.2.

The discretization yields the system of equations

$$M_A \dot{\boldsymbol{J}}_v - \Lambda_\rho(\boldsymbol{J}) \boldsymbol{J}_v - D\boldsymbol{V} = 0. \tag{9.3}$$

where $\boldsymbol{J}_v$ is not the local continuous current density but a vector containing the DOFs J_i for $i = 1, .., n$ at each computation node of the mesh, M_A is a dense invertible matrix of size $n \times n$ and Λ_ρ is a diagonal matrix of size $n \times n$ containing the resistivity associated with each DOF. The vector $\boldsymbol{V}$ contains the DOFs V_i for $i = 1, ..., nbcond$, where $nbcond$ is the number of conductors and D is a matrix of size $n \times nbcond$. Depending on how this problem is driven, the system to solve is either a system of DAE of index 0 or 2. Note that not all the entries of Λ_ρ depend on $\boldsymbol{J}$. If a DOF is in a conductor that has a constant resistivity, e.g. copper, the associated entry in Λ_ρ is constant.

9.2.1 System of DAE of index 0

In the case of a voltage driven problem, the system of equations to solve is

$$M_A \dot{\boldsymbol{J}}_v - \Lambda_\rho(\boldsymbol{J}) \boldsymbol{J}_v = D\boldsymbol{V}. \tag{9.4}$$

This system of equations only contains differential equations. As a result, it is a system of DAE of index 0, i.e. a system of ODEs. We propose two different strategies to discretize this system of DAE in time, i.e. by direct discretization of by reformulation. Let us write the

system of DAE of index 0 in residual form:

$$\boldsymbol{F}(t, \boldsymbol{J}_v, \dot{\boldsymbol{J}}_v) = M_A \dot{\boldsymbol{J}}_v - \Lambda_\rho(\boldsymbol{J})\boldsymbol{J}_v - D\boldsymbol{V} = \boldsymbol{0}. \tag{9.5}$$

If we discretize the system of DAE directly using a BDF time-integration scheme, we have the nonlinear system of equations

$$\boldsymbol{F}\left(t_m, \boldsymbol{J}_{v,m}, \frac{1}{\beta_0 \triangle t} \sum_{j=0}^{k} \alpha_j \boldsymbol{J}_{v,m-j}\right) = \boldsymbol{0}, \tag{9.6}$$

where m is the time-step number, t_m is the time at time step m, $\triangle t$ is the time-step size, and β_0 and α_j are the coefficients of the BDF scheme. The vector $\boldsymbol{J}_{v,m}$ contains an approximation of the DOFs at time step m, i.e.

$$\boldsymbol{J}_{v,m} = \begin{bmatrix} J_{1,m} \\ J_{2,m} \\ \vdots \\ J_{n,m} \end{bmatrix}, \tag{9.7}$$

where $J_{i,m} \approx J_i(t_m)$ for $i = 1, ..., n$. This nonlinear system of equations can be linearized using Newton's method.

It is also possible to reformulate the system of DAE of index 0 in semi-explicit form by isolating $\dot{\boldsymbol{J}}_v$:

$$\dot{\boldsymbol{J}}_v = M_A^{-1}\left(\Lambda_\rho(\boldsymbol{J})\boldsymbol{J} + D\boldsymbol{V}\right). \tag{9.8}$$

We then discretize $\dot{\boldsymbol{J}}_v$ using an explicit method. However, this strategy is not recommended since we need to invert M_A, a dense matrix and because the problem is nonlinear.

9.2.2 System of DAE of Index 2 in Hessenberg Form

If the problem is current driven, we need to add n_c current constraints I_i for $i = 1, ..., n_c$ to the system of equations (9.3). Those current constraints are given by

$$I_i = \int_{\Omega_i} \boldsymbol{J}\, d\Omega_i = \boldsymbol{C}_i^T \boldsymbol{J}_v \tag{9.9}$$

where $\boldsymbol{C}_i$ is a vector obtained from the discretization of the integral for I_i. As a result, the system of equations to solve is:

$$\begin{cases} M_A \dot{\boldsymbol{J}}_v - \Lambda_\rho(\boldsymbol{J})\boldsymbol{J}_v - D\boldsymbol{V} = 0; \\ C\boldsymbol{J}_v = \boldsymbol{I}, \end{cases} \tag{9.10}$$

where C is a matrix whose lines are given by the vectors $\boldsymbol{C}_i$ for $i = 1, ..., n_c$ and $\boldsymbol{I}$ is a vector containing the constraints I_i for $i = 1, ..., n_c$. In matrix form, we have

$$\begin{bmatrix} M_A & 0 \\ 0 & 0 \end{bmatrix} \begin{bmatrix} \dot{\boldsymbol{J}}_v \\ \dot{\boldsymbol{V}} \end{bmatrix} - \begin{bmatrix} \Lambda_\rho(\boldsymbol{J}) & D \\ -C & 0 \end{bmatrix} \begin{bmatrix} \boldsymbol{J}_v \\ \boldsymbol{V} \end{bmatrix} = \begin{bmatrix} \boldsymbol{0} \\ \boldsymbol{I} \end{bmatrix}. \tag{9.11}$$

We see that the the vector $\boldsymbol{V}$ only appears in the differential equations and not in the algebraic equations. Moreover, we see that there is only one vector, $\boldsymbol{J}_v$ with the time derivative $\dot{\boldsymbol{J}}_v$. Therefore, this system of equations is a system of DAE of index 2 in Hessenberg form:

$$\begin{cases} \boldsymbol{q}(t, \boldsymbol{V}, \boldsymbol{J}_v, \dot{\boldsymbol{J}}_v) = \boldsymbol{0}; \\ \boldsymbol{p}(t, \boldsymbol{J}_v) = \boldsymbol{0}. \end{cases} \tag{9.12}$$

This system of DAE of index 2 in Hessenberg form has the same structure as the one studied in the previous chapter. We recall this system of equations for comparison purpose without assigning new variables:

$$\begin{bmatrix} M & 0 \\ 0 & 0 \end{bmatrix} \begin{bmatrix} \dot{\boldsymbol{H}}_v \\ \dot{\boldsymbol{\lambda}} \end{bmatrix} + \begin{bmatrix} A(\boldsymbol{J}) & G \\ C & 0 \end{bmatrix} \begin{bmatrix} \boldsymbol{H}_v \\ \boldsymbol{\lambda} \end{bmatrix} = \begin{bmatrix} \boldsymbol{0} \\ \boldsymbol{I} \end{bmatrix}. \tag{8.69}$$

We see that the voltage vector $\boldsymbol{V}$ plays the role of the Lagrange multipliers contained in $\boldsymbol{\lambda}$.

Since the two systems of equations have the same structure, the same strategies can be applied, i.e the direct discretization and the reduction of the index. The reformulation of the system of DAE and the reduction of the index are investigated in the next section. Note that this investigation serves as an introduction to the discretization of systems of DAE in time.

9.3   Investigation of the Proposed Strategies

In this section, we investigate some of the proposed strategies with a simple problem for which we built a manufactured solution. We wrote a code to investigate the two following strategies:

- System of DAE of index 2 in Hessenberg form discretized directly;

- Reduction of the index from 2 to 1 for a system of DAE of index 2 in Hessenberg form and then reformulated in a semi-explicit form.

9.3.1 System of DAE of Index 2 in Hessenberg Form Discretized Directly

The problem and manufactured solution go as follows. Let us consider the system of DAE of index 2 in Hessenberg form:

$$\begin{cases} M_A \dot{\boldsymbol{x}} = \Lambda_\rho \boldsymbol{x} + D\boldsymbol{z}; \\ 0 = C\boldsymbol{x} - \boldsymbol{I}, \end{cases} \tag{9.13}$$

where the entries of Λ_ρ are constant in space and time. If we isolate $\boldsymbol{x}$ by inverting M_A, we then have:

$$\begin{cases} \dot{\boldsymbol{x}} = -M_A^{-1} \left(\Lambda_\rho \boldsymbol{x} + D\boldsymbol{z} \right); \\ 0 = C\boldsymbol{x} - \boldsymbol{I}, \end{cases} \tag{9.14}$$

where $\boldsymbol{x}$ and $\boldsymbol{z}$ are vectors containing the DOFs $x_i(t)$ and $z_j(t)$ for $i = 1, ..., n$ and $j = 1, ..., n_c$. If $n = 2$ and $n_c = 1$, and if all the entries of Λ_ρ are constant, we have the simple system:

$$\begin{cases} \dot{x}_1 = a_1 x_1 + a_2 x_2 + a_3 z; \\ \dot{x}_2 = b_1 x_1 + b_2 x_2 + b_3 z; \\ I = s_1 x_1 + s_2 x_2, \end{cases} \tag{9.15}$$

where a_i and b_j for $i, j = 1, 2, 3$ are constant entries coming from the product $M_A^{-1}\Lambda_\rho$ or $M_A^{-1}D$ and s_1 and s_2 are the values in C.

Let us consider the manufactured solution:

$$\begin{cases} x_1 = A\sin(\omega t); \\ x_2 = B\sin(\omega t); \\ z = C\sin(\omega t), \end{cases} \tag{9.16}$$

where ω is an arbitrary angular frequency, and A, B and C are arbitrary constants. For the manufactured solution to be a solution to the system of equations (9.15), we need to add two functions to the first two equations of system (9.15), i.e.

$$f_1(t) = A\omega\cos(\omega t) - a_1 A\sin(\omega t) - a_2 B\sin(\omega t) - a_3 C\sin(\omega t), \tag{9.17}$$

and

$$f_2(t) = B\omega\cos(\omega t) - b_1 A\sin(\omega t) - b_2 B\sin(\omega t) - b_3 C\sin(\omega t), \tag{9.18}$$

and we define

$$I(t) = s_1 A\sin(\omega t) + s_2 B\sin(\omega t). \tag{9.19}$$

This yields:

$$\begin{cases} \dot{x}_1 = a_1 x_1 + a_2 x_2 + a_3 z + f_1; \\ \dot{x}_2 = b_1 x_1 + b_2 x_2 + b_3 z + f_2; \\ I = s_1 x_1 + s_2 x_2. \end{cases} \qquad (9.20)$$

According to Brenan [27]: *The k-step constant-step-size BDF method ($k < 7$) applied to constant coefficient linear systems of DAE of index ν is convergent of order $\mathcal{O}(h^k)$ after $(\nu - 1)k + 1$ steps.* Let us verify this by discretizing the system of DAE of index 2 (9.20) with BDF integration schemes of order 1, 2 and 3. The BDF integration scheme of order 1, i.e. the implicit Euler scheme, is given by

$$y^m = y^{m-1} + \triangle t g^m, \qquad (9.21)$$

where y^m is an approximation of $y(t)$ at time $t = t_m$, $m = 1, ..., nstep$ is the index of the time step, $\triangle t$ is the time-step size and g includes, for example, the RHS of equation (9.20). For the system of DAE (9.20), this yields:

$$\begin{cases} \dfrac{x_1^m - x_1^{m-1}}{\triangle t} = a_1 x_1^m + a_2 x_2^m + a_3 z^m + f_1^m; \\ \dfrac{x_2^m - x_2^{m-1}}{\triangle t} = b_1 x_1^m + b_2 x_2^m + b_3 z^m + f_2^m; \\ I^m = s_1 x_1^m + s_2 x_2^m, \end{cases} \qquad (9.22)$$

and therefore, the system of linear equations to solve at each time step is

$$\begin{bmatrix} 1 - a_1\triangle t & -a_2\triangle t & -a_3\triangle t \\ -b_1\triangle t & 1 - b_2\triangle t & -b_3\triangle t \\ s_1 & s_2 & 0 \end{bmatrix} \begin{bmatrix} x_1^m \\ x_2^m \\ z^m \end{bmatrix} = \begin{bmatrix} x_1^{m-1} + f_1^m \\ x_2^{m-1} + f_2^m \\ I^m \end{bmatrix}. \qquad (9.23)$$

The BDF time integration schemes of order 2 and 3 are respectively given by:

$$y^{m+1} - \frac{4}{3}y^m + \frac{1}{3}y^{m-1} = \frac{2}{3}f^{m+1}\triangle t, \qquad (9.24)$$

and

$$y^{m+2} - \frac{18}{11}y^{m+1} + \frac{9}{11}y^m - \frac{2}{11}y^{m-1} = \frac{6}{11}f^{m+2}\triangle t. \qquad (9.25)$$

The additional initial conditions necessary for the higher order BDF integration schemes are obtained recursively by using the results from the lower order methods, as described in [26].

Let us consider the dimensionless coefficients and parameters shown in Table 9.1. Using these parameters, the maximum norm of the error $||\boldsymbol{E}||_{max}$ as a function of the time-step size

Table 9.1 Coefficients and parameters for the simple system of DAE of index 2 (9.20) and the manufactured solution (9.16).

a_1	10000000
a_2	20000000
a_3	$a_1 + a_2$
b_1	30000000
b_2	40000000
b_3	$b_1 + b_2$
s_1	1
s_1	1
A	1
B	50
C	3
f	60
ω	$2\pi f$
t_{nstep}	$20/f$
$x_1(0)$, $x_2(0)$, $z(0)$	0

$\triangle t$ for the approximation of $x_1(t)$ using BDF schemes of order 1, 2 and 3 is shown in Figure 9.1. As predicted by Brenan [27], the BDF integration scheme of order 1 is convergent of order $\mathcal{O}(h)$, the BDF integration scheme of order 2 is convergent of order $\mathcal{O}(h^2)$ and the BDF integration scheme of order 3 is convergent of order $\mathcal{O}(h^3)$ for the approximation of $x_1(t)$. The same orders of convergence are achieved for the approximation of the algebraic variable $z(t)$, as illustrated in Figure 9.2. A description of the calculation of the error in the discrete maximum norm is available in Appendix D.

9.3.2 Reduction of the Index of a System of DAE from Index 2 to Index 1

If we differentiate the algebraic equations in the system of equations (9.13), we have

$$\begin{cases} M_A \dot{\boldsymbol{x}} = \Lambda_\rho \boldsymbol{x} + D\boldsymbol{z}; \\ \dot{\boldsymbol{I}} = C\dot{\boldsymbol{x}}. \end{cases} \tag{9.26}$$

For $n = 2$ and $n_c = 1$, let us define

$$M_A = \begin{bmatrix} M_{A_{11}} & M_{A_{12}} \\ M_{A_{21}} & M_{A_{22}} \end{bmatrix} \tag{9.27}$$

Figure 9.1 Maximum norm of the error as a function of the time-step size $\triangle t$ for the approximation of $x_1(t)$ using BDF schemes of order 1, 2 and 3.

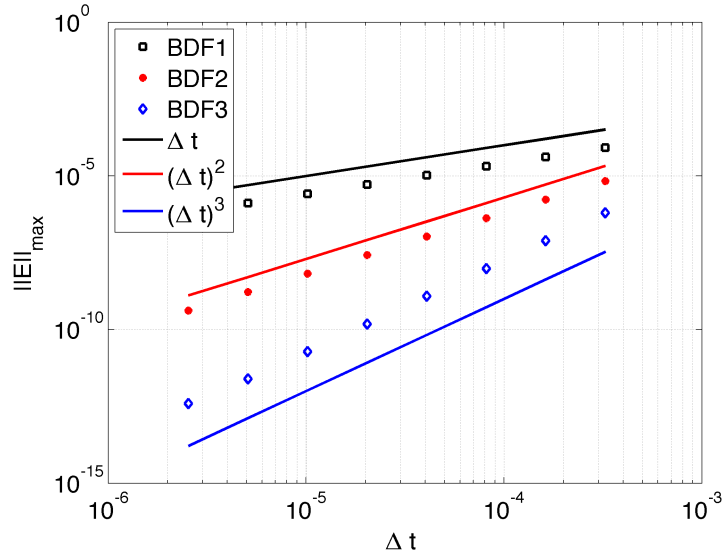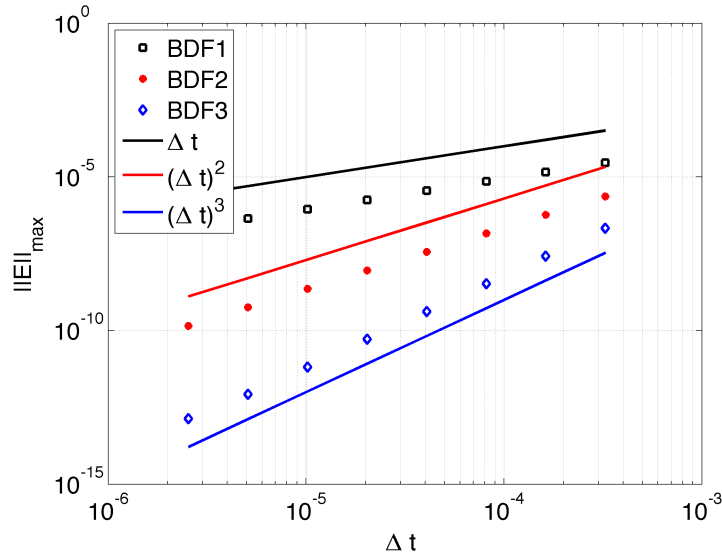Figure 9.2 Maximum norm of the error as a function of the time-step size $\triangle t$ for the approximation of $z(t)$ using BDF schemes of order 1, 2 and 3.

and write the system of equations (9.26) as

$$
\begin{bmatrix}
M_{A_{11}} & M_{A_{12}} & -1 \\
M_{A_{21}} & M_{A_{212}} & -1 \\
s_1 & s_2 & 0
\end{bmatrix}
\begin{bmatrix}
\dot{x_1} \\
\dot{x_2} \\
z
\end{bmatrix}
=
\begin{bmatrix}
\rho_1 x_1 \\
\rho_2 x_2 \\
\frac{dI}{dt}
\end{bmatrix},
\tag{9.28}
$$

where ρ_1 and ρ_2 are the diagonal entries of Λ_ρ. The matrix on the left is the augmented matrix based on M_A, written M_A^+. If we multiply this system of equations by the inverse of the augmented matrix $(M_A^+)^{-1}$ whose entries are given by d_{ij} for $i, j = 1, 2, 3$, we have:

$$
\begin{cases}
\dot{x}_1 = d_{11}\rho_1 x_1 + d_{12}\rho_2 x_2 + d_{13}\dfrac{dI}{dt}; \\[2mm]
\dot{x}_2 = d_{21}\rho_1 x_1 + d_{22}\rho_2 x_2 + d_{23}\dfrac{dI}{dt}; \\[2mm]
z = d_{31}\rho_1 x_1 + d_{32}\rho_2 x_2 + d_{33}\dfrac{dI}{dt},
\end{cases}
\tag{9.29}
$$

which is a system of DAE of index 1. Note that in order to find x_1 and x_2, we only need to solve the first two equations, which are ODEs.

For systems of ODEs, the forward Euler scheme is first order accurate. If we use the same manufactured solution as for the index 2 case and discretize these two equations using the forward Euler time integration scheme, we have:

$$
\begin{cases}
x_1^m = x_1^{m-1} + \triangle t \left(d_{11}x_1^{m-1} + d_{12}x_2^{m-1} + d_{13}\dfrac{dI}{dt}^{n-1} + f_1^{n-1} \right); \\[2mm]
x_2^m = x_2^{m-1} + \triangle t \left(d_{21}x_1^{m-1} + d_{22}x_2^{m-1} + d_{23}\dfrac{dI}{dt}^{m-1} + f_2^{m-1} \right).
\end{cases}
\tag{9.30}
$$

The algebraic variable at each time step m can then be calculated with the values obtained from x_1^m and x_1^m, i.e.

$$
z^m = d_{31}x_1^m + d_{32}x_2^m + d_{33}\dfrac{dI}{dt}^m .
\tag{9.31}
$$

Let us consider the dimensionless coefficients and parameters shown in Table 9.2. Note that we chose these parameters to be in the stability region of the forward Euler scheme. Using these parameters, the maximum norm of the error as a function of the time-step size $\triangle t$ for the approximation of $x_1(t)$ and $x_2(t)$ using the forward Euler scheme is shown in Figure 9.3. As expected, the forward Euler scheme is convergent of order $\mathcal{O}(h)$. Figure 9.3 also shows the order of convergence for the approximation of the algebraic variable $z(t)$. We see that it is also $\mathcal{O}(h)$.

With both strategies, i.e. the direct discretization and the reduction of index, we achieved the expected orders of convergence. Based on those results, we cannot conclude that one strategy is better than the other. However, to reduce the index of the system of DAE, we had to do additional mathematical manipulations. These mathematical manipulations are additional steps in the solving process and as a result, the strategy of the reduction of the index is less straightforward than the direct discretization. Moreover, when reducing the

Table 9.2 Coefficients and parameters for the system of DAE of index 1 (9.20) and the manufactured solution (9.16).

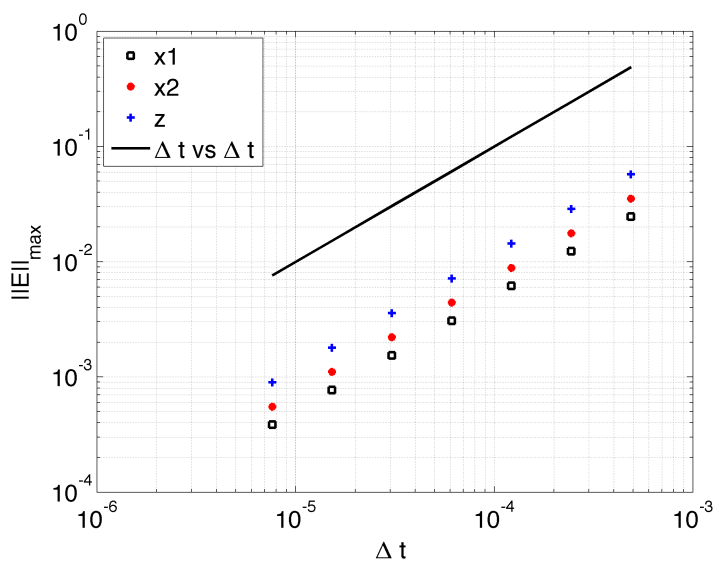|	
d_{11}	1
d_{12}	2
d_{13}	$d_{11} + d_{12}$
d_{21}	3
d_{22}	2
d_{23}	$d_{21} + d_{22}$
s_1	1
s_1	1
A	1
B	0.5
C	3
f	4
ω	$2\pi f$
t_{nstep}	$^2/_f$
$x_1(0),\ x_2(0),\ z(0)$	0

Figure 9.3 Maximum norm of the error as a function of the time-step size $\triangle t$ for the approximations of $x_1(t)$, $x_2(t)$ and $z(t)$ using the forward Euler integration scheme.

index, we need to make sure that the initial conditions satisfy the algebraic equation

$$s_1 x_1 + s_2 x_2 = I(t) \tag{9.32}$$

but also, the differentiated algebraic equation

$$s_1 \dot{x}_1 + s_2 \dot{x}_2 = \dot{I}(t). \tag{9.33}$$

As a result, from what we discussed in this chapter, it is less risky and more straightforward to use the strategy of direct discretization than to reduce the index of the system of DAE.

CHAPTER 10

CONCLUSION

In this thesis, we showed that the discretization of HTS problems using nodal finite elements in 1-D results in a system of DAE of index 0 or 1, depending on how the Dirichlet boundary conditions are enforced. We described two strategies to discretize the system of DAE of index 0 in time, i.e. the direct discretization strategy and the reformulation strategy. In practice, direct discretization is preferable to reformulation because the latter requires a matrix inversion, which is not practical with a nonlinear problem such as that encountered in HTS modeling. We described two strategies to discretize the system of DAE of index 1 in time, i.e. the reduction of the index strategy and the direct discretization strategy. We concluded that the direct discretization is more straightforward than the reduction of the index because it does not require as many mathematical manipulations. It is also less risky because there are no hidden constraints. We implemented a code in which we discretized the systems of DAE of index 0 and 1 directly. We verified the code against an analytical nonlinear solution and we showed that it gives a good approximation of the solution for both systems of DAE. We did not face any issues when we computed the approximations. We concluded that the direct discretization strategy works for the typical 1-D HTS problem described in chapter 7.

The system of DAE that results from the discretization of HTS problems using edge elements in 2-D is either of index 0 or 2 depending if Dirichlet or Neumann boundary conditions are applied. The system of DAE of index 2 is in Hessenberg form. We described two strategies to discretize the system of DAE of index 2 in time, i.e. the direct discretization and the reduction of the index. We noted that reducing the index from 2 to 1 leads to a system of ODEs. We were not able to conclude if the direct discretization strategy is better than the reduction of the index. However, the reduction of the index requires additional mathematical manipulations such as inverting a matrix, which is a downside of the strategy. We implemented a code and we verified this code against two analytical solutions for three problems. In all cases, we showed that the code gives a good approximation when the solution is nearly linear in space. When it is not, we observed small discrepancies. We explained that those discrepancies are due to the coarseness of the mesh and to the fact that the normal component of the approximation of the magnetic field between two elements is not necessarily continuous. We showed that the approximation converges, when the size of the elements is reduced.

We also showed that the discretization of HTS problems using the SAM leads to a system of DAE of index 0 or 2, depending if the problem is voltage or current driven. The system of DAE of index 2 is in Hessenberg form. We described two strategies to discretize the system of DAE of index 0 in time, i.e. the direct discretization and the reformulation. We mentioned that the reformulation is not the best strategy because it requires inverting a dense matrix and because the system of DAE is nonlinear. We showed that the system of DAE of index 2 in Hessenberg form obtained with the SAM is similar to the system of DAE of index 2 in Hessenberg form obtained with the FEM using edge elements. Therefore, the same conclusions for the discretization strategies still hold. We investigated the strategy of direct discretization and the strategy of reduction of the index using a simple system of DAE of index 2 in Hessenberg form with a manufactured solution. We showed that we get the expected order of convergence with both strategies. However, we noted that the reduction of the index is less straightforward than direct discretization. It is also riskier since the initial conditions must satisfy both the algebraic equations and their time derivatives.

This project gives a background for the systems of DAE encountered in the numerical modeling of HTS devices. However, we have not done a thorough investigation of the proposed strategies for HTS devices problems. Generally, the direct discretization seems like the best strategy but we have not quantified how well it works compared to the other strategies. Maybe there is a limit at which one of the strategies becomes better than the others. In Future work, we would like to assess the proposed strategies for a given HTS problem and give recommendations based on data such as the rate of converge and the computation time.

REFERENCES

[1] A. C. Rose-Innes and E. Rhoderick, *Introduction to superconductivity*. Oxford: International Series in Solid State Physics, 2nd ed., 1977.

[2] P. Tixador and Y. Brunet, "Supraconducteurs, Bases Théoriques," 2003.

[3] F. Sirois and F. Grilli, "Numerical Considerations About Using Finite-Element Methods to Compute AC Losses in HTS," *IEEE Transactions on applied superconductivity*, vol. 18, no. 3, pp. 1733–1742, 2008.

[4] A. Fortin and A. Garon, *Les éléments finis: de la théorie à la pratique*. Quebec city: unpublished, 2011.

[5] J. Jin, *The finite element method in electromagnetics*. New York, NY: Wiley, 2nd ed., 2002.

[6] F. Sirois and F. Roy, "Computation of 2-D Current Distribution in Superconductors of Arbitrary Shapes Using a New Semi-Analytical," *ieeexplore.ieee.org*, vol. 17, no. 3, pp. 3836–3845, 2007.

[7] F. Sirois, *Modélisation de la caractéristique E-J des supraconducteurs à haute température critique*. Ph.D. Thesis, École Polytechnique Montreal, 2002.

[8] M. Tinkham, *Introduction to superconductivity*. Mineola: Dover publications Inc., 2nd ed., 1996.

[9] N. W. Aschroft and N. D. Mermin, *Solid State Physics*. Orlando: Harcourt, Inc., 1st editio ed., 1976.

[10] S. Elliott, *The Physics and Chemistry of Solids*. Chichester: John Wiley and & Sons, 1st ed., 1998.

[11] Y. B. Kim, C. Hempstead, and A. Strnad, "Resistive States of Hard Superconductors," *Rev. Mod. Phys.*, 1964.

[12] A. Wan, *Adaptive Space-Time Finite Element Method in High Temperature Superconductivity*. Ph.D. Thesis, École Polytechnique Montreal, 2014.

[13] R. Brambilla, F. Grilli, and L. Martini, "Development of an edge-element model for AC loss computation of high-temperature superconductors," *Superconductor Science and Technology*, vol. 20, pp. 16–24, Jan. 2007.

[14] E. H. Brandt, "Superconductors of finite thickness in a perpendicular magnetic field : Strips and slabs," *Physical Review B*, vol. 54, no. 6, pp. 4246–4264, 1996.

[15] M. Siahrang, S. Member, F. Sirois, and S. Member, "Fast Numerical Computation of Current Distribution and AC Losses in Helically Wound Thin Tape Conductors : Single-Layer Coaxial Arrangement," *IEEE Transactions on applied superconductivity*, vol. 20, no. 6, pp. 2381–2389, 2010.

[16] K. Carlier, *Modèle Intégrale Axisymétrique pour le Calcul des Pertes AC dans les Bobinages Supraconducteurs*. Master Thesis, École Polytechnique Montréal, 2012.

[17] R. Brambilla, F. Grilli, L. Martini, and F. Sirois, "Integral equations for the current density in thin conductors and their solution by the finite-element method," *Superconductor Science and Technology*, vol. 21, p. 105008, Oct. 2008.

[18] R. Brambilla, F. Grilli, D. N. Nguyen, L. Martini, and F. Sirois, "AC losses in thin superconductors: the integral equation method applied to stacks and windings," *Superconductor Science and Technology*, vol. 22, p. 075018, July 2009.

[19] F. Sirois and F. Grilli, "Potential and limits of numerical modelling for supporting the development of HTS devices," *Superconductor Science and Technology*, vol. 28, p. 043002, Apr. 2015.

[20] A. Sanchez and C. Navau, "Magnetic properties of finite superconducting cylinders. I. Uniform applied field," *Physical Review B*, vol. 64, p. 214506, Nov. 2001.

[21] N. Amemiya, S.-i. Murasawa, N. Banno, and K. Miyamoto, "Numerical modelings of superconducting wires for AC loss calculations," pp. 16–29, 1998.

[22] S. Stavrev, F. Grilli, B. Dutoit, N. Nibbio, E. Vinot, I. Klutsch, G. Meunier, P. Tixador, Y. Yang, and E. Martinez, "Comparison of Numerical Methods for Modeling of Superconductors," vol. 38, no. 2, pp. 849–852, 2002.

[23] S. Dufour, "Notes de cours MTH6207, Mathématiques des éléments finis," 2009.

[24] J. Nedelec, "Mixed finite elements in R3," *Numer. Meth.*, vol. 35, pp. 315–341, 1980.

[25] J. Webb, "Edge Elements and What They can do for you," *IEEE Transactions On Magnetics*, vol. 29, no. 2, pp. 1460–1465, 1993.

[26] U. Ascher and L. Petzold, *Computer Methods for Ordinary Differential Equations and Differential-Algebraic Equations*. Philadelphia: SIAM, 1998.

[27] K. Brenan, S. Campbell, and L. Petzold, *Numerical solution of Initial-Value problems in Differential-Algebraic Equations*. Philadelphia: SIAM, 1996.

[28] S. Cambell, *Singular System of Differential Equations*. Boston: Pitman, 1980.

[29] L. Petzold, "A Description of DASSL: A Differential/Algebraic System Solver," in *10th international mathematics and computers simulation congress on systems simulation and scientific computation*, (Montreal Canada), 1982.

[30] A. Hindmarsh, R. Serban, and A. Collier, "User Documentation for IDA v2.6.0," tech. rep., Center for applied Scientific Computing, LLNL, 2009.

[31] I. Mayergoyz, *Nonlinear Diffusion of Electromagnetic Fields With Applications to Eddy Current and superconductivity*. San Diego, CA: Academic, 1998.

[32] O. Dubois and F. Sirois, "Edge elements pour la calcul du champ magnétique en 2D et 3D: application au contrôle non destructif.," tech. rep., École Polytechnique Montréal, Montreal Canada, 2010.

[33] G. B. Arfken and H. J. Weber, *Mathematical Methods for Physicists*. Burlinghton, MA: Elsevier Academic Press, 6th ed., 2005.

APPENDIX A

Expression of the power law in terms of the discrete degrees of freedom for 1-D nodal elements

We recall equations (7.5) and (7.6):

$$\rho(J) = \frac{E_c}{J_c}\left|\frac{J}{J_c}\right|^{n-1} \quad \text{and} \quad J = -\frac{1}{\mu_0}\frac{\partial B}{\partial x}. \tag{A.1}$$

On an arbitrary element K, using the approximation

$$B(x,t)\Big|_K \approx b^K(x,t) = \sum_{j=1}^{2} b_j^K(t)\Psi_j^K(x), \tag{A.2}$$

an approximation of the current $J(x,t)$ can be computed using

$$J(x,t)\Big|_K \approx j^K(x,t) = \frac{-1}{\mu_0}\left[\frac{\partial}{\partial x}\left(b_1(t)\Psi_1^K(x) + b_2(t)\Psi_2^K(x)\right)\right]. \tag{A.3}$$

Using the transformation over the reference element $\hat{K}$, we have, from equation (7.24),

$$j^K(\xi,t) = \frac{-2}{\mu_0 h^k}\left(b_1(t)\frac{d\hat{\Psi}_1(\xi)}{d\xi} + b_2(t)\frac{d\hat{\Psi}_2(\xi)}{d\xi}\right). \tag{A.4}$$

Since we know that

$$\begin{cases} \dfrac{d\hat{\Psi}_1(\xi)}{d\xi} = \dfrac{-1}{2}; \\ \dfrac{d\hat{\Psi}_2(\xi)}{d\xi} = \dfrac{1}{2}, \end{cases} \tag{A.5}$$

the resistivity $\rho^K(t)$ can be computed with

$$\rho^K(t) = \frac{E_c}{J_c}\left|\frac{b_1^K(t) - b_2^K(t)}{\mu_0 J_c h^k}\right|^{n-1}. \tag{A.6}$$

APPENDIX B

Analytical solution for a 1-D HTS problem

For a one sided slab with the boundary and initial conditions:

$$
\begin{cases}
B(-a, t) = B_a t^p; \\
B(x, 0) = 0.
\end{cases}
\tag{B.1}
$$

Using the power law

$$
\rho(J) = \frac{E_c}{J_c} \left| \frac{J}{J_c} \right|^{n-1},
\tag{B.2}
$$

the magnetic flux density is given by

$$
B(x, t) =
\begin{cases}
B_a t^p \left(1 - \frac{\epsilon(x+a)}{\xi_0 t} \right)^p, & -a \leq x < x_f(t), \\
0, & x > x_f(t),
\end{cases}
\tag{B.3}
$$

with

$$
p = \frac{n}{n-1},
\tag{B.4}
$$

$$
\epsilon = B_a^{\left(\frac{1-n}{n+1} \right)} \kappa^{\left(\frac{-1}{n+1} \right)},
\tag{B.5}
$$

$$
\kappa = \frac{E_c}{(\mu_0 J_c)^n},
\tag{B.6}
$$

$$
\xi_0 = p^{\frac{n}{n+1}},
\tag{B.7}
$$

and

$$
x_f(t) = \frac{\xi_0}{\epsilon} t.
\tag{B.8}
$$

This solution can be extended to a two-sided slab using the proper symmetry.

APPENDIX C

Expression of the power law in terms of discrete degrees of freedom for 2-D edge elements

Knowing that

$$\boldsymbol{J} = \nabla \times \boldsymbol{H}. \tag{C.1}$$

On an arbitrary element K, we have

$$\boldsymbol{H}(\boldsymbol{x},t)\Big|_K \approx \boldsymbol{h}^K(\boldsymbol{x},t) = \sum_{j=1}^{3} h_j^K(t)\boldsymbol{N}_j^K(\boldsymbol{x}). \tag{C.2}$$

Therefore, on the element K:

$$\boldsymbol{J}(\boldsymbol{x},t)\Big|_K \approx j^K(\boldsymbol{x},t)\hat{\boldsymbol{k}} = \sum_{j=1}^{3} h_j^K(t)\nabla \times \boldsymbol{N}_j^K(\boldsymbol{x}), \tag{C.3}$$

which yields for an approximation of the current $\boldsymbol{J}$:

$$j^K(t) = \sum_{j=1}^{3} h_j^K(t)\frac{l_j^K}{\triangle^K}. \tag{C.4}$$

Therefore, on element K, the resistivity with the power law is time dependent and is given by

$$\rho^K(t) = \frac{E_c}{J_c(\triangle^K)^{n-1}}\left|\frac{\sum_{j=1}^{3} h_j^K(t)l_j^K}{J_c}\right|^{n-1}. \tag{C.5}$$

APPENDIX D

Calculation of the error in the discrete maximum norm $||\boldsymbol{E}||_{max}$

Let us consider y_m an approximation of the solution $y(t)$ at time t_m, where $m = 1, ..., nstep$ is the index of the time-step. The error in the approximation of the solution at time t_m is given by $E_m = y_m - y(t_m)$. For a simulation that lasts t_{nstep}, the maximum norm of the error is given by:

$$||\boldsymbol{E}||_{max} = \max(|E_1|, |E_2|, ..., |E_{nstep}|), \tag{D.1}$$

where $\boldsymbol{E}$ is a vector containing the error E_m for $m = 1, ..., nstep$.